universität wien

MASTERARBEIT / MASTER'S THESIS

Titel der Masterarbeit / Title of the Master's Thesis

„Elucidation of function of proteins taking part in the Reelin Pathway“

verfasst von / submitted by

Magdalena Teufl Bsc

angestrebter akademischer Grad / in partial fulfilment of the requirements for the degree of

Master of Science (MSc)

Wien, 2023 / Vienna, 2023

Studienkennzahl lt. Studienblatt / degree programme code as it appears on the student record sheet:	UA 066 834
Studienrichtung lt. Studienblatt / degree programme as it appears on the student record sheet:	Molekulare Biologie UG2002
Betreut von / Supervisor:	ao. Univ.-Prof. Dipl.-Ing. Dr. Johannes Nimpf

Contents

Acknowledgements

First, I want to thank ao. Univ.-Prof. Dipl.-Ing. Dr. Johannes Nimpf for being my supervisor. His advice and feedback throughout my project were always valued highly. He helped me several times by giving me new ideas I could include in my projects or showed me new ways to interpret my results. Especially, his explanations of various matters were always clear and easy to understand, which helped me a lot.

I am extremely grateful for the help I got from Paula. Without her I would not have become the scientist I am today. She showed me how work in the lab is done in general. Through her expertise I could gain a lot of knowledge of how to organize matters and how planning of projects should look like. Additionally, she helped me to learn how to establish and maintain clean techniques during experiments and how precise writing of protocols is done. What I valued the most, was her way of establishing a great atmosphere in the lab. Even though, we were working hard the whole week, there was always time for a quick question, and she always helped me out when I needed help. Thinking back to the times, when the “awesome mix” was improving our moods during long days in the lab, still makes me smile. I am extremely grateful for her being my supervisor and friend during my master project.

Of course, I also want to thank my colleague Max, who was always there for great conversations and discussions while working or going for lunch together.

I’d like to mention my parents, who always were there for me and encouraged me a lot and last, I want to thank Christoph, who was my greatest supporter during my masters. He always knew what to say to me when doubts rose and cheered me up when I needed it. If I ever had some technical problems, he was there to help me out. I could not have undertaken this journey without him pushing me to achieve my goals and become the person I am now.

Abstract

The Reelin pathway plays a crucial role during embryonic development in mammals. Especially for the formation of the central nervous system, its presence is essential. In this project, the search for hitherto unknown functions of key players of the Reelin pathway was the main goal. Apo-E Receptor 2 (ApoER2) which is phosphorylated upon Reelin stimulation, and its isoforms were used for different experimental setups to uncover distinct mechanisms taking part during Reelin signalling. Based on existing data, suggesting an influence on cell shape and, a closer evaluation of the specific subcellular location of the isoforms was performed. To approximate our results as close as possible to the in vivo situation, experiments were not only carried out with cell lines, but also primary cells were included, when possible. Additionally, Disabled 1 (Dab1) the direct adaptor protein of ApoER2 was studied in detail. With the help of a Knockout cell line, reduced cell growth due to the lack of Dab1 could be identified. Furthermore, a yet unknown function of Dab1 in the EGFR pathway could be identified. As EGFR is expressed in nearly any tissue and is involved in many processes and, many different diseases can arise because of its dysregulation. Maybe, the discovery of this link can provide the base of a future treatment of diseases in tissues where these two proteins are expressed in.

Der Reelin-Signalweg spielt eine entscheidende Rolle in der Embryonalentwicklung von Säugetieren. Besonders während der Bildung des zentralen Nervensystems ist er essenziell. Während diesem Projekt wurde nach bisher unbekannten Funktionen der Schlüsselproteine des Reelin-Signalweges gesucht. Apo-E Rezeptor 2 (ApoER2) und dessen Isoformen wurden durch verschiedene experimentelle Setups darauf untersucht, welche verschiedenen Funktionen sie im bereits bekannten Signalweg einnehmen können. Aus Vorversuchen wurde vermutet, dass diese Isoformen in Abhängigkeit ihrer subzellulären Expression einen Beitrag zur Morphologie der Zellen liefern könnten. Um unsere Ergebnisse so weit wie möglich and die in-vivo Situation anzunähern, wurden nicht nur Experimente mit Zelllinien gemacht. Wenn es möglich war, wurden auch primäre Zellen verwendet. Weiters wurde Disabled 1 (Dab1), das direkte Adapter-Protein von ApoER2 genauer untersucht. Mithilfe eine Knockout Zelllinie konnte ein reduzierter Zellwachstum und reduzierte metabolische Aktivität durch fehlendes Dab1 identifiziert werden. Zusätzlich wurde eine bis jetzt unbekannte Funktion von Dab1 im EGFR-Signalweg entdeckt. Da EGFR an einer großen Anzahl an Prozessen beteiligt ist und es in fast jedem Gewebe gefunden wird, gibt es viele Krankheiten, die aufgrund von Fehlregulierungen dieses Proteins entstehen können. Vielleicht könnte die Entdeckung dieser Verbindung die Basis einer, in der Zukunft zu entwickelnden Behandlung von einer Krankheit sein, die auf Fehlfunktionen dieser beiden Proteine beruhen.

Aims

The aim of this master thesis project was to uncover hidden functions of proteins involved in the Reelin pathway. The focus was primarily set on ApoER2 and Dab1, whose major functions in the Reelin pathway are already known. As there are different isoforms of the receptor exist, subcellular localisation and signals can differ in certain situations. Additionally, there is a possibility that those proteins also take part in other signal pathways and have unknown functions that can still be discovered. My goal was to get a better understanding and to deepen our knowledge about certain responses to Reelin by proteins further down the signal cascade. One protein included in this research was N-Wasp. Additionally, I wanted to determine the location of proteins/receptors in the plasma membrane and check whether the localization of some of them changes upon Reelin treatment.

Introduction

The canonical Reelin pathway (Figure 1) also called core Reelin pathway has been studied extensively and involves binding of Reelin to VLDLR and ApoER2 which induces phosphorylation of Dab1 via SRC family tyrosine kinases. Dependent on the phosphorylation of different tyrosines

of Dab1, special signal cascades such as Crk, Crk-like and phosphatidylinositide 3-kinase are activated and orchestrate neuronal migration during development. Involvement in dendritic growth, branching and spine formation, synaptogenesis and synaptic plasticity and many other important processes have been reported so far[1–3].

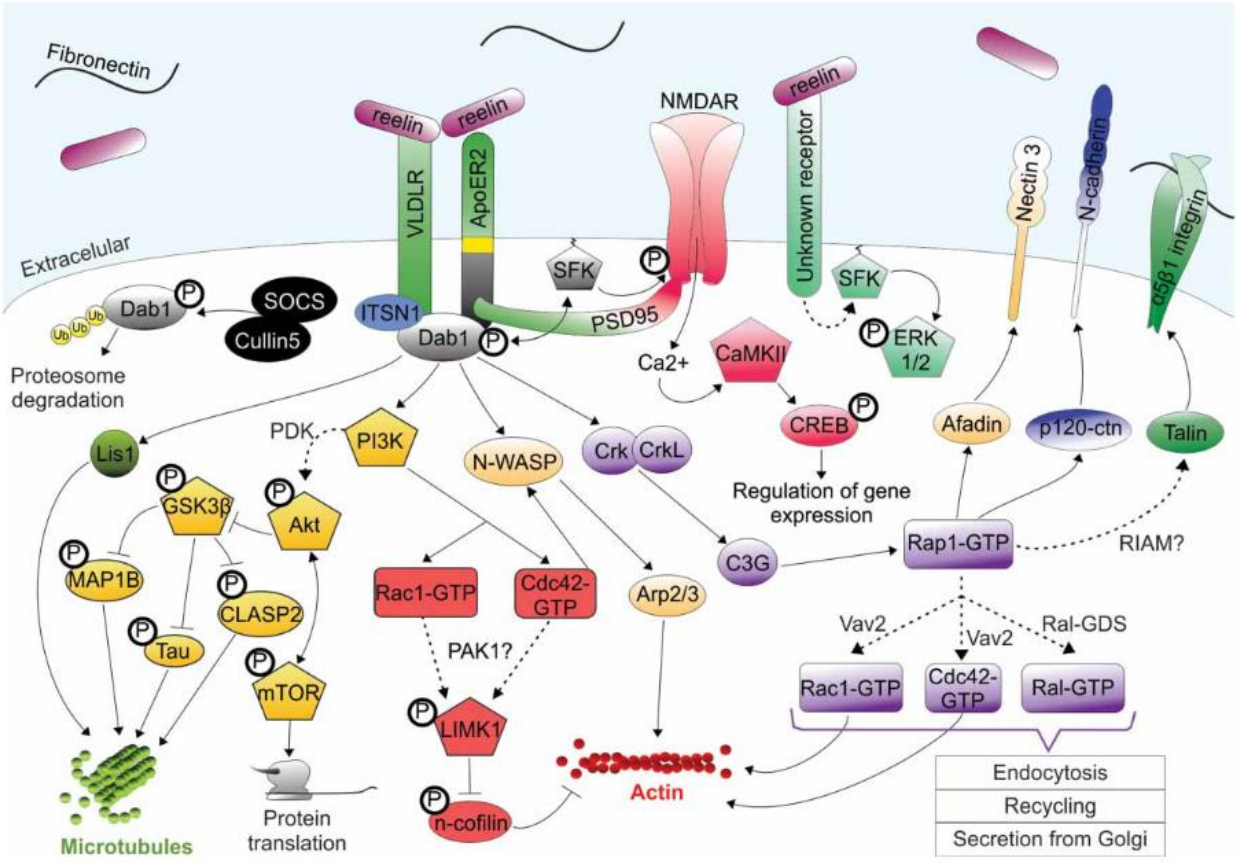

Figure 1 The Reelin Pathway[1]

Reelin

The protein Reelin is an extracellular glycoprotein which orchestrates the inside-out layering of neurons of the neocortex during development of the brain. It was first discovered in mice which lost the functional protein by a spontaneously acquired recessive mutation. This phenotype was termed “Reeler” according to the observed reeling gait of the affected animals. Other symptoms of those mice were, that they are ataxic, tremble, walk with a wide gait and often drag their hind limbs, sometimes they even flip onto their backs[4,5]. Without functional Reelin present during embryonic development, ectopic layering of neurons in the cerebral cortex, cerebellum and hippocampus occurs. When taking a closer look at other parts of the nervous system, such as the olfactory bulb, the spinal cord, the thalamus and others, one can see that these areas are moderately affected as well as a consequence of the absence of Reelin. As it is not only found in neuronal tissues, the loss of Reelin can adversely impact other signalling pathways of the body as well. Development of lymphatic vessels, mammary and submandibular glands, the small intestine, cartilage and bone can be altered. In adults, involvement of Reelin in immune system function, liver fibrosis, multiple cancers and Alzheimer’s disease has been implied[2].

During embryogenesis neuronal precursors are made in the subventricular zone of the neocortex by asymmetric cell division of precursor cells. The newly built neuroblasts start migrating in radial direction towards the brain surface. A switch between different types of neuronal migration occurs. Starting with short bipolar migration neuronal movement changes into multipolar migration. Next bipolar locomotion guided by glia cells takes place and finally the movement is finished via terminal somal translocation. This process is tightly regulated in a time and cell-type specific

manner. Attraction of neurons, detachment from glia, and stop signals have to happen at the right moment[6–8].

Initially, the development of the reeler neocortex is normal. Neurons are formed in germinative zones, of the ventricular zone and migrate normally. If present, Reelin is abundantly expressed in some of the preplate forming pioneer neurons, called Cajal-Retzius bodies. Glutamatergic excitatory projection neurons invade and split the preplate with the help of Reelin signalling and the cortical plate is formed. The split preplate is called marginal zone on the outer side, where Reelin expressing cells are located and the transient subplate, where Reelin negative cells reside. If Reelin is absent, this invasion cannot take place, later born neurons cannot surpass their progenitors and their location is changed. This results in poorly organized, inside-out cortical layering as shown in Figure 2. The main source of Reelin secretion is switched from Cajal-Retzius bodies to cerebellar granule cells and a subpopulation of GABAergic (inter)neurons.[9,10].

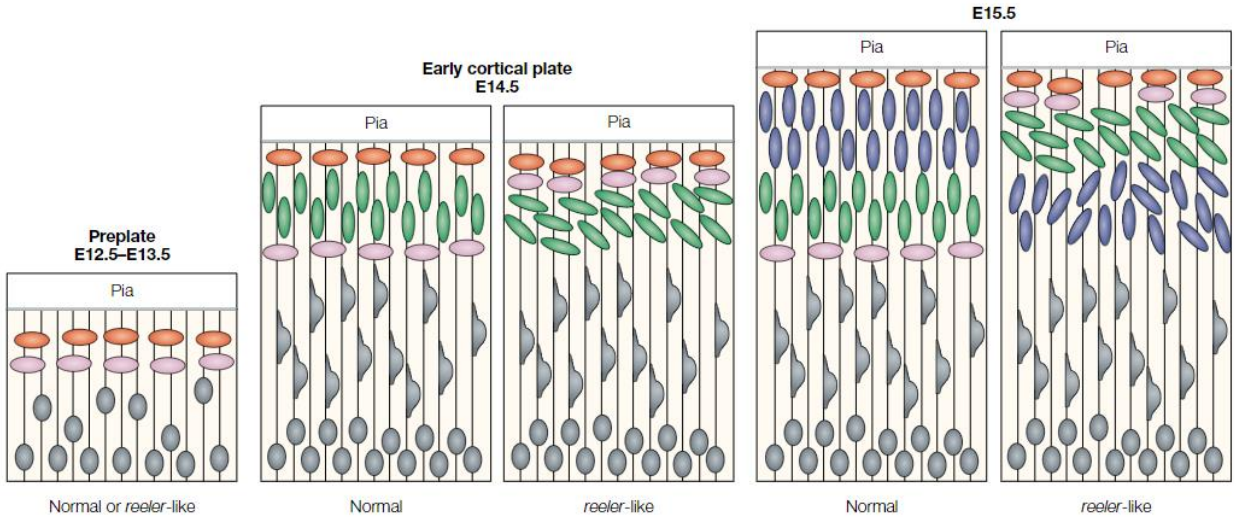

Figure 2 Neuronal layering in laminated brain structures during development in wt and -reeler mice. Preplate splitting does not occur in the early cortical plate in reeler mice (E14.5) and later born neurons(blue) cannot pass early born neurons (pink and green) and locate in close proximity to the Reelin expressing pioneer neurons (red).[122]

Reelin is built from a 450kbp long gene, which gives rise to a large extracellular matrix glycoprotein that consists of 3461 amino acids. It has a relative molecular mass of 388kDa, which is increased to up to 450kDa when N-glycosylation is performed in the Golgi. The different functional parts of Reelin are, a signal peptide, a F.spondin homology domain, an unique region, eight Reelin-specific repeats (R1-R8) which consist of sub-repeats A and B that flank an EGF-like motif and a 33 amino acid C terminal stretch that is positively charged. Most homologues of Reelin, that were identified so far are found in the phylum Chordata, but some also belong to Mollusca and Arthropoda. According to phylogenetic data, the protein might have originated in Arthropoda[11–13].

Reelin expression is promoted by neuronal silencing and its secretion is constitutive[14]. The two major sites where Reelin is proteolytically processed after secretion are located between Reelin-specific repeats two and three and six and seven. The five following fragments are produced by cleavage with extracellular matrix metalloproteinases: N-R6, R3-8, R3-6, N-R2 and R7-8. (Figure 3) It was found that fragments containing the C-terminal part of the protein reside in the marginal zone[15]. The active central fragment (R3-6) can diffuse further into the tissue as it is smaller than the full-length protein. Some controversial data, regarding its ability to phosphorylate Dab1 exists. Therefore, its function to relay Reelin signalling is still questioned. The full length and central fragment (R3-6) changes clustering size of the receptors and phosphorylation of Dab1 occurs. Dab1 could not be phosphorylated via treatment with R3-6 but it was achieved via treatment with full-length Reelin[16]. The binding site of its two major receptors (ApoER2 and VLDLR) is built by

the A subdomain of R6. If both receptors are lost, an increase of the central fragment is detected, which suggests, that it may be taken up by the receptors and degraded to prevent enhanced/prolonged signalling. Additionally, the covalent homo-dimerization region of Reelin is located on R3-6 which is essential for Dab1 phosphorylation[17]. Recent studies have shown that the N-terminal cleavage is important for the duration of Reelin signalling. Through introduction of a mutation at the N-terminal cleavage site of Reelin, a loss of both the N-terminal and the central fragment was generated. High numbers of N-R-6 were present which caused excessive Reelin signalling leading to a low number of improperly located neurons, enhanced dendritic growth and Dab1 protein levels were reduced[18]. There is an existing crosstalk of the Reelin and the Notch pathway maintaining hippocampal plasticity[19]. Further, the activity of the NMDA receptor and its subunit composition are regulated via Reelin signalling through the postsynaptic density protein (PSD95)[20].

Reelin not only plays an important role in neuronal development, its dysregulation or anomalous procession contributes to various diseases as well. Decreased mRNA levels of the protein correlate with autistic spectrum disorder and schizophrenia[21,22]. Elevated levels of Reelin, which arise due to failure of Cajal-Retzius programmed death, can affect memory and epileptic seizures can occur[23]. Frontotemporal dementia, Alzheimer's disease and Down syndrome symptoms are linked to enhanced Reelin processing. It also has the ability to bind to amyloid precursor protein (APP) a protein which is located at synapses. Because of this connection and the major role of APP in Alzheimer's disease (AD), the involvement of Reelin in this complex condition is suggested [24–26]. Depression, bipolar disorder, epilepsy and some types of schizophrenia are associated with decreased Reelin procession[27–29].

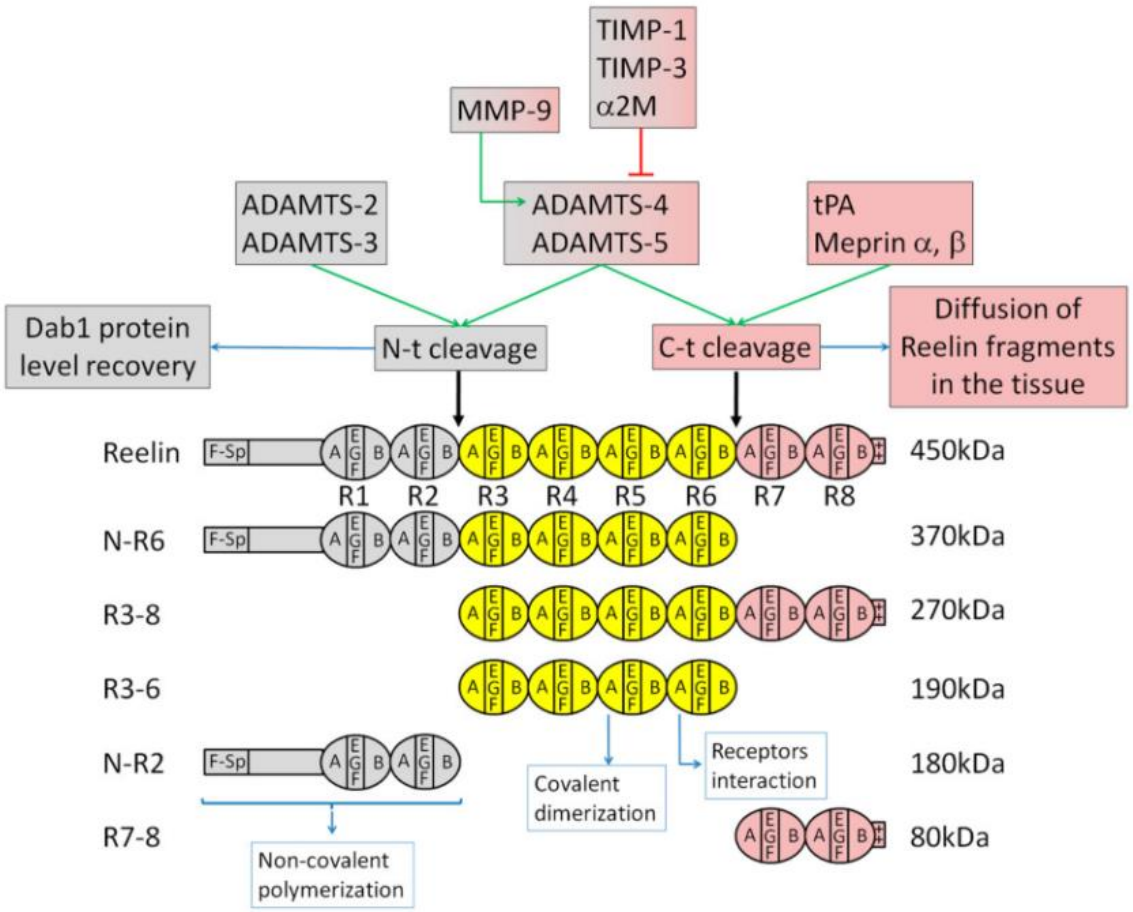

Figure 3 Reelin structure including cleavage sites and discovered proteases. [2]

ApoER2+VLDLR

ApoE receptor 2(ApoER2), also known as LRP8 (this is the gene name as well) and very low-density receptor (VLDLR) are type-I transmembrane proteins and members of the low-density lipoprotein receptor family class. These receptors are thought to have evolved from one ancestor through several rearrangements and duplications. The type-I transmembrane receptors are responsible for endocytosis and signal transduction.

They share six important structural properties which consist of a N-terminal ligand binding domain, with differing numbers of LDL receptor type A repeats (LA) followed by three EGF precursor-like repeats. Another common feature of this receptor family is the β-propeller domain that is built up by LDL receptor class B repeats containing the YWTD motif, that is located between the second and third EGF like repeat. The next important element is the O-linked sugar domain (OLSD). The other two elements of this receptor type family are the transmembrane domain followed by the short cytoplasmic tail where the NPXY motif is found. Clathrin mediated endocytosis and recycling as well as interaction with the disabled 1 (Dab1) adaptor protein and further signal transduction is possible through this highly conserved motif[30–32].

Dendritic spine formation, cortex, hippocampus and cerebellum development are depending on a functional canonical Reelin pathway. The loss of both receptors, ApoER2 and VLDLR leads to the reeler-like phenotype which is described above. Although both Receptors have many structural features in common, and the sequence identity between them is 47%, there are some very important differences. As only mild spatiotemporal alterations occur in single knockouts, divergent functions of the receptors exist and some of them still have to be discovered[33,34].

ApoER2 is a key player in cortical lamination during development and as well important for cytoskeletal and synaptic plasticity, learning and memory and it also regulates Tau phosphorylation[33,35–40]. The corresponding gene consists of an open reading frame of 2889 bp, which is translated into proteins with a relative molecular mass of 120-140 kDa, built by 963 amino acids. ApoER2 expression is restricted to mostly nervous tissue such as the central nervous system where especially high numbers are found in the neocortex (apical dendrites and cell bodies), cerebellum (Purkinje cells), hippocampus (pyramidal cells of CA and granule cells of dentate gyrus) and the olfactory bulb but some amounts are also found in the periphery (sciatic nerve and the Schwann cells). Additionally, ApoER2 is also found in testis, placenta, ovary, bone, vascular endothelial and smooth muscle cells and immune cells of the myeloid lineage[32]. In the small intestine, ApoER2 is found in the upper half of the villi[41]. During development ApoER2 is predominantly found in the lower part of the intermediate zone and in the multipolar accumulation zone. VLDLR is absent in these regions. Lower numbers of ApoER2 are expressed in the upper part of the marginal zone. Neurons expressing ApoER2 normally do not express VLDLR, even though they are found in the same area during brain development. It is thought that ApoER2 signalling is essential for migration of late born cortical neurons and VLDLR is needed to terminate this movement[34].

Splice variants of both receptors, ApoER2 and VLDLR are existing to modulate signals, especially in the brain. Altered ligand binding properties, glycosylation, processing and downstream signalling of ApoER2 has been reported so far[37,42,43]. For a better understanding, the most common variants found in humans and mice are shown in Figure 4 and were visualized in Dlugosz et al, 2018[44].The full-length human receptor consists of 7LA repeats (1-7), the murine version is built by 5 LA repeats (1-3,7,8). The isoform that is found primarily in humans is missing exon 5 and only 4 LA repeats (1-3,7) are included. This isoform is also found in mice. An even shorter variant is built, including only LA repeats 1-3. Low numbers of an isoform including a furin cleavage site situated after the last LA repeat, can be found in humans and mice. Isoforms lacking the middle EGF-like domain are existing in humans as well. Through addition of O-linked sugars by posttranslational mechanisms, the access for proteolytic cleavage of the extracellular part of the receptor is modified, altering the signal transduction, stability and recycling of the ApoER2

receptor itself. Proteolytic processing, synaptic formation and function can be modulated through sugar attachment. Glycosylation and splicing have an impact on expression, processing, and turnover of the receptor: In human and murine organisms, the OLSD, located on exon16/15 in mice/humans, can be spliced out. Without presence of this domain, glycosylation is not possible and the extracellular cleavage by matrix metalloproteases is lost. Interestingly, hyperglycosylation, a process where N- and O-linked sugars are added to the receptor prevents the procession of the receptor as well. Through loss of the OLSD an increased (overall) number of ApoER2 is found, which causes enhanced long-term potentiation (LTP) and reduced fear response in mice[37]. Uniquely, in ApoER2 a proline rich region (PXXP) can be found, which is thought to be important for signal transduction. If this region, which is located on exon 19/18 in mice/humans, of ApoER2 is missing, associative learning ability and spatial memory formation are impaired. Moreover, it also has a role in neuronal protection and selective cell death during aging. Alternatively spliced receptor isoforms lacking the proline rich region are present in humans and mice.

The receptor can undergo sequential steps of proteolytic cleavage via α- and γ-secretases[45]. First, a soluble extracellular receptor fragment that has an antagonistic function via binding potential ligands of unprocessed ApoER2, is cleaved off (in vitro data). Reelin triggers this cleavage. Second, the intracellular domain (ICD) is cleaved off. This small part is able to migrate into the

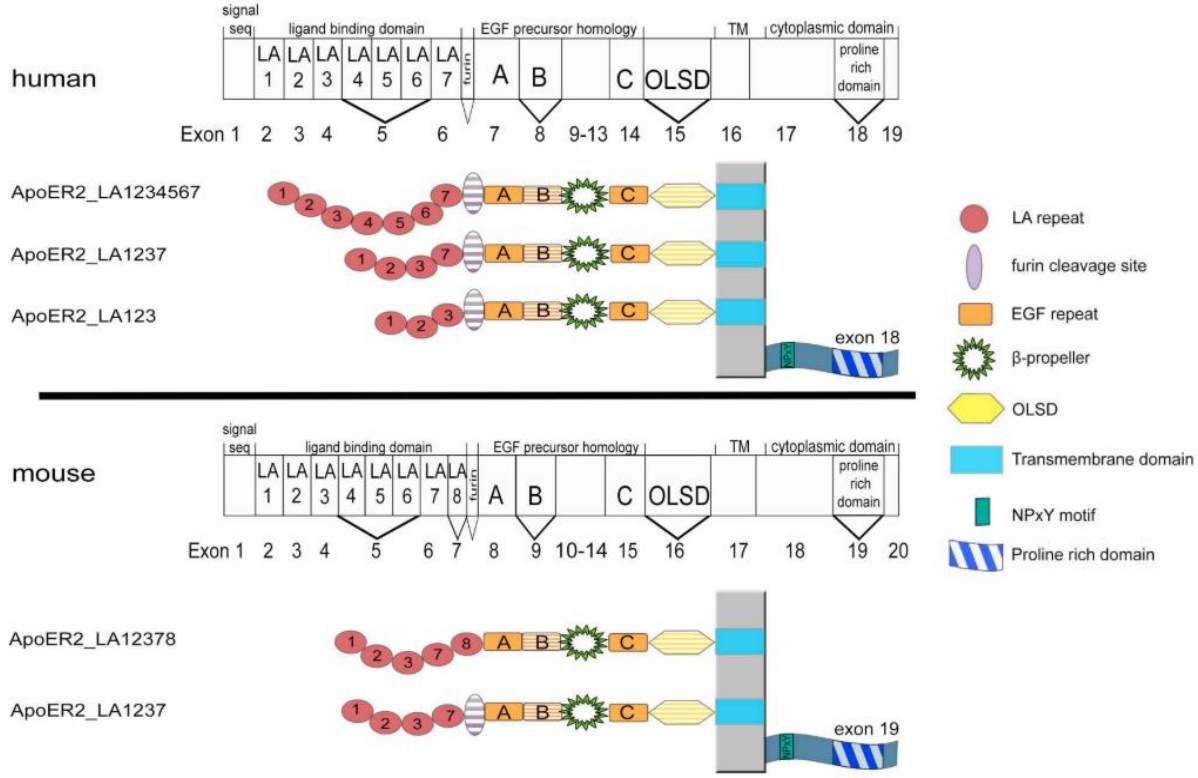

Figure 4 Splice variants of ApoER2[44]

nucleus and regulates the transcription of Reelin in a supressing manner but enhancing learning and memory gene profiles[46,47]. For proper brain function it is essential, that ApoER2 levels are tightly regulated, both, over- and underrepresentation can have malicious effects[48]. Therefore, it is also highly important that its degradation is working properly. Proteins that play a role in these processes are E3 ubiquitin ligase IDOL, proprotein convertase PCSK9 and Nexin 17[48–50]. The ligand binding domain of ApoER2 binds Reelin, ApoE, Clusterin (ApoJ), and some other ligands that are mentioned in the review by Dlugosz[32]. One special ligand, that binds at a unique position is Selenoprotein P (Sepp1), as it binds to the YWTD domain.

There are some well-known diseases that are associated with an impaired ApoER2 function. For example, a role in sporadic Alzheimer's disease already is known[51]. Sperm motility and

morphology are affected by ApoER2 deficiency, as the Selenoprotein transport is not functional[52]. One single nucleotid polymorphism has been identified to increase the risk of coronary artery disease and myocardial infarction. This happens through premature cell cycle arrest in smooth muscle cells by loss of the PP2A catalytic subunit that leads to loss of CDC20 interaction[53,54]. Additionally, endothelial cells reparation is slowed down by ApoER2 loss, and NO production doesn't work properly[55]. Interestingly, the switch from M1 to M2 macrophages also is not possible without ApoER2, because ApoE signalling doesn't work[56].

The VLDLR is highly conserved throughout species, consists of 873 amino acids that are translated from a 2619 bp transcript. There are alternative splicing variants of VLDLR existing as well and the most common one expressed in humans is lacking exon16. This isoform is therefore built without O-linked sugar attachment and has a relative molecular mass of 75-100 kDa[57]. In addition to the full-length version one without exon 3 and one without the OLSD in mice and humans was described. It is expressed in the nervous system, with high concentration in the cerebellum and the cerebral cortex. VLDLR can also be found in skeletal muscles, heart, adipose tissue, kidney, ovary, testis and lung. In the small intestine, VLDLR is expressed in crypt and villus cells[41]. It has a lower affinity to Reelin than ApoER2 as the unique PXXP region is not present in this receptor. During development it is mainly found in the marginal zone of the brain, in the non-raft fraction of the plasma membrane of neurons. Through loss of VLDLR the termination of neuronal migration is impaired, and the cerebellum is smaller and less foliated, additionally granule and Purkinje cell layer organization is affected. Its recycling is done via Clathrin coated pit endocytosis which works in a faster way than ApoER2 endocytic mechanisms[44].

Dab1

The nucleocytoplasmic-shuttling adaptor protein disabled 1 (Dab1) is crucial for Reelin pathway function[58]. Its loss also leads to the Reeler-like phenotype, which was described in yotari and scrambler mice[59]. The full-length protein consists of 555 amino acids and has a relative molecular mass of 75 kDA.

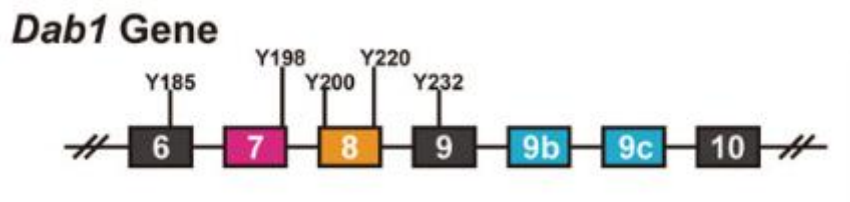

Figure 5 Dab1 gene consisting oft exons which are differently spliced. The tyrosines (Y) which can be phosphorylated in the Dab1 protein are included.[73]

It gets phosphorylated via binding of full length Reelin to its receptors and interacts with ApoER2 and VLDLR via their NPXY motif and a special phosphotyrosine binding domain (PTB) has to be present for Dab1 to localize in membrane regions. Phosphorylation of Dab1 is mediated by Src and Fyn kinases and there are 5 tyrosines, which are shown in Figure 5, that can be phosphorylated. Dab1 gets downregulated via Reelin signalling and to relay a downstream signal it has to be phosphorylated. This phosphorylation is triggered through homo-/heterodimerisation of ApoER2 and VLDLR which occurs through binding of the Reelin central fragment[11,16,60–62].

Regulation of Adhesion and cell-cell interactions, actin cytoskeleton rearrangements, cell migration, neuronal differentiation, dendritic outgrowth are mediated via Dab1 signalling. The activation of different Src Family tyrosine kinases can have various outcomes, depending on the phosphorylation pattern of Dab1. For proper cell migration and brain development the AKT and JNK signalling/ Wnt/β-catenin signalling pathway is needed. Activation of this cascade is enabled through PI3K activation which is triggered by phosphorylation of residues 185 and 198 or 200. Through Lis1, ependymal cell placement can be regulated and via interaction of Nckβ adaptor protein through SH2-SH3 domains Dab1 mediates actin cytoskeleton remodelling. For example, if tyrosines 220 and 232 are phosphorylated, Crk pathway is mainly activated. Crk-family proteins are known to be involved in the regulation of adhesion of cells, through C3G and Rap1.They are also able to stimulate phosphorylation of Tyr 220 in presence of Src. Glia independent neuronal

migration requires Dab1/Rap1 as well as N-cadherin and activated integrin β1. Altogether, many downstream processes of Dab1 involve Rho-GTPases. One of these proteins becoming phosphorylated involving Rho-GTPase is Neural Wiskott-Aldrich syndrome protein (N-WASP). The downregulation of Dab1 is mediated via its phosphorylation and by the presence of Cullin 5 that has an antagonistic function to Dab1[63–72]. A process where alternative splicing of Dab1 plays a crucial role is during development of the cortex. Migration of neurons and their multipolar-to-bipolar transition are mediated via Dab1 signalling. Differential splicing of Dab1 differs greatly in a (time and location dependent/spatiotemporal) manner and is tightly regulated. For example, during early development Exon7 and 8 are differently spliced out, in late-born neurons both exons are included. The switch from multipolar to bipolar migration is managed via exon 9bc silencing and 7,8 expression[73]. Fine tuning of neuronal migration seems to be dependent on differential splicing events of Dab1. However, the exact mechanisms, how this may be regulated still need to be discovered. Recently it could be proven that one of those underlying processes very likely is Dab1 dosage. Layer 1 thickness differences and some ectopic dendrites in the neocerebral cortex were found in mice carrying only one functional dab1 allele[74]. Dab1 is not exclusively found in neuronal tissue, but also in mammary gland tissue where it is necessary for branching of epithelial cells. In the small intestine it may contribute to crypt-villus stability and regulation of cartilage and bone during limb development is preserved. In adults Dab1 is also contributing to immune system function[42].

One function of Dab1, independent of the core Reelin pathway, is the interaction of the protein with VEGF/VEGFR. Signalling of this receptor is important for vascularisation and Dab1 is known to play a role in this process[75].

However, even though extensive research has been already done to find out as much as possible about Reelin and the proteins involved in its core pathway, there are still functions existing which are not fully understood and a number of processes that need to be elucidated.

Lipid rafts

The phospholipid bilayer of the plasma membrane of eucaryotic cells is not laterally homogenous. Because of this heterogeneity, specialized microdomains are present and defined as lipid rafts or liquid-ordered functional area (Lo). Lipid rafts have a distinct protein and lipid composition, and cholesterol and sphingolipid concentrations are increased in these special areas. Processes such as adhesion, migration, cell growth, signalling and trafficking are thought to be taking part in these areas. The size of lipid rafts is defined as 10-200nm dynamic structures. However, it is still debated whether proteins are concentrated in these self-organizing lipid-rich areas or rather excluded from there. Special protein structures are supporting the formation of rafts, and some have the potential to stabilize them. MLRs (membrane/lipid rafts) can form complexes with cytoskeletal structures. Through this support, lipid rafts can reach a size larger than 300nm. The protein Caveolin is found in the MLR and takes part in the processes of trafficking. The integration of cholesterol and its binding is also facilitated by it. Additionally, Caveolin is also involved in organising, scaffolding, aggregating, and activating a huge amount of signalling factors. For caveolin to build caveolae, the protein cavin has to be present. If that is the case, the caveolin isoforms can build the invaginations in the MLR. It is known, that full length ApoER2 is found in the caveolin-rich light membrane, also known as lipid raft domain, whereas VLDLR localizes outside of lipid rafts in the plasma membrane. Until present day there it is still a debate going on, if lipid rafts, and how they are defined now, are actually existing or are on a high extent artefacts produced by methods of cell membrane preparation[76–80].

EGFR

Epidermal Growth Factor Receptor (EGFR) pathway is known to be involved in the processes of cell proliferation and division, and development of cancer. Its most important components are the Ligand EGF and its receptor EGFR (also HER1/ERBB-1) are the widely known. The pathway very likely evolved in Metazoans and is found in the majority of them, excluding placozoans and

cnidarians[81,82]. EGFR is a receptor tyrosine kinase, which is located in the plasma membrane and a member of the ERBB-receptor family, which originally got its name from an erythroblastosis virus, that had been discovered before and acquired its sequence structures from the avian EGFR homologue. Other members of this family are the Neu/ErbB-2/HER2, HER3 and HER4. The gene for EGFR has a length of 189 kbp, is composed of 31 exons and gives rise to a 130 kDa polypeptide chain that goes through N-glycosylation resulting in a 170kDa mature protein[83]. It is widely expressed throughout the human body as it can be found in tissues such as: eye, intestine, brain, endocrine tissues, proximal digestive tract, gastrointestinal tract, liver, lung, gallbladder, pancreas, kidney, urinary bladder, muscle, mammary glands, skin, bone marrow& lymphoid tissue, tonsils and an especially high expression is seen in the nasopharynx, bronchus and placenta[84]. In the brain, at embryonic day E14.5, the majority of EGFR expressing cells found on the apical surface of the VZ are embryonic neural progenitor cells. Cells that stop to express EGFR, differentiate in neurons, oligodendrocytes and astrocytes. Additionally, EGFR signalling could be detected in regenerative mouse brain and the EGFR positive cells discovered are transit-amplifying precursors and a small number of class B1 stem cells[85,86]. The receptor consists of an extracellular ligand-binding domain, at transmembrane domain, a short juxtamembrane section, a tyrosine kinase domain and a tyrosine containing c-terminal tail. The formation of three intramolecular disulfide bonds is crucial for EGFR to function and to bind EGF. The ligand itself also has to form three intramolecular disulfide bonds to build its active center. EGFR gets either homo or heterodimerized as a result of ligand binding and the intracellular kinase domain of it is activated, enabling it to relay signals downstream. The binding partners of EGFR in heterodimers are other ERBB-family members, and each of them has a slightly different function. 7 Ligands which bind to EGFR are known so far. Their binding is different as their affinity and strength varies and they are capable of altering intracellular trafficking and can induce specific responses in cells. Upon ligand dependent activation, a signal transduction via Ras/MAPK, PI3K/AKT, Jak/STAT and PLC (phospholipase c)/PKC (protein kinase C) is triggered as shown in Figure 6[87,88]. There are eight different splice variants of EGFR, playing important distinctive roles. They are described in the Review by Abou-Fayçal[89].The regulation of EGFR is maintained via endocytic pathways such as ubiquitination via E3ligase. At a certain threshold of EGF concentration internalisation via NCE, (nonclathrin endocytosis), CME (clathrin mediated endocytosis) and FEME (fast endophilin mediated endocytosis) also regulate total levels of it[90].

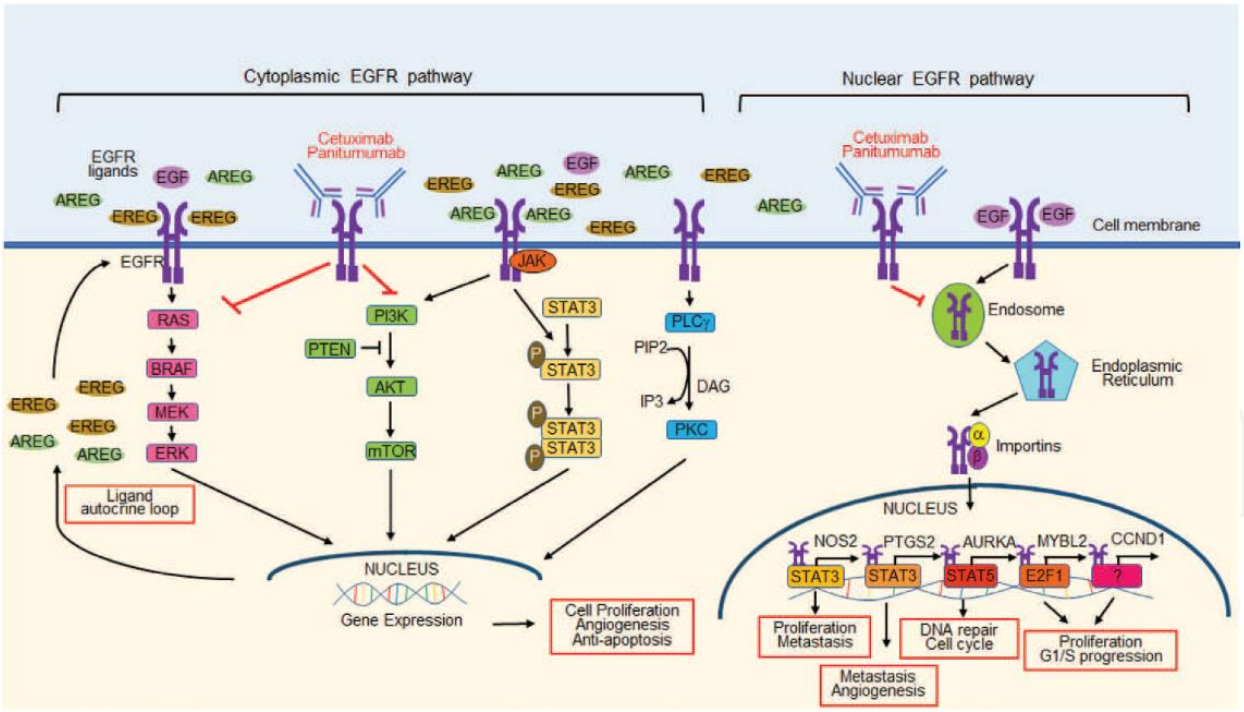

Figure 6 EGFR signal pathway [91]

Many genetic alterations of EGFR are already known, which result in abnormal trafficking and altered signalling leading to promoted tumor growth. The most common types of mutations are gain of function mutations (deletions in exon 19 and point mutation L858R) and kinase activating mutations (associated with the ATP binding pocket). Through these mutations increased signalling and ligand independent activation are caused. The third type of mutation that is quite common is constitutive activation (exons 18-21) of EGFR, which means that signalling is continued in the absence of ligands. Further, amplification of EGFR signalling can be cause by gene duplication. Increased signalling can also be caused by decreased receptor endocytosis. Through an alteration of the E3 ligase binding site, this interaction can be disrupted, and ubiquitination and further degradation cannot take place[92]. As EGFR is involved in cell growth and migration, differentiation, and survival, it is not surprising that mutations of it can lead to increased cell motility, building of invadopodia and increased survival and proliferation. Not all mutations that promote survival are depending on the kinase function of EGFR. Also, increased heterodimerisation with ERBB family members can lead to reduced internalization and increased stability. Additionally, EGFR overexpression can be stress induced and lead to increased survival of the cells that experience it. This stress can be induced by UV light, hypoxia and oxidative and ionizing radiation. In this case EGFR is able to translocate into the nucleus to alter gene expression. Genes for DNA repair and increased cell survival are upregulated for example[93,94]. Many tyrosine kinase inhibitors (TKI) are already known and also used as cancer treatment with varying success. As cancers are driven to acquire escape mutations, resistance against the TKIs arises frequently. In these recent reviews by Levantini and Li, problems and future ideas to overcome this are mentioned[94,95].

Material and Methods

Cell lines and Plasmids

The cell lines used during this project were Human Embryoinc Kidney (HEK293) and NIH3T3 fibroblasts. They were grown at 37°C with 5%CO2. The medum used for their growth was Dulbecco's Modified Eagle Medium (DMEM, GIBCO)+10% fetal calf serum (FCS).

The used constructs are mentioned in the following table (Table 1).

Table 1 Constructs used during the project.

Plasmid	Host	Backbone	Resistance	Author
Dab1				Howel
pClneo	Top10F'	pClneo	Ampicillin	
pClneo_ApoER2	Top10F'	pClneo	Ampicillin	DF
pClneo_EGFR	DH5alpha	pClneo	Ampicilin	PD, MT
pClneo VLDLR	Top10F'	pClneo	Ampicillin	DF
pcDNAflux3_HA_ApoER2_myc_wt/tYF				Bill Rebeck
pClneo_EGFR	DH5alpha	pClneo	Ampicilin	PD, MT
ApoER2Δ16	DH5alpha	pClneo_mmApoER2 #70	Ampicilin	AV,PD
ApoER2_mGFP	DH5alpha	pHomMem1	Ampicillin	PD
VLDLR_mGFP	Top10	pHom1 (Clontech)	Ampicilin	PD
EGFR_mCherry	DH5alpha	pmCherry_N1 #300	Kanamycin	PD
mGFP	DH5alpha	pHom1 (Clontech)Ampicilin		PD
mCherry	Top10		Kanamycin	RK
ApoER2Δ16_mGFP	DH5alpha	pmGFP_mmApoER2 #188	Ampicilin	PD

Discontinuous gradient

Cells were grown confluent and the whole procedure was carried out at 4°C, all machines used were tempered at 4°C and the cells and later on their isolates were either processed in the cold room or on ice. 10cm or 6cm dishes were used in the following protocols. The Isolation was carried out in three different protocols, with varying gradient forming agents as well as different lysis buffers. In all protocols the SW40Ti Rotor and propylene centrifuge tubes (Beckman coulter (Lot Z71113SCA, REF 331374)) were used.

In the protocol, where sucrose and sodium carbonate were used, the cells were washed with TBS and directly scraped in MES-buffer (15mM NaCl, 25mM MesHydrate, pH 6,47) with Na_2CO_3 (500mM) and PI. This step was followed by a 2s sonication with 100% sonication time and 70% power repeated three times. Isolates were rotated for some time and centrifuged for 15' at max speed. Input control was taken and the lysate was mixed with 90% (w/v) sucrose in MES buffer to reach a final concentration of 35% (w/V). A 4ml 35% and a 5% sucrose phase was added on top. Centrifugation was carried out at 160,000xg for 18h and 1ml fractions were taken from the top of the tube to be analysed via SDS-Page and Western blot.

The second protocol was carried out with a sucrose gradient and the NP-40 lysis buffer. Cells were washed with 1xTBS, scraped in fresh TBS and pelleted at 1400xg. The supernatant was removed and the pellet resuspended in 2ml of Lysis buffer (TBS, 2%Birj 78P (Fluka) and PI (Roche). Afterwards the cells were passaged 10x through a 23. gauge needle. The isolate was centrifuged for 15' at 21.000xg to remove cell debris. An input control was taken and the supernatant was transferred into an ultracentrifuge tube. 1,67ml of lysate was mixed with 1,67ml of 90% sucrose in MES-buffer to get a concentration of 45% sucrose. A layer of 35% (6,98ml) and a layer of 5% (1,67ml) was carefully added on top. The centrifugation was set for 20h at a speed of 160 000xg(36000rpm). 1ml fractions were taken and analysed in the same way as in the protocol described above.

In the third protocol, the used gradient was Optiprep in combination with buffer. The plates were washed with ice cold PBS and scraped. They were pelleted via centrifugation at 1,400g for 5'. 220µl lysis buffer B (50mM Tris/HCl, pH 7,4, 150mM NaCl, 5mM EDTA, 0,1% Triton X-100) was added and cells were passaged 3x through a 27-gauge needle. 60µl of lysate were spun down for 15' at max speed and taken as input control. Lysate was mixed with Optiprep gradient solution in a 4,5 ml ultracentrifugation tube until it was homogenous, and a 35%(w/v) concentration was reached (360µl). A layer of 30% Optiprep (3,2ml) and another layer containing only buffer B (0,5ml) were carefully added to create a discontinuous gradient. The gradient was centrifuged at 150, 000xg with the SW40Ti rotor for 4h. 500µl fractions were taken from the top of the tube and analysed via SDS-Page and Western blot.

Transfection of Cell Lines

Transient transfection of HEK293 cells was done with PEI (polyethyleneimine). DMEM without FCS was mixed with the desired receptors and PEI was added last. The used volumes, corresponding to the size of culture dishes are listed in Table 2. Reagents were mixed by pipetting up and down and left at RT for 15min. Afterwards they were added dropwise to the cell culture.

Table 2 Volumes for PEI transfection

HEK293							
Culture vessel size	96 well	24 well	12 well	35 mm	60 mm	100 mm	150 mm
Surface area per well (cm^2)				28		93	186
Vol of plating medium (mL)	0,1	0,5	1	3	3	10	20
Volume of dilution medium (µL)	5	25	50	150	200	500	1000
DNA (ng) from:	100	500	1000	2000	4000	9000	18000
to:				3000			
Transfection reagent (µL)	0,3	1,5	3	9	18	30	60

For co-transfection the mentioned amount of DNA was taken as total amount.

Transient transfection of NIH3T3 cells was achieved with Ultracruz reagent (Santa Cruz Biotechnology; SC-395739). DNA and transfection reagent were diluted separately in transfection medium and let sit for 5min at RT. The DNA (6,67 ng/µl Transfection Mix) mixture was added dropwise to the Reagent mixture, mixed via vortexing and incubated for 20min at RT before transfection. The used volumes for different culture sizes are shown in Table 3.

Table 3 Volumes for Ultracruz transfection

NIH3T3						
Culture vessel	96 well	24 well	35 mm	60 mm	100 mm	150 mm
Surface area per well (cm^2)			28		93	186
Vol of plating medium (mL)	0,1	0,5	3	3	10	20
Volume of transfection mix total	5	25	150	200	500	1000
DNA (ng)	33,3333333	166,666666	1000	1333,3333	3333,33333	6666,66666
Transfection reagent (uL)	0,33333333	1,6666666	10	13,333333	33,3333333	66,6666666

Isolation, Electroporation and nucleofection of Neurons

Dishes were coated with Poly-L-Ornithine (150µg/ml), incubated at 30°C for 30', washed 2x with H2O and dried. Culture dishes were filled with 0,5 ml of complete Neurobasal medium and preincubated for 1h prior addition of cells at 37°C and 5%CO2 in an incubator to adjust temperature to 37°C and pH to 7.4. Mouse was sacrificed via cervical dislocation and embryos were extracted as fast as possible. Decapitation was carried out and brains of embryonic day 15,5-18,5 were dissected, and all meninges removed. Brain tissue was collected in 5ml of Hibernate®-E supplemented with 2% B-27® Serum-Free Supplement and 0.5 mM GlutaMAX™-I at 4°C. After centrifugation at 300xg for 4min at RT, the supernatant was removed and 1ml of HBSS was added per brain. After 30s the washing was repeated. Afterwards 1mL Complete Neurobasal medium was added, and the cells were resuspended gently for 5x with a 10mL pipette, for 5x with a 5mL pipette and for 15x with a fire polished Pasteur pipette. After 30s to let the remaining parts of meninges settle, the supernatant, which is the cell suspension was transferred and ml were adjusted to brain numbers (5ml/5brains).

100µl of Amaxa neuronal cell suspension (18µl supplement/ 82µl Nucleofection solution)/nucleofection were prewarmed to RT. 3µg of plasmid DNA in ddH20 were pipetted into a sterile 1.5ml Eppendorf tube. As a control GFP only control should be included. Neuronal cell suspension (scaled up to total number of nucleofections/500µl/condition) was taken (between $2x10^5$ and $6x10^6$ cells/condition) and centrifuged at 80xg for 5min at RT. The supernatant was removed carefully and as complete as possible. Resuspension of the cells was done with a 1000µl pipette and in 100µl(/condition) of Amaxa cell line neurons solution. Subsequent steps were carried out individually. Neuronal cell suspension (100µl) was put into the prepared Eppendorf tube containing the plasmid DNA. By genltle flicking for 20s the contents were mixed. Carefully the cells were transferred into the cuvette and placed into the nucleofector device. The program used was O-005 for mouse neurons. Directly after nucleofection 500µl of prewarmed Complete Neurobasal medium were added into the cuvette and cells were taken via a fire polished Pasteur pipette and seeded into the previously equilibrated 6cm dishes.

SDS-Page and Western blots

6% to 15% Polyacrylamid-Gels were done to separate proteins. Gels were either run constant current or constant voltage. The maximum values set were either 115V or 30mA/Gel.

Wet western blots were carried out and proteins were transferred onto AmershamTM Protran nitrocellulose membrane (GE Healthcare, Chicago, IL, USA). Transfer buffer was mixed with 10% MeOH when the size of the protein of interest exceeded 200 kDa. Western blots with 1,5/1 mm thick gels were run for 1,5/1 h at constant current (350mA) at 4°C. Blocking of the Membrane was

done with 5% Milk or BSA in PBS/TBS-Tween for at least 20min. TBS-Tween was added to keep phosphorylations detectable. Fresh primary ABs were added and the and incubation was done overnight at 4°C. Membranes were washed 3x with PBS/TBS-Tween and horseradish peroxidase- conjugated secondary Antibodies were directly added (Jackson ImmunoResearch Laboratories, West Grove, PA, USA). After an incubation time of 1h membranes were washed 3x and incubated with an ECL Illumination solution. For Proteins, which were difficult to detect, either nova or supernova ECL solution from Cyanagen (Bologna, Italy) was used. Development was done via Chemidoc from BioRad or in the darkroom. Some membranes were stripped of the Antibodies with Stripping buffer (25mM glycine-HCl pH 2.0, 2% SDS) for 30 min. Afterwards they were washed 2x with PBS/TBS-Tween and checked in the darkroom. Then another round of blocking and staining, as mentioned above, was carried out to detect an additional protein.

In some cases, further analysis was done with ImageLab software from BioRad. Data was then exported to Excel for further analysis and visualized and statistically tested with GraphPad Prism.

RCM and MCM production and treatment

Production of Reelin conditioned medium was done with cultivated Reelin-expressing HEK293 cells. Those contained the pCrl construct (a kind gift of Tom Curran, Perelman School of Medicine at the University of Pennsylvania, Philadelphia, PA, USA). Cells were cultivated in DMEM with GlutaMax (Thermo Scientific), 10% fetal calf serum (FCS, Sigma) and 0,5mg/mL G418 (Roth) at 37°C and 5%CO2. After 70% confluency were reached, the medium was replaced by serum-free medium (OptiMEM, Gibco). After 48h the conditioned medium was sterile filtered and used for experiments. To get mock-conditioned medium (MCM) for control experiments, the same procedure was carried out, with HEK293 cells, lacking the construct for Reelin expression. For treatment cells were previously washed with PBS and incubated with imaging medium (IM) for 30 min. IM was removed and treatment with RCM/MCM was done for 15min.

About Reelin conditioned medium:

One crucial part during the varying projects for the thesis was the preparation of Reelin- and mock conditioned medium. As already mentioned above RCM and MCM were collected from HEK293 cells expressing Reelin, so there probably are a bulk of cytokines and other factors included in the medium, which could influence the behavior of the treated cells. Of course, Reelin treatment with a pure full-length protein would be the best option to avoid these difficulties. Unfortunately, full length Reelin is not available at the market, as it is not easy to stabilize it. Only R3-6 central fragment can be ordered. Of course, a stable cell line that expresses Reelin attached to a tag to purify it would be the best option, but due to time limits it was not possible to carry this out. So, the best option for treatment was to use freshly produced Reelin from a HEK293 stable cell line, which was available in the lab. As they are a great vehicle for producing high amounts of functional protein this seemed to be a good choice. But it is also known that HEK293 have a very heterogenous expression of genes which can change considerably between passage numbers. HEK293 wt are capable to endogenously express low amounts of Reelin, which was something that had to be avoided strictly, as MCM was designed a negative control. Because of this, the quality of RCM and MCM differed between experiments, and it had to be tested thoroughly every time. As the direct cause for the activation of the Reelin gene expression in HEK293 could not be found and full length Reelin was not available at the market, another solution had to be found for this problem. Therefore, it was decided to make a stock of MCM with a good quality, where Reelin was not present, and freeze it for further usage.

Wound healing assay

HEK293 were seeded with a density of $4x10^5$ cells/ml in a 96 well plate. Confluent cells were transfected with a plasmid carrying the GOI attached to a fluorophore via PEI 24h after seeding. After 24h medium was changed to DMEM+1%FCS to initiate starvation. Again, an incubation of 24h was carried out. Wells were scratched with a 200µl tip and medium was changed to clear DMEM. Ligands were added and time course on the CellDiscoverer7 microscope was started.

Analysis was done via Zen blue, Fiji/ImageJ MRI_wound_healing tool, excel and Graph pad prism.

Fluorescent microscopy

Coverslips were added to plates and coated with Collagen for up to 1h, washed 2x and 2x10^5cells/ml were added. On the same day medium of a full 10cm dish of a Reelin producing HEK293 cell line was changed to Optimem to induce RCM (Reelin conditioned medium) production. MCM (mock conditioned medium, produced by HEK293 wt) was previously produced in a high quantity and thawed when needed. On the next day cells were transiently transfected with the respective proteins/receptors attached to a fluorophore, including all necessary controls. After 24h fresh RCM was filtered, MCM thawed, and cells were treated. After 3' of incubation at 37°C medium was aspirated, and cells were washed 2 with ice cold PBS. 4% FA (formaldehyde) was added and incubation at RT for 15min at darkness was carried out. Cells were washed 3x with cold PBS and blocking was done in 1% BSA in PBS for another 30' at RT. Coverslips were put upside down on droplets of primary AB solution pipetted on parafilm. Everything was put in a wet chamber and incubated overnight in the fridge. In the morning coverslips were transferred back to the plate and washed 3x with cold PBS. Secondary ABs in PBS were added, and cells were incubated for 1h at RT in darkness. Another washing step and DAPI staining (5µl/ml) for 5min at RT in darkness was done.

For the Phalloidin staining 3.7% formaldehyde (without MeOH) in PBS was used for fixation at RT for 10min. After two cold PBS washing steps permeabilization was done with h0.1% Triton X-100 in PBS for 3-5min. Another washing step (2x PBS) was carried out and preincubation with 1%BSA was done for 30min. The staining was done with Phalloidin red (1:40,4,95µM, A12380 Thermo Fisher) in 1%BSA in PBS for 20min at RT with coverslips put on 30µL drops placed on parafilm.

After a final washing step (3x PBS), coverslips were mounted with Ibidi mounting medium and fixed with nail polish. Glass slides were further analysed, and images were taken with LSM700 and Zen blue/black software.

RT-PCR

gDNA digestion reaction mix was prepared at 4°C according to manufacturer's protocol and 2µg of sample were added.(Invitrogen; MAN0015862, 05-31-23) Digestion was carried out at 37°C for 2 minutes. After a short centrifugation RT was added to the reaction mixes at 4°C. The primer annealing step was done at 25°C for 10 minutes and followed by the RT reaction at 50°C for another 10 minutes. The RT was inactivated for 5 minutes at 85°C. For the following PCR the Platinum™ SuperFi™ II Polymerase provided by Invitrogen was used. (MAN0018859, 05-31-23) The master mix was prepared for 20µl reactions and 5ng of DNA were added.

EdU Click-iT Assay

Cells were seeded with a density of 3.5x10^5 cells/ml. After reaching 50-70% confluency, they were transfected as described in the section transfection. After 24h a concentration of 10µM/well of EdU (5-ethynyl-2'-deoxyuridinde, Invitrogen, C10337) was added to the 12 well plate and the cells were incubated for 2h at 37°C/CO2. Afterwards they were fixed with 3,7% FA in PBS for 15' at RT. Two washing steps with 3% BSA were carried out and cells were permeabilized with 0,5% Triton X-100 in PBS for 20'. 10min before usage, 1X Click-iT reaction buffer and cocktail were prepared according to manufacturer's kit. Another washing step (3x with 3%BSA in PBS) was done and 500µl of reaction cocktail was added and rocked for 30' at RT in darkness. Cells were again washed with 3%BSA in PBS and additionally with PBS only. 1:2000 Höchst and 1:1000 DAPI in PBS were added and cells were incubated for another 30' at RT in darkness. After another washing with PBS for 2x 5µl of ibidi mounting medium and a coverslip was added. The sealing of

the coverslip was done with nail polish. With the Laser Scanning Confocal microscope (LSM 700, Zeiss, Jena, Germany) pictures were taken and analyzed via Fiji/ImageJ. Colour channels were split, the threshold was adjusted, and pictures were processed to binary. Watershed option was applied to separate overlapping nuclei too close to each other. All particles bigger than 50µm^2 were counted.

WST-proliferation/metabolic activity assay

HEK293 wt and Dab1 k.o. cells were seeded with a density of 3x10^5cells/ml on a 96 well plate coated with 50µg/mL collagen I (A10483-01, Gibco). After 24h the medium was changed to clear DMEM, and cells were transfected with Dab1_555 or pClneo with PEI transfection reagent. After another 24h cells were treated with EGF (10ng/ml) and 10µl of Cell proliferation agent WST-1 was added to each well according to manufacturer's protocol (100nM stock, Roche, 11644807001, Version August 2018). The plate was shaken thoroughly, and absorbance was measured via the VictorTM Nivo Plate reader after 0,5; 1; 2 and 3h. 600/10nm absorbance and blank values were subtracted from 480/30nm absorbance for quantification.

EGF Treatment

HEK293/NIH3T3 cells that were treated with inhibitors were incubated with them 2h before EGF treatment. 1µM of either Neratinib (MCE, Cat. No.: HY-32721) or Gefitinib/Iressa (MCE, Cat. No.: HY-50895) were added to 2ml of growth medium. Then cells were put in IM consisting of 4mM Glutamine in Hank's Balanced Salt solution (HBSS) for 30 min at 37 ◦C + 5% CO2. Treatment was done with 10 ng/mL of human EGF (PHG0315, Thermo Scientific, Waltham, MA, USA) or 20 ng/mL of murine EGF (130-094-036, Miltenyi Biotec, Bergisch Gladbach, Germany) and cells were incubated for 3, 10, or 20 min at 37 ◦C + 5% CO2. For a negative control one dish was left untreated. In the conditions including inhibitor treatment, the concentration was kept at 1µm during the whole time.

Antibodies

Table 4 Antibodies

epitope	reference name in thesis	target size	company	catalog number	lot number	application	blocking solution	secondary AB
ApoER2		100-160kDa						
	A20		in house			WB 1:5000 fresh	5%Milk, PBS-Tween	rabbit
	a186		in house			IP 10µl undiluted		
VLDLR		~100 kDa	R&D Systems	AF2258		WB 1:1000	5%BSA, PBS-Tween	goat
Dab1		80kDa						
	D4		Andre Goffinet			WB 1:1000, 1:8000	5%BSA, PBS-Tween	mouse
	a54		in house			IP 10µl undiluted		
Reelin	G10	380kDa	Andre Goffinet			WB 1:10 000	5%BSA, PBS-Tween	mouse
Caveolin1	Cav1	21kDa	BD	610406		WB 1:1000	5%BSA, PBS-Tween	mouse
	Cav1		CST	3238	3	WB 1:2500	5%BSA, PBS-Tween	rabbit
Caveolin2	Cav2	23kDa	BD	610684		WB 1:500	5%BSA, PBS-Tween	mouse
pEGFR	pEGFR	170kDa	Santa Cruz	SC-12351		WB 1:1000	5%BSA in TBS-Tween	goat
Phosphotyrosines	pY99		Santa Cruz	SC-7020	I1009	WB 1:500	5%BSA, TBS-Tween	mouse
N-Wasp		66kDa	St. Johns	STJ96261	62613	WB 1:1000	5%BSA, PBS-Tween	rabbit
EGFR		170kDa	Santa Cruz	SC-373746	K1617	WB 1:2000	5%BSA, PBS-Tween	mouse
GAPDH		37kDa	Sigma	G8795		WB 1:10 000	5%BSA, PBS-Tween	mouse

Results

Caveolin rich fraction isolation of NIH3T3, HEK293 and Neurons via sucrose gradient.

The goal of this project was to reproduce previously published results determining the location of the ApoER2 receptor and its variants in different plasma membrane regions, and to evaluate changes of the localization of the receptor upon lipid raft disruption treatment. Higher amounts of the hyperglycosylated isoform of the ApoER2 receptor were mainly found in specific regions of the plasma membrane, also known as lipid rafts. This hypothesis was built on data previously acquired by raft isolation based on discontinuous gradient ultracentrifugation. Disturbance of lipid rafts was done by addition of Methyl-ß-cyclodextrin. Discontinuous gradient ultracentrifugation was used for separation of different subdomains of the membrane. Cells were lysed with either detergent or sodium carbonate. The same method to enrich for the caveolin rich fraction was already used before in our laboratory with the cell line NIH3T3. These experiments revealed that the isoforms of ApoER2 (hyper/hypo glycosylated) were not evenly distributed between the two membrane subdomains. We tried to repeat these experiments with HEK293 cells[98]. Since we had experienced problems with reproducibility, we also compared another method to isolate rafts in parallel.

As shown in Figure 7A there was a problem to properly isolate the caveolin rich fraction in all cell lines that were used as well as in primary neurons. In the first panel ApoER2 distribution in the membrane is shown. The receptor is located in fractions F5-F8 in neurons, but nothing is present in the caveolin-rich light membrane (CLM) fraction which is the fraction taken at the interface of 5% and 35% sucrose/optiprep gradient (F2). Caveolin1 is not detected in F2 where the majority should be present but found in F5-8. As we wanted to check the cause, why we could not detect Caveolin 1 in the CLM, we included a different antibody, binding to Caveolin 2., which is another cavin protein known to form heterodimers with Caveolin 1 to build deep invaginations. Interestingly we could detect high amounts of Caveolin 2, in F2 and F5 - F7.

As the use of new buffers and changes of reagents did not improve the results sufficiently, a different protocol, used for caveolin rich fraction isolation, was carried out[99]. First, a comparison of both protocols, sucrose versus Opti prep discontinuous gradient centrifugation, was carried out and is shown in Figure 7B. In this case, NIH3T3 cells were used and transfected with ApoERΔ16 and Dab1. This ApoER2 receptor splice variant used in this experiment is lacking the OLSD, which is mentioned in the introduction and was studied by Wasser et al, 2014[37]. As some of the functions and the sorting of this variant is not yet fully resolved, we decided to include it in our studies. No treatment of the cells was carried out, as the focus was set on separation of different membrane fractions. In both protocols the majority of the receptor is found in the non-caveolar membrane (NCM ,F4-8)-fraction, only small amounts of ApoER2Δ16 are found in F2 of the Opti prep protocol. The Opti prep protocol worked nicely, Caveolin1 is found in F1 and F2 and not distributed in all fractions as it was the case before, when using sucrose gradient ultracentrifugation also shown in the upper blot of Figure 7B. Still, very low amounts of Caveolin1 are found in F3-F5 of the Opti prep centrifugation, most likely due to a spill over by transferring the fractions out of the ultracentrifuge tube into separate tubes after centrifugation. Unfortunately, problems with separation of fractions occurred again even using the protocol with Opti prep/Buffer B. Luckily the cause for this problem was found as shown in Figure 7C. Using fresh buffer B directly before usage, the separation of CLM and NCM works nicely, compared to one week old buffer B. Again, small amounts of Caveolin are found in all fractions, due to reasons already mentioned. Because of these results it was decided to change to the Opti prep protocol during my work. However, as I already had results with the discontinuous sucrose gradient using sucrose, at some points both methods were used in parallel.

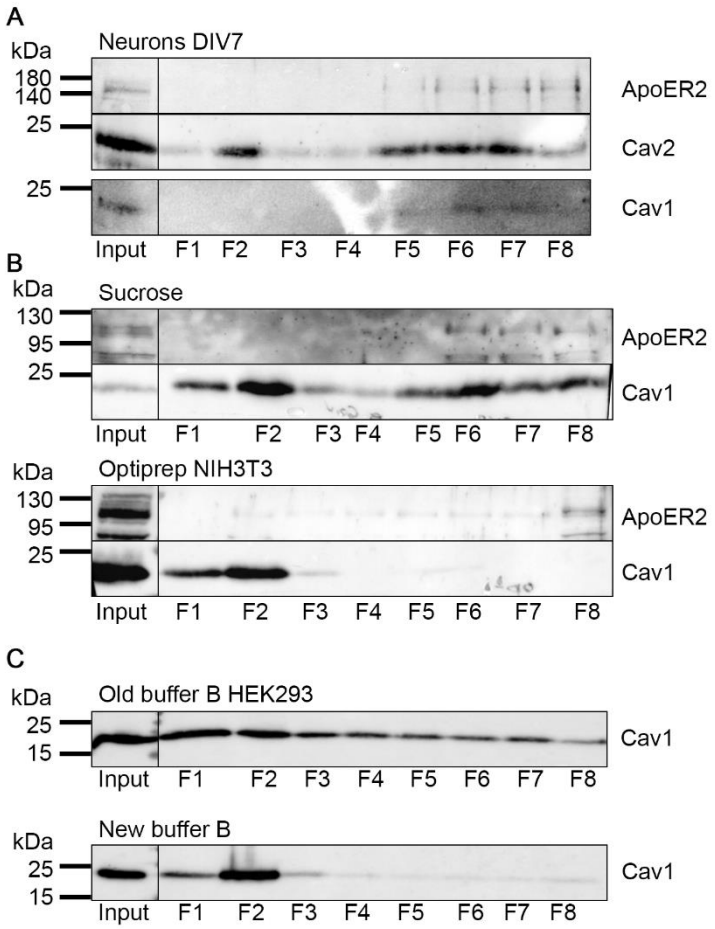

Figure 7.A.Discontinuous sucrose gradient ultracentrifugation of DIV7 Neurons. B. Comparison of Birj lysis and Sucrose gradient with Buffer B lysis and Optiprep. C. Comparison of one week and one-hour old buffer B.

The results of the CDX-treatment to disrupt Caveolin rich membrane fractions are shown in Figure 8A. HEK293 cells were transiently transfected with full length ApoER2 and treated with Methyl-β-Cyclodextrin at a concentration of 4,4mM for 1h. The cells were kept at 37°C and 5%CO2. Lysis was done with Birj 78P(Fluka) and the membrane fractionation was carried out via discontinuous sucrose gradient ultracentrifugation at 160.000xg for 20h. Subsequent analysis was done via SDS-PAGE and Western blot. Both forms of ApoER2 (hyper- and hypogoycosylated 120-140kDa) as well Caveolin (20kDa) are visible in the Input controls of both setups (Control and CDX-treatment). The hyperglycosylated form of ApoER2 is majorly found in fraction 2, where the amount of Caveolin 1 is high as well. The hypoglycosylated form is detected in fractions 6 to 9. In the CDX treatment, the hyperglycosylated form of ApoER2 shifted to F6-F8, whereas localization of Caveolin1 can still be observed in F1 and F2. The first step, a reproduction of already published results worked nicely[98].

The next question we wanted to answer, was whether Dab1 is localized in the CLM-fraction or in the NCM-fraction and if there is a shift of receptor and Dab1 to one of the two different membrane compartments when treatment with Reelin is done. As already mentioned, problems with the Birj lysis buffer and sucrose ultracentrifugation occurred, so the method was changed to buffer B lysis and opt prep ultracentrifugation (see above). Caveolin rich fraction isolation of HEK293 cells transiently transfected with full length ApoER2 and Dab1 and analysis via SDS-Page and Western blot was carried out as described. Different conditions were used, as cells were treated with either Mock- or Reelin conditioned medium. For Western blot antibodies against Dab1 and Cav1 were used. The corresponding results are shown in Figure 8B. Dab1 is found in fractions 7 and 8 in both conditions and the majority of Caveolin1 can be seen in fractions 2 and 3 in both conditions. Therefore, we suggest, that Dab1 is mainly bound to the hypoglycosylated form of ApoER2, as it could only be detected in the NCM fractions. Reelin treatment did not change this interaction.

Next, we evaluated whether phosphorylation of both forms of the receptor changes upon Reelin addition. The results are shown in Figure 8C. Cells were treated in the same way as already mentioned for the previous experiment. As a control for the efficiency of transfection of both, the receptor and the adaptor protein, were included for detection after ultracentrifugation. All panels, that are presented together, were acquired from the same sample. In this case, ApoER2 was visualized first, and phosphorylation levels were checked after membrane stripping using a phosphotyrosine specific antibody. Dab1 presence was checked in another blot. As the majority of Caveolin1 is found in fractions one and two, the experiment was rated successful. When

checking the Input levels of ApoER2, more of the hyperglycosylated variant is present in the lysate. Interestingly, in this experiment, ApoER2 as well as Dab1 can be found in all fractions, which would suggest that both proteins are found in CLM and NCM. When taking a closer look at ApoER2 levels in different fractions, it can be seen, that the hyperglycosylated form of ApoER2 with a size of 140kDa is more abundant in the CLM (F2), whereas the hypoglycosylated form with a size of 120kDa is not present. In the fractions representing the NCM, both variants are present. One interesting thing is that only the hyperglycosylated ApoER2 gets phosphorylated on its tyrosines. There is another prominent band at the size of 180kDa (arrow) present as well, which runs above the hyperglycosylated form of ApoEr2 and was considered another protein which

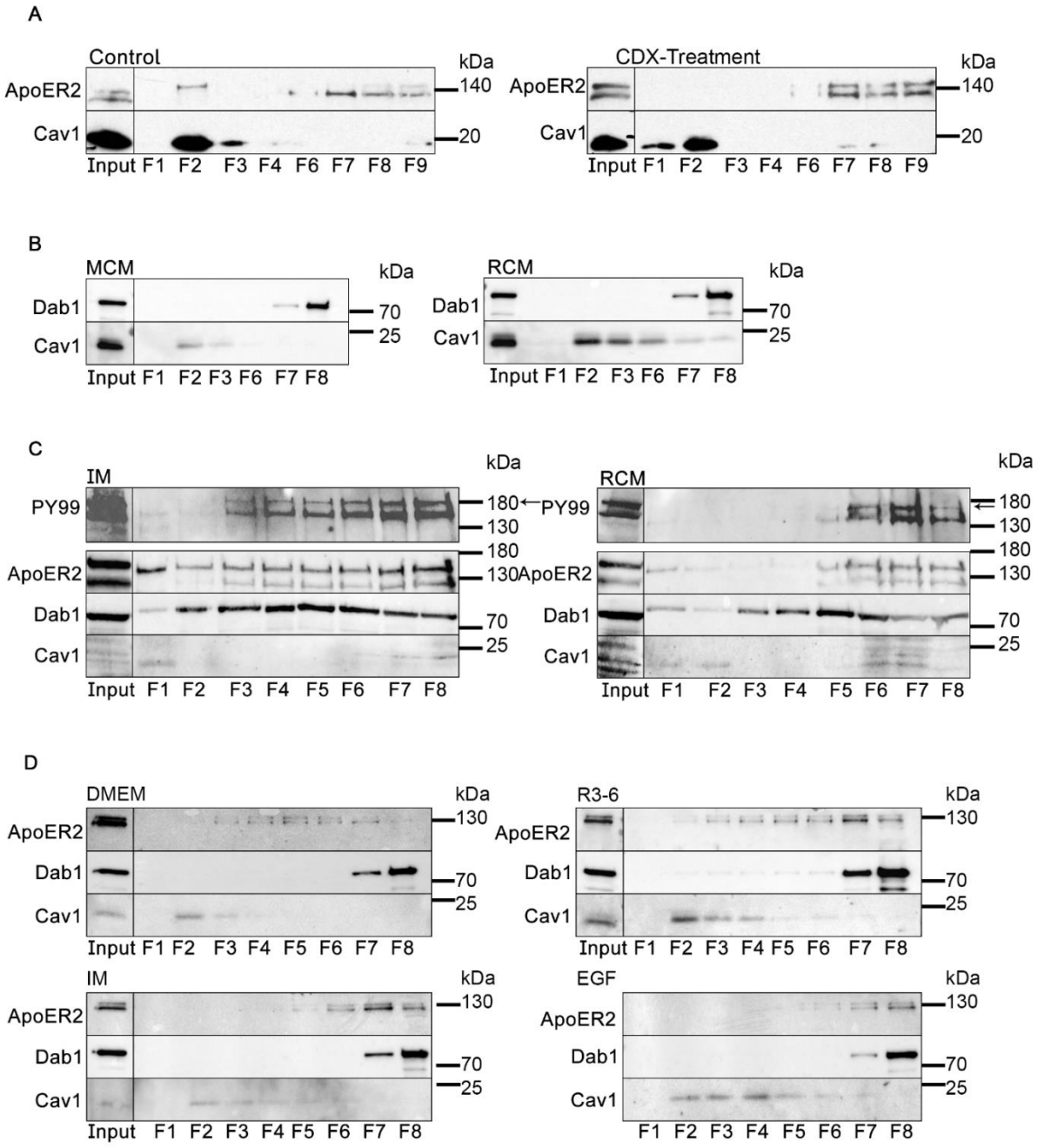

Figure 8.CDX treatment (4,4mM, 1h) of transiently transfected HEK293 with pClneo_ApoER2 for caveolin rich fraction disruption and isolation. Caveolin rich fraction isolation of transiently transfected HEK293 with ApoER2fL and Dab1. Treatment with Mock- or Reelin conditioned medium (B), with IM and RCM (C), and treatment with R3-6(30nM,20') and EGF (100ng/ml,7'), including controls with DMEM and IM (D). Analysis was done via discontinuous sucrose gradient ultracentrifugation, SDS-Page and Western blotting with the indicated antibodies, which is described in Material and methods section.

becomes phosphorylated under these conditions. Although, there are high levels of hyperglycosylated ApoER2 present in the NCM, no phosphorylation takes place there. Dab1 levels are very low in the CLM when compared to the NCM. Differences of phosphorylation or localization of the proteins of interest between IM and RCM conditions could not be found, only that total expression levels of ApoER2 are a bit lower in the RCM condition. These results strengthen the suggestion that ApoER2 phosphorylation and Dab1 binding take place in the NCM.

In the experiment presented in Figure 8D HEK293 cells were transiently transfected with pClneo_ApoER2 and Dab1_555 again. Treatment was done with the central Reelin fragment R3-6 (30nM, 20'), and EGF (100ng/ml, 7') and controls were included (DMEM, IM). In the experiment without treatment and starvation (DMEM) both isoforms of ApoER2 can be seen in the Input as well as in F3-F6. In F7-F8 only the hypoglycosylated variant is present. Full length Dab1 (80kDa) is seen in the Input and in F8-F9 and Caveolin1 is detected in Input and F2-F4. In the second control, where cells were starved (IM), both receptor isoforms are present in F2-F8 in varying concentrations. In the condition where cells were treated with Reelin central fragment both receptor isoforms are visible in the Input and in F2-F8. Low amounts of Dab1 can be seen in F2-F6 and high amounts are found in F7 and F8. Caveolin1 is also visible in the Input and found in F2-4, as well as very low amounts can be seen in F5-F7. In the EGF treated condition the Input control results were negative because of a very low amount of lysate was loaded to the gel. ApoER2 variants s are visible in F6-F8, Dab 1 is present in F7 and F8 and Caveolin is present in F2-F6.

ApoER2 pull down and phosphorylation

The goal of this experiment was to check the phosphorylation levels of the full-length receptor protein ApoER2 upon Reelin treatment. Another goal was to check for bound proteins. The system of choice was an in vitro cell culture with HEK293 cells, transiently transfected with the desired proteins. HEK293 are easily transfected and produce large amounts of proteins, so their detection is facilitated. The Antibody used for the pull down was ab186, which was produced against the entire ligand binding domain of the receptor[62]. For detection after Immunoprecipitation a20 was used which detects the cytoplasmic tail of ApoER2[100]. PY99 is an unspecific antibody for detection of phosphotyrosines obtained from Santa Cruz.

First, the capability of the antibody to pull down ApoER2 was assessed and a condition for preserving the phosphorylation level was searched for. The results are shown in Figure 9A. Transiently transfected HEK293_ApoER2 cells were treated with RCM. ApoER2 was pulled down with AB186 (IP) and protein levels were checked via SDS-Page combined with Western blotting. Blocking and incubation with Antibody was done with Phosphoblocker in PBS-Tween (lanes 1-3), TBS-Tween (lanes 4-6) or PBS-Tween only (lanes 7-9). The phosphorylation was detected best, where TBS-Tween was used (as seen in lanes 4-6). At a first glance it looks like there is a strong phosphorylation of the hyperglycosylated variant (180kDa) and the phosphorylation of the hypoglycosylated variant is barely visible (120kDa). The same blot was stripped and reblotted with a20 to evaluate the amount of ApoER2 (lower panel, lanes 4-9). To check if and to what extend the immunoprecipitation worked, Input and Flowthrough (FT) are included in the lower panel. Arrows indicate where the bands representing receptor isoforms can be seen. In the upper panel at around 160kDa the phosphorylated hyperglycosylated isoform is expected to be seen. As a control the blot images were overlayed via photoshop and the bands showing a phosphorylation via PY99 and the ones representing ApoER2 aligned. This experiment confirmed, that the hyperglycosylated form is mainly phosphorylated in presence and absence of Reelin treatment.

In Figure 9B transiently transfected HEK293 cells with ApoER2 and Dab1 treated with RCM are shown. An IP with a186 was carried out and phosphorylation was detected with pY99 and can be seen in the upper panel. In the lower panel total levels of ApoER2 and Dab1 are depicted. A positive control was added in lanes 1 and 4. Detection of phosphorylation of hyperglycosylated ApoER2(160kDa) was possible in the Flowthrough (1-3) and IP (4-6) lanes. Unfortunately, Dab1 phosphorylation can only be seen in the flowthrough samples as well as in the RCM control lane (4). Additionally, there is a low amount of phosphorylated Dab1 present in the flowthrough derived from cells of the untreated condition (2). The strongest bands are present in the control. Through this experiment we could show that Co-IP of Dab1 is possible, and phosphorylation of the protein can be detected.

As a next step the focus was set on an ApoER2 mutation where the tyrosines, we expected to be phosphorylated upon Reelin treatment, were all mutated to phenylalanines (tYF). Our goal was to see, if loss of the tyrosines diminishes receptor phosphorylation and if binding and phosphorylation of Dab1 is reduced. In the experimental setup cells were transfected with three different plasmids coding for: wild type receptor (fL_ApoER2), wild type receptor containing a N-terminal HA and a C-terminal Myc tag (HA_wt_myc), and a receptor with both previously mentioned tags as well as three mutated tyrosines, two in the NPXY-region and one in exon 19 (HA_tYF_myc). All cells were co-transfected with Dab1 and treated with IM, mock-conditioned medium (MCM) or Reelin-conditioned medium (RCM). A Co-IP was carried out were ApoER2 was pulled down with a186 and the eluates were loaded on two different gels. With the first blot phosphorylation levels were detected (panel1), then the blot was stripped and checked for total receptor level (panel2). The second blot was used for Dab1 detection (panel3). Because of the addition of the tags by the Rebeck lab[101], the expressed proteins migrate slightly slower (1-6, first panel) than the full length ApoER2 frequently used in our lab (7-9, first panel). One thing that was interesting, is that the second band representing the hyperglycosylated form of ApoER2 in the wt

(4-6) and tYF (1-3) versions of the receptor is missing. Normally, it is visible when full length ApoER2 is expressed, as it can be seen in the added control lanes (7-8) at around 140kDa. The cause of this phenomenon could be the addition of the HA and myc tags to the receptor, which may alter the rate of successful hyperglycosylation in the Golgi. This is just a hypothesis based on my speculation, as the only difference of these variants, expressed in the cells of this experiment, should be the attached HA and myc tag. Of course, this can be validated by a sequence analysis of the plasmids. Maybe some sterical hindrances through tag attachment can reduce the process of hyperglycosylation and therefore the full-length mature/hyperglycosylated receptor is not present in such high numbers. This could be the reason, why the bands of the hypoglycosylated isoforms (in 1-6) are stronger when compared to the hypoglycosylated forms of full length ApoER2 (7-9) even though cells were transfected with the same amounts of plasmid. Similar results are shown in Burrell et al 2014, where no hyperglycosylated isoform is detected after transfection with ApoER2-Myc. Only after co transfection with Fyn the hyperglycosylated isoform of HA-ApoER2-Myc is detected through phosphotyrosine pull down and subsequent detection via ApoER2 antibody. The tYF-mutant is unable to build a hyperphosphorylated isoform. Another difference that was detected is the very different migration of receptor bands. In our experiment the bands of the hypoglycosylated receptors were found at a size of 110 kDa, in Burrell et al, 2014[101] they migrated at around 130kDa. In our experiment all bands corresponding to phosphorylated proteins (1-7, first panel) have the same size and do not change upon RCM treatment which means the band detected at around 155kDa, most likely, does not correspond to ApoER2. Therefore, the bands detected in previous experiments (Figure 9A and B) very likely do not depict phosphorylated ApoER2 as well. One cause, why pApoER2 could probably not be detected would be that there are not high enough levels of Fyn present, which is known to indirectly increase and stabilize ApoER2 phosphorylation. What is also known is, that ApoER2 does not contain a domain that enables autophosphorylation, therefore other proteins, that are capable of phosphorylation of ApoER2 upon ligand treatment, have to be present. This can be achieved either via transfection of Fyn or Src or endogenous expression by the stable cell line itself[101]. The literature found about endogenous Fyn expression of HEK293 is sparse and controverse. For example, expression of Fyn is only mentioned once as it is downregulated in special mutational clones of HEK293, or not found at all[102,103]. One approach would be to test HEK293 via SDS-Page and Western blot for Fyn expression or to co express proteins known to phosphorylate tyrosines, especially in NPXY motives. All three receptors are able to bind Dab1(~80kDa, lower panel) and no differences between the wild type and the tagged wild type receptor are visible. As expected, the ability to bind Dab1 is reduced in the tYF-mutant (1-3). Slight differences are also seen when comparing the RCM treated conditions to MCM or IM. The highest amount of Dab1 is bound by all three receptors when cells are treated with RCM (1, 4, 7).

As conclusion of this part of the project we encountered a big setback, regarding the evaluation ApoER2-phosphorylation during Reelin signalling. Unfortunately, the detected band, previously thought to represent ApoER2 phosphorylation is an unknown protein endogenously expressed in HEK293, pulled down with a186 and phosphorylated (also in the absence of Reelin). This could have been realized earlier by a simple control experiment where untransfected HEK cells would have been analyzed in parallel. It has been published, that phosphorylation of ApoER2 and VLDLR is dependent on Fyn or Src, as both receptors have no kinase domain and cannot autophosphorylate themselves. [16] A positive outcome is that we were able to pull down Dab1 via Co-IP which binds robustly and directly to ApoER2 which led us to the observation that Dab1 binding is reduced when Reelin is dependent on tyrosines present in the intracellular domain of the receptor.

In the experiment presented in Figure 9 HEK293 cells were transiently transfected with plasmids coding for ApoER2 variants (fL_ApoER2 and ApoER2Δ16) and Dab1. Cells were treated with RCM, lysed and an IP with a186 was carried out. Phosphorylation of the receptor was evaluated via SDS-PAGE and Western blot with PY99 antibody. In this situation a band was detected at around 140kDa (1,3). The blot was stripped and reblotted with a20 to detect ApoER2 (hyper and

hypoglycosylated), which are running at 140 and 120kDa (2). ApoER2Δ16 was detected at around 110kDa (4). As the only phosphorylated band runs at 140kDa and is also present in the cells transfected with the Receptor lacking the o-linked sugar domain, it becomes even clearer that the pulled down, phosphorylated protein cannot be ApoER2.

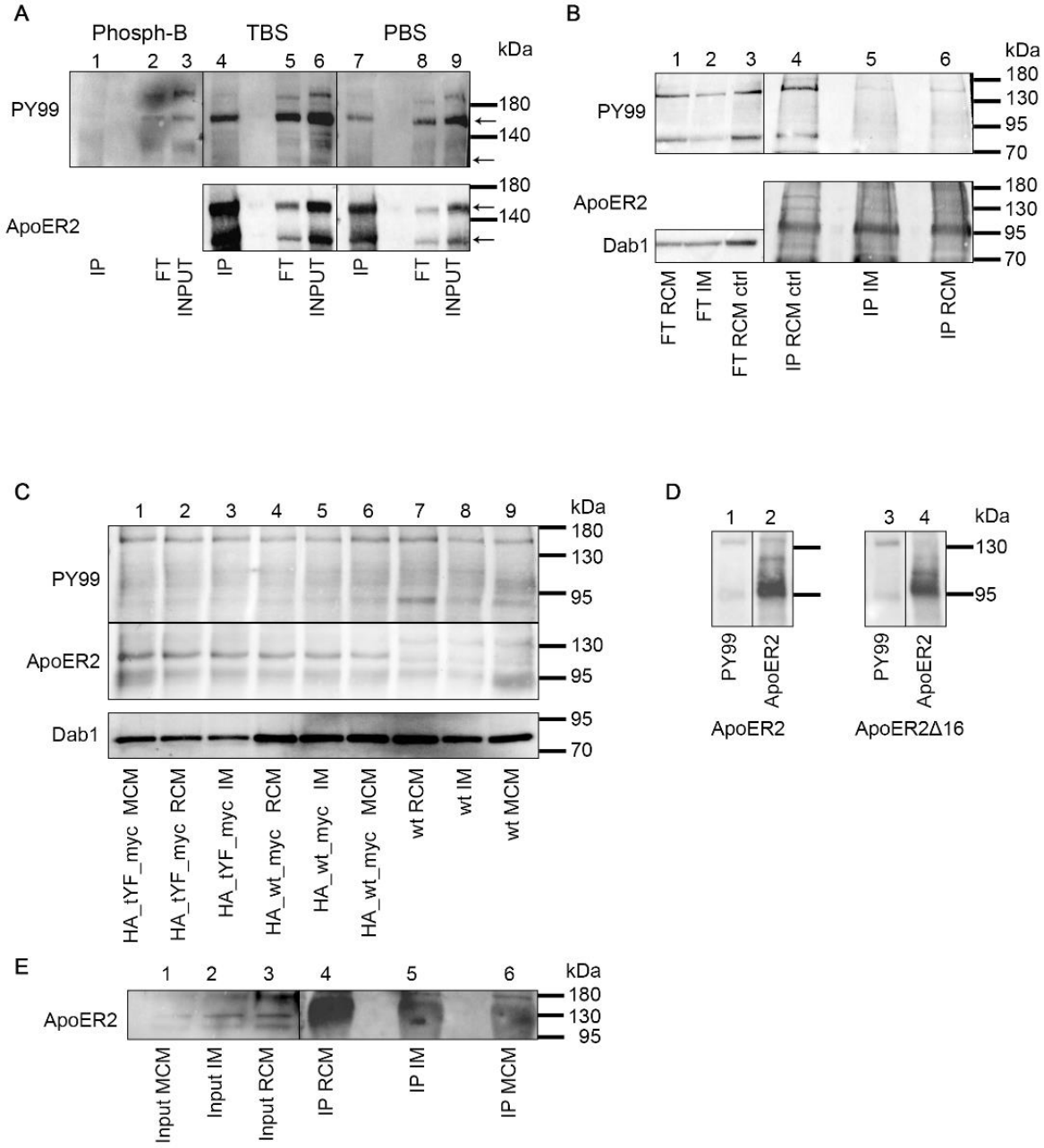

Figure 9. *ApoER2 pull down* **A**. Optimisation of Phosphorylation detection. Phosphoblocker, TBS-Tween and PBS-Tween phosphorylation levels are compared. Blots were stripped and total protein levels are shown in the lower panels. **B**. IP with a186 and Flowthrough (FT), detection of phosphotyrosines, stripping and detection of pulled down ApoER2 and Dab1 in FT.**C**. Co-IP and phosphorylation detection of Dab1 with mutated ApoER2 upon Reelin treatment. D. IP and detection of phosphorylation of ApoER2 and ApoER2Δ16. E. Quality control of ApoER-pull down in neurons, IP and Input comparison upon treatment.

As the most accurate situation in terms of the presence of all proteins needed for the Reelin pathway are neurons, we tried to pull down our desired proteins in primary neuronal culture as well. In Figure 9E the result of an experiment is presented, where Neurons of DIV11 were treated with RCM, MCM or were left in IM. IP of ApoER2 was done, SDS-PAGE carried out and proteins were evaluated via Western blot. ApoER2 could be found in the Input samples (lanes 1-

3;140kDa,110kDa) but was not detected in the IP eluates (lanes 4-5). Unfortunately, a huge signal was always present when ApoER2 or the phosphorylation was evaluated. This could have been caused by the heavy chain of an antibody used. Thus, maybe the use of other antibodies might solve this problem in further investigations. Due to time limits during my thesis this particular project was not continued further, but a lot of knowledge could be gained through those experiments.

Dab1 pull down and phosphorylation

The aim of this project was to discover proteins bound to Dab1 and to pull them down via Co-IP. Dab1 pull down was done with Ab54[33,62], which was raised against the first 15 amino acids of the C-terminal part of the short splice variant of murine Dab1. As this antibody was established long time ago and stored over years, first trials were carried out where we tested if the antibody is still functional, and under which condition the pull-down works best. A corresponding experiment was carried out and the results are shown in Figure 10A. First HEK293 cells that were transiently transfected with ApoER2 and Dab1 were used. After lysis the pull down of Dab1 was carried out using Ab54, the details are mentioned in material and methods section. As a control the Input was included in lane 1. To ensure that the antibody binding is working efficiently, and highly specific and cross reactivity can be excluded, the experiment was carried out including spiking. For this we added a protein lysate of another organism to our experiment, where no proteins are present to which our antibodies used can bind to. In one condition a lysate for spiking only was included as a negative control (2) and in the second condition with spiking Ab54 was included as well (3). IP efficiency was tested with freshly thawed (4) and at 4°C stored antibody (5), and it was tested if a difference could be detected when using magnetic instead of Sepharose beads (6). After IP, the captured proteins were separated via SDS-Page and transferred to nitrocellulose. A20 for ApoER2 detection was used and the presence of hyper and hypoglycosylated forms of the receptor could be confirmed. The corresponding bands are found slightly above and below the 140kDa mark. After this evaluation the membrane got stripped and was reblotted with D4 against Dab1. Dab1 is present at around 80kDa. The strongest band of Dab1 can be observed in lane 4, representing the experiment where magnetic beads were used. This set up worked best as the background is much less in comparison to the other set ups. As it was proven now that it is possible to pull down proteins bound to Dab1 detection of Dab1 in primary mouse neurons was the next step that had to be checked. In Figure 10B an IP of Dab1 from lysates derived from neurons (DIV12) was carried out. Dab1 could be detected nicely (~80kDa, 2) and could be pulled down effectively as no band could be detected at the same size within the flowthrough of the IP (1). The ability of an antibody to detect N-Wasp in neurons in our experimental setup was tested and is shown in lane 3. The protein is found and migrates with a rel. mol. Mass of 65kDa (3). Next, a Co-IP of N-Wasp with Dab1 was tried, and neurons were treated with RCM or left in IM to check for a possible effect Reelin binding could have on this interaction (Figure 10C). After IP, SDS-PAGE and Western blot very low levels of N-Wasp are found in lane 3 at around 65kDa. For comparison, the Input was included, and N-Wasp levels detected (lane 1,2). As the bands are barely visible, and the secondary Ab chain migrated very close to the protein band the experiment was repeated with a special Ab carrying a specific light chain, to improve detection. The results are shown in Figure 10D. Neurons of DIV13 were treated with RCM or kept in IM. Dab1 pull down was carried out, and bound N-Wasp was detected (lane 3,4, lower panel~65kDa). The same blot was stripped and reblotted for Dab1 (lane 3,4, upper panel, ~80kDa). The Input and flowthrough controls were included (lanes 1,2,5,6). To quantify the detected bands Image Lab Software provided by BioRad was used. Background subtractions were carried out and the adjusted values of N-Wasp were put into relation with Dab1 levels via Excel. The results were visualized in Graph pad and are depicted in Figure 10E. Interestingly, the amount of bound N-Wasp relatively to Dab1 levels is dramatically decreased, when Neurons are treated with RCM.

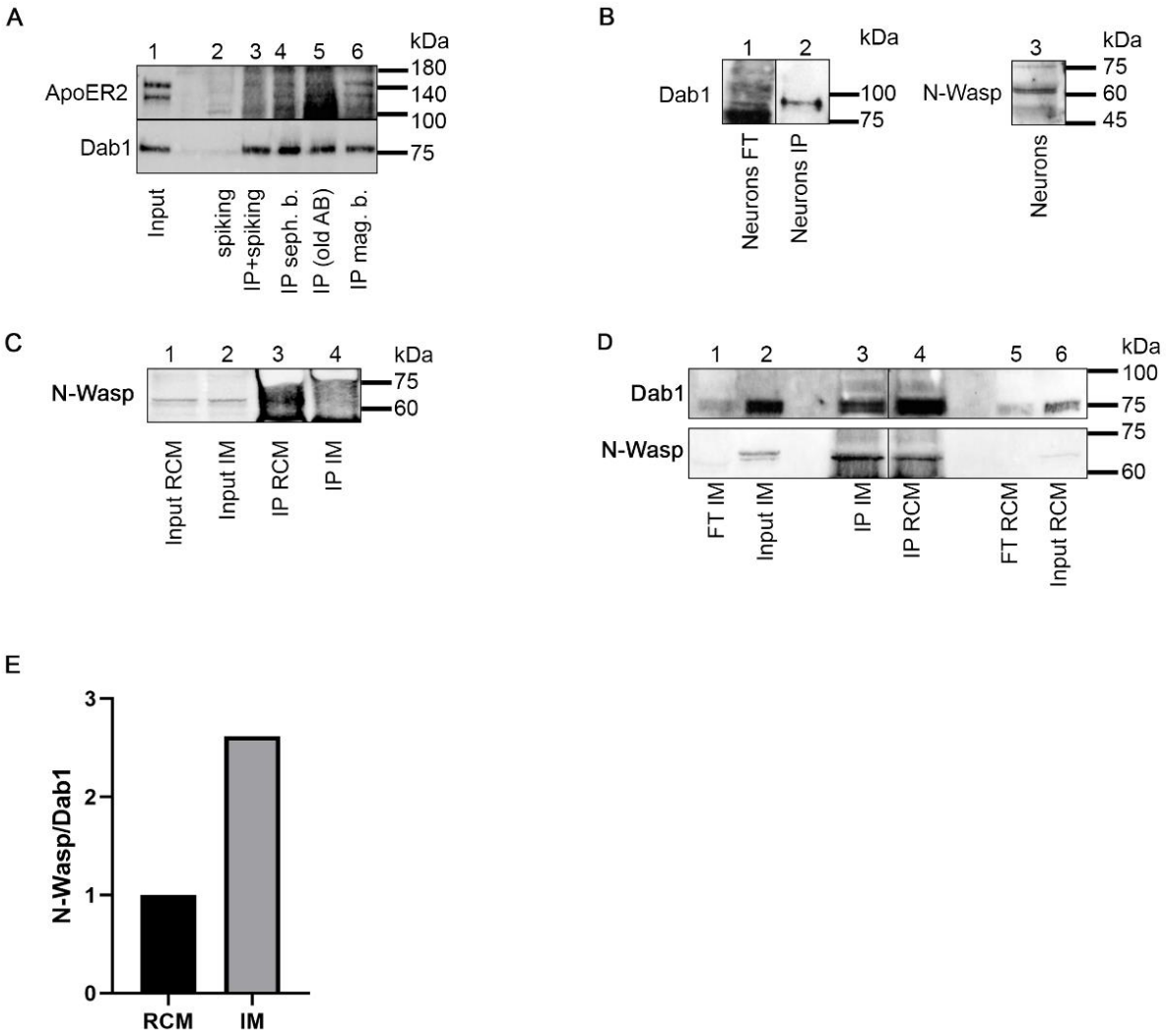

Figure 10. Dab1 pull down. In all lanes labelled with IP a pull down with Ab54 was carried out. Separation and detection were done with SDS-PAGE and Western blot. A20 and D4 were used for ApoER2 and Dab1, N-Wasp Ab was used for N-Wasp. A. Pull down and Co-IP optimization. IP with HEK293 ApoER2/Dab1 lysate was carried out including Sepharose beads. Other steps that were included: usage of spiking protein only (2), Ab54 and spiking (3), Ab54 alone (4), an old antibody aliquot of Ab54 (5) and Ab54 was pulled down with magnetic beads (6) instead of Sepharose beads. Input was included as a control (1). B. IP in Neurons DIV12 (2). Flowthrough control is included (1). Total cell lysate was used for N-Wasp detection (3). C. Co-IP of N-Wasp. Neuron treatment with Reelin (RCM), control (IM) is included. Input conditions are included. D. Co-IP of N-Wasp but Flowthrough (FT) is added as well (lower panel). Additionally, membrane stripping was carried out and Dab1 levels of pull down are analysed (upper panel). E. Adjusted Volumes of the bands were assessed and exported from Chemidoc, put into relation via Excel and visualized via Graph pad.

Dab1 Phosphorylation

To preserve and properly evaluate phosphorylation of Dab1 as good as possible, some steps during our experimental procedures were checked and altered accordingly. First, different ways of antibody blocking to reduce background signals during Western blotting were tested. HEK293cells were transiently transfected with ApoER2 and Dab1 and the results aiming to detect Dab1 and its phosphorylation status by Western blotting are shown in Figure 11A. Treatment with RCM (3,4,5) and controls such as IM (2) and MCM (1) were included. The blots were blocked with BSA (3), Milk (4) and BSA with PHosSTOP (5). Even though the background signal was slightly reduced in the condition were blocking with Milk was done the phosphorylation of Dab1 (~80kDa, PY99) was not preserved nicely and the level detected can be compared with the control conditions shown in lane 1 and 2. Blocking with BSA worked slightly better, but the best result preserving phosphorylation could be detected when blocking was done with BSA including PHosSTOP. Thus, for further phosphorylation detection blocking was done in this way. As a next

step, it was tested, if some differences can be detected upon stimulation of HEK293 ApoER2/Dab1 with Reelin when different concentrations of cells were used for production of RCM and MCM. Data are shown in Figure 11B. With both seeding concentrations (3x10^5, 4,5 and 6x10^5, 2,3) a clear increase of phosphorylation could be detected, when comparing RCM treatment (3,5) to MCM/IM controls (1,2,4). Although the seeding number of cells was doubled for medium production, no visible change in phosphorylation intensity could be seen between MCM (2,4) and RCM (3,5) conditions. As a next step, cells were transiently transfected with different isoforms of ApoER2, to detect if there is a change of phosphorylationof Dab1. For this experiment HEK293 were transiently transfected with full length ApoER2 and Dab1 (1,2,6-9) or ApoER2Δ16 and Dab1(4,5). As a control condition Dab1 only transfection was included (3). In Figure 11C lane 4 it is clearly visible that indeed ApoER2Δ16 is capable of phosphorylating Dab1. As nicely seen in Fluorescent microscopy/Phalloidin staining, ApoER2Δ16 is not always located in the plasma membrane, which seems to have no effect on Dab1 phosphorylation. Additionally, CDX (1h, 5mM) treatment was carried out prior to RCM addition, which is described above. As rafts get disrupted upon treatment, it was tested if Dab1 phosphorylation may be altered through re-localization of hyperlgycosylated ApoER2. In lane 8 it is visible that upon CDX treatment Dab1 phosphorylation is also not impaired. Another thing that can be observed, is that the phosphorylation of tyrosines is in general increased in conditions when cells are treated with CDX, which can be explained by increased stress levels of cells as cholesterol cannot be inserted into the membranes. Even though the highest phosphorylation of Dab1 is always found in conditions when cells are treated with RCM.

A quantitative analysis of the blot shown in Figure 11B and two other additional experiments was done via image lab and excel. pDab1/Dab1 intensities relative to GAPDH were assessed and levels produced by the addition of MCM were set to 1. The acquired Data is shown in Figure 11D. In Figure 11E the blot depicted in Figure 11C was analysed in the same way as described above. Unfortunately, only two individual experiments were available for this analysis. In Figure 11F phosphorylation levels displayed in Figure 11E are shown as phosphorylation ratios between stimulated (Reelin) cells and unstimulated (IM) cells. There it is visible that the phosphorylation difference in cells is not as big as in the two other conditions as the overall phosphorylation is already elevated due to stress induced by CDX treatment.

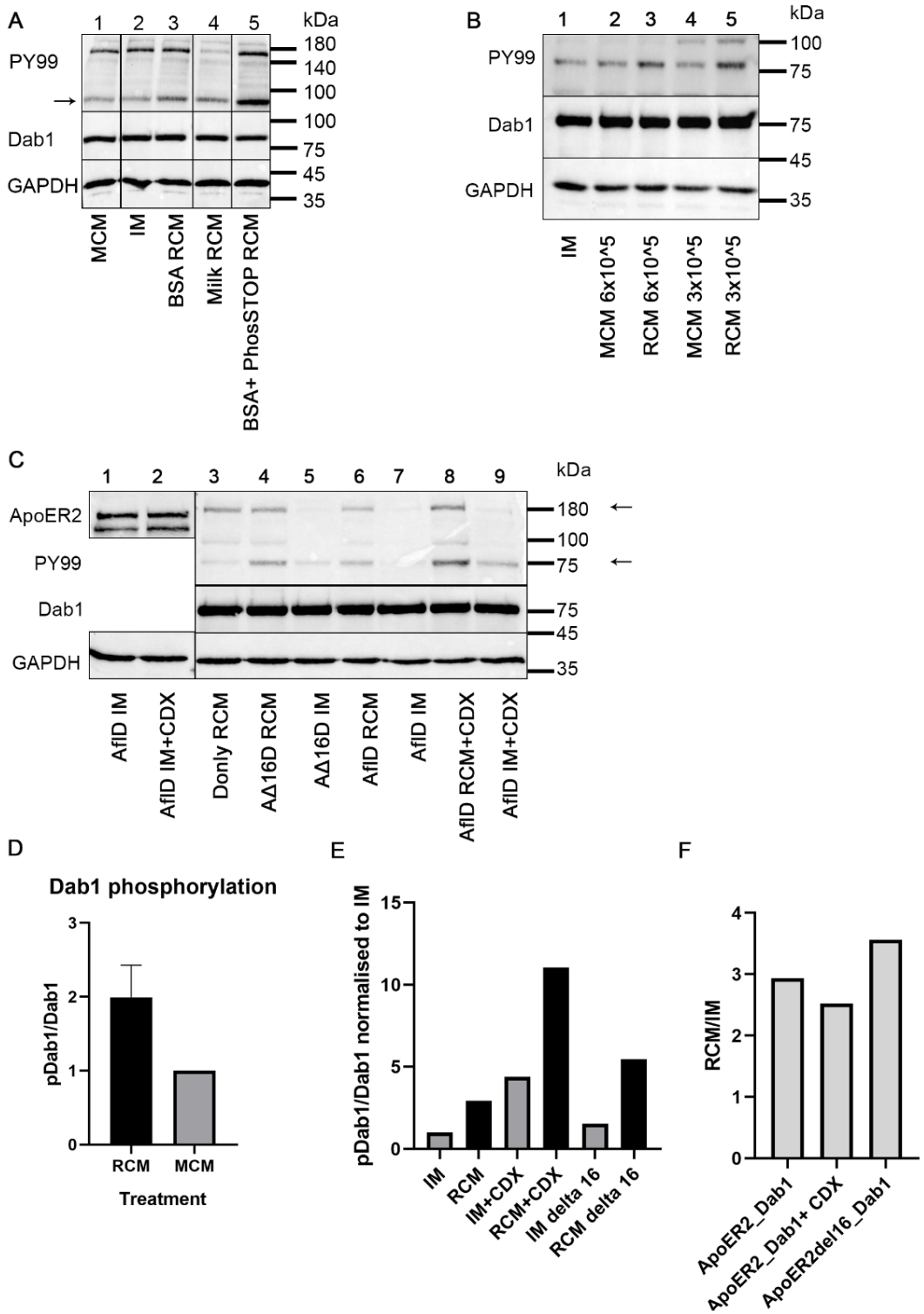

Figure 11. Dab 1 phosphorylation. The shown panels of each figure part are corresponding to one single blot, which was stripped between protein detections. A. Optimization of phosphorylation detection. Double transfected (ApoER2/Dab1) HEK293 cells were either left in IM (1) or treated with MCM (2) or RCM (3). TBS-Tween and BSA (1-3), TBS-Tween and milk (4) or TBS-Tween with BSA and PhosSTOP (5) were used to during blocking. Tyrosine phosphorylation was assessed (upper panel, PY99) and bound Dab1(middle panel, D4) detected. GAPDH loading control was included (lower panel). The arrow indicates where phosphorylated Dab1 is detected(~80kDa). B. Again HEK293 ApoER2/Dab1 cells were treated, this time with freshly produced MCM (2,4) and RCM (3,5) extracted from dishes with differing cell concentrations, or they were left in IM (1). C. Transient transfection was carried out with ApoER2 and Dab1 (1,2,6-9), ApoER2Δ16 and Dab1(4,5), or with Dab1 alone (3). CDX(1h,5mM) was added (2,8,9) and cells were treated. (RCM, 3, 4, 6, 8). Additionally, ApoER2 levels were included in two conditions (a20,1,2). D/E. Analysis of phosphorylation was done with ImageLab (BioRad) and Excel. The amounts of pDab1/Dab1 relative to GAPDH levels is shown. The graphic shown in D is acquired from data shown in B and two other independent experiments. Analysis in E was done with Data acquired from the blot shown in C. F Phosphorylation changes of E were set into relation.

Isolation of mouse neurons, electroporation/nucleofection

The following experiment was carried out with neurons extracted from embryonic mouse brains (embryonic day 14) transfected with GFPmax from Lonza. The plan was to optimize the protocol to transfect neurons by nucleofection with different isoforms of ApoER2 to test if morphological differences of the cells can be detected upon expression of different isoforms of ApoER2. In addition, the localization of the isoforms in the plasma membrane as well as inside the cells was planned to be evaluated. Unfortunately, only neurons that did not express GFP survived longer than 24h. As it takes longer for neurons to build their dendritic connections to each other, we could not get any satisfying results. As we were taking care of all the troubleshooting recommendations provided by the Lonza manual, we suspect, that our AMAXA nucleofector device did not work properly anymore. Unfortunately, we could not use any other device to redo the experiment. HEK293 that were included as a control are way more robust and they survived the nucleofection which is visible in Figure 12. However, this could not be achieved with neurons. For further experiments I would focus on a lentiviral approach to achieve expression of desired genes in neurons[104].

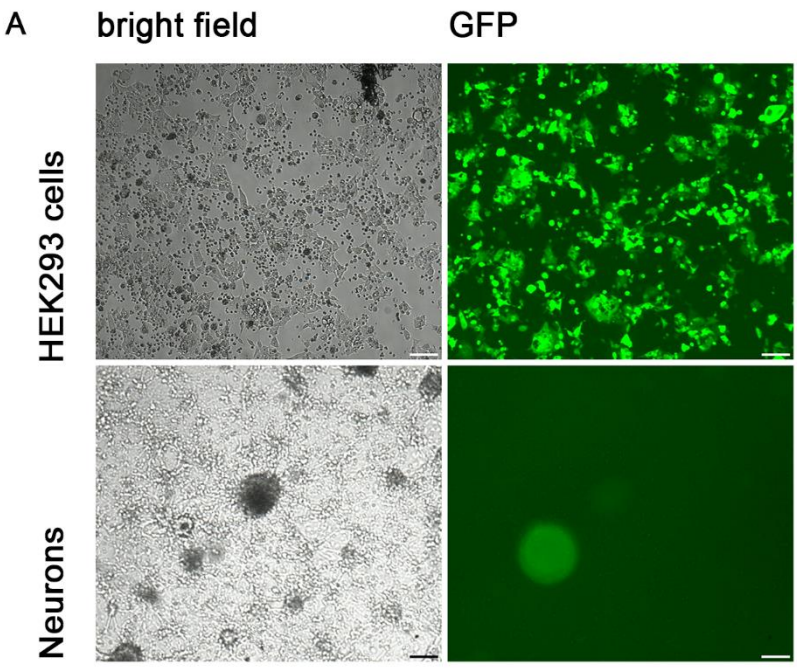

Figure 12 Nucleofection of HEK293 and Neurons with GFP via AMAXA nucleofector.Scale bars represent 100µm.

Wound healing assay with HEK293, transfected with different variants of ApoER2, and treated with RCM/IM

The goal of this experiment was to evaluate differences in growth or motility of cells expressing different isoforms of ApoER2 when treated with full length Reelin or central Reelin fragment. The protocol for this experiment has been newly established in the lab, using suggestions, recommendations from colleagues and according to protocols found in the literature [105–108]. Indifferent steps the protocol was optimized and adapted for our specific situation. The goal of this experiment was to find out if any differences in growth or motility between cells expressing the ApoER2 or its isoform lacking the exon 16 can be found when treated with the ligand Reelin. In the beginning experiments were started with a 96 well plate coated with collagen, and cells were transfected with plasmids coding for ApoER2, ApoER2Δ16 and as well as for VLDLR. Before seeding, the wells were marked with a thin marker on the bottom to make sure the same area of the well was evaluated after different timepoints. The scratch which was made later was done perpendicular to this marking. At the beginning treatment with RCM and IM was carried out and pictures were taken after 2, 4, 8, 24 and 28h. Later, MCM was used as control to have the same components in the medium as in RCM, but it didn't work well as media, that were produced via cell culture, still had a lot of debris inside after sterile filtering. During the optimization process 96 well plates with a glass bottom were tested as well, but the cells or the collagen which was added before was not adhering nicely to this surface. To get a better effect during the treatment it is recommended to starve the cells before the actual experiment. As our cells did not survive this treatment, we tried different low concentrations of serum and decided to use 1% serum for the assays. At the beginning we used a normal light microscope to take pictures of the scratch,

but later on we decided to use the CD7 microscope to reduce stress and to get images which were always taken exactly at the same spot as defined at 0h. We started our wound healing assay with two cell lines, HEK293 and NIH3T3. Different cell numbers were seeded to get 90% confluent

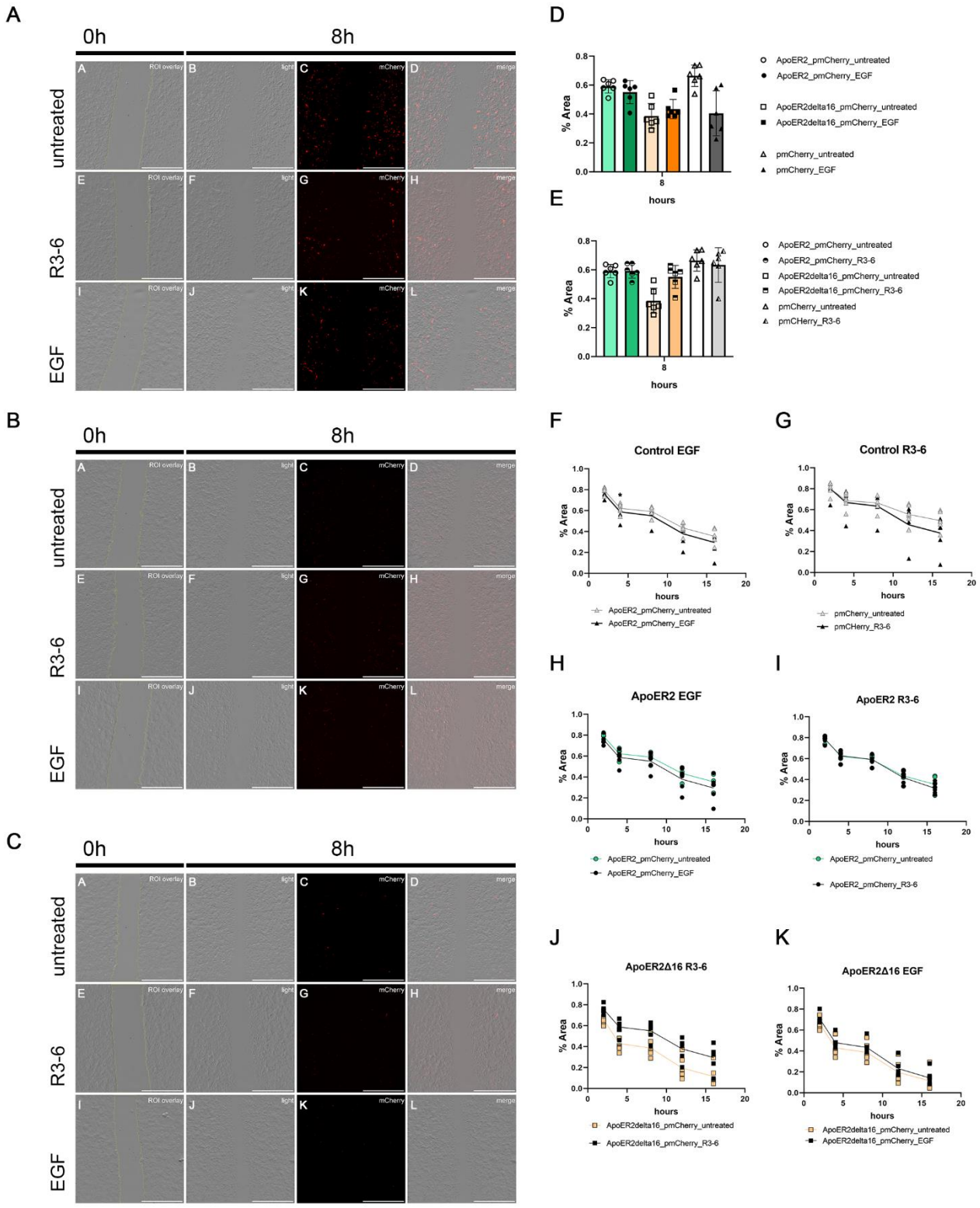

*Figure 13.*Scratch area for wound healing assay with HEK293 cells at 0 and 8h is shown in A, B and C. In A. cells were transfected with a plasmid carrying mCherry (A; A-L), in B. cells were transiently transfected with ApoER2_mCherry (B; A-L) and in C. cells were transfected with ApoER2Δ16_pmCherry. All conditions were treated with R3-6(E-H) or EGF(I-L). Scratch size comparison was carried out via Fiji MRI_wound_healing_tool and Graph pad prism. Bars represent 1mm. In D.-K. comparisons of the decrease of the free area after indicated hours is shown.

cells at the day of transfection. Unfortunately, we were not able to seed NIH3T3 for this experimental setup, as they were either dying rapidly or the wells were overgrown 24h after seeding. Also, one recommendation we tried to follow was addition of collagen after seeding on top of the cell layer additionally to the layer on the bottom. The idea of this procedure was to embed the cells properly and to give them the possibility to grow better at the area where the scratch was made. In our case this did not work well as the cells fully detached, therefore it was decided to keep the original procedure. Regarding the concentration of EGF which had to be added during the experiment. First, an experiment was carried out with different concentrations of EGF for treatment. According to the results obtained We decided to use a concentration of 100ng/ml. For R3-6 30nM were decided to be the optimal concentration under the established conditions. The final protocol which was working best, and used for the described results can be found in the material and methods section.

The data of the optimized experiment is displayed in Figure 13. In the panels A-C the scratches which were made by a 200µl pipette are depicted and in panels D-K the analysis of the primary scratch data is shown. In panel A, cells which were transfected with a plasmid containing the mCherry reporter gene alone. The first row (A-D) shows the control condition where no treatment was carried out. In the second and third row, the results produced by the addition of R3-6 and EGF was monitored. The images in column 1(A, E, I) represent time point 0, which was taken directly after scratching and addition of the (ligands?). To analyze all images, the ROI (region of interest, cell free area after scratch) was defined by MRI_wound_healing_tool in Fiji/ImageJ. In the other tree columns, the same area as in column one is shown again but after 8h of treatment. The second column (B, F, J) shows the light microscopy image of the scratch. Additionally, the mCherry fluorescence is shown in column 3 (C, G, K) to show transfection efficiency, and indirectly the expression of the genes expressed by the plasmids. In column four (D, H, L) the merge of the light microscopy and the fluorescence image is shown. Panel B shows the conditions where cells were transfected with the ApoER2_mCherry plasmid, and it is arranged in the same way as panel A. For panel C the same system was used again and the results with cells transfected with ApoER3Δ16_mCherry are depicted. As can be seen, the scratch sizes are relatively uniform at 0h and the cell free areas can be detected easily by the MRI_wound_healing_tool in Fiji/imageJ. As already mentioned, the cells were monitored for 24h, but with a low serum concentration used here they are not in the best condition after such a long time. Therefore, it was decided to analyze the wound closure only until 16h post scratch. After this time point, the cells were getting round and many of them died. What can be seen as well after 8h is that the scratch gets smaller in all conditions and fluorescence is still present. When comparing the different conditions one can see that with the control experiment, where cells were transfected with the plasmid coding for mCherry only, the highest transfection efficiency was achieved. The lowest transfection efficiency is found in conditions transfected with ApoER2Δ16_mCherry. This could contribute highly to the obtained results. However, after so many steps of optimizing the experiment, the outcome was rather disappointing. Unfortunately, the data were highly variable. Therefore, it was quite difficult to get consistent results throughout the replicates. After images were taken, they were opened with the Zen blue program to process them via time concatenation. Therefore, the images were put together via drag and drop and saved in between until all timepoints were linked in one file. Then the scenes were split again to get each condition alone. Further, the processing was done with Fiji, where the channels were split as fluorescence is not needed for wound size calculation. The smooth option was used and the parameters for MRI_ wound_healing_tool were defined. The variance filter radius was set to 5, the threshold to 254, the radius open to 5 and the min. size to 5000. With the M button measuring was done and all images were checked by hand to delete and add measurements that were not detected properly by the program. It is crucial to check that areas are added to the corresponding time points, so the total remaining area is correct. Area size was copied from ROI manager to excel and areas from each time point were divided by the value derived from time point zero. The results were copied to Graph Pad and analyzed via RM two-way ANOVA with the

Geisser-Greenhouse correction followed by a Tukey's multiple comparisons test with individual variances computed for each comparison. The Geisser-Greenhouse correction was chosen as the variance between different treatments was not equal. In panels D and E response of all cells to EGF or R3-6 treatment is shown. One can see that there is a smaller area of the wound in the control group (mCherry transfected) when treated with EGF (white and grey bar;D), which was expected as this conditions were used as positive control. Also, in the analysis the decrease of area was significant after 2h which is shown with the asterisk in F. There is no response to R3-6, which was expected as well, as HEK293 wt cells should not have receptors to react to Reelin and this was the negative control included in this experiment[98]. With analysis using graph pad, no significant size differences of the wound healing area between the conditions could be found. What is interesting is, that cells transfected with either isoform of ApoER2 seem to be insensitive to EGF treatment, as the wound size doesn't decrease significantly after treatment with EGF. We can only speculate about the cause of this effect but maybe the amount of EGFR on the surface of the cells is decreased, when ApoER is expressed. Another explanation could be that there exists a cross talk between the EGF/EGFR pathway and the Reelin pathway (see later). After Reelin treatment, there seems to be no increased motility/growth of cells expressing an ApoER2 isoform as no significant reduction of cell free area could be monitored. A surprising observation was, that without treatment, cells expressing the ApoER2Δ16 isoform seem to close the wound faster than other conditions, which may be due to an already smaller scratch size at the beginning of the experiment. Through analysis of this data, the conclusion is, that Reelin central fragment does not increase motility or growth of cells expressing ApoER2 full length and Δ16 receptor variants.

Binding of EGF/Reelin to different receptors

So far, no connection between the EGFR and the Reelin pathway has been published. One of our goals was to test whether EGF might be a ligand for VLDLR or ApoER2. This came to our mind, because we found the NPXY motif, which is where Dab1 binds to VLDLR and ApoER2, on EGFR in the cytoplasmic region ([109], Figure 1 A). First, we tested if there is a cross talk between the two pathways on ligand/receptor level. For this we transfected HEK293 cells with different receptors and ligands attached to varying fluorophores. As controls, plasmids containing genes of already known ligands tagged with a fluorophore as well as some containing the fluorophore alone were included. To test whether EGF binds to any of the expressed receptors fluorescence microscopy was carried out using EGF labelled with Dylight 488.

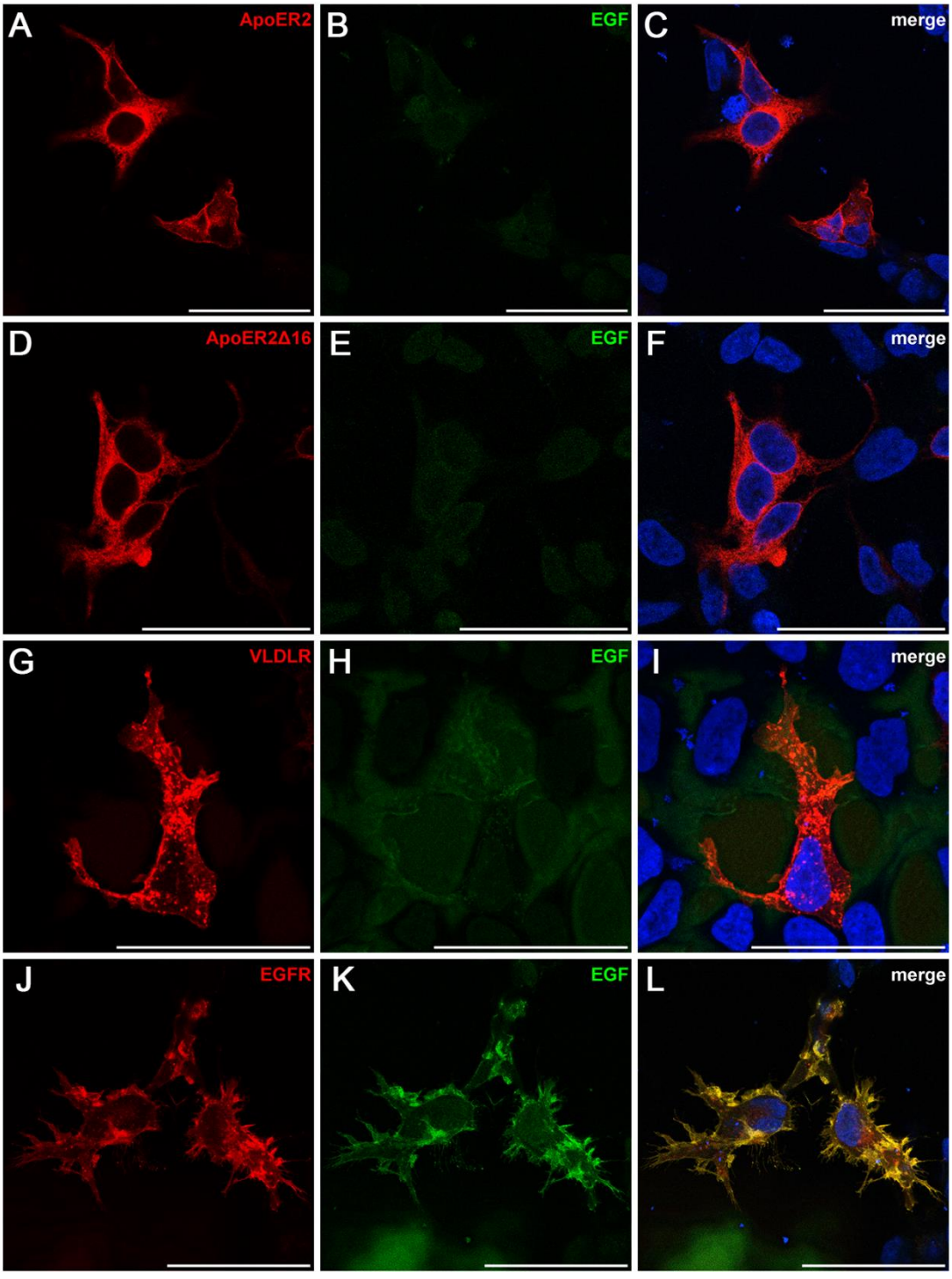

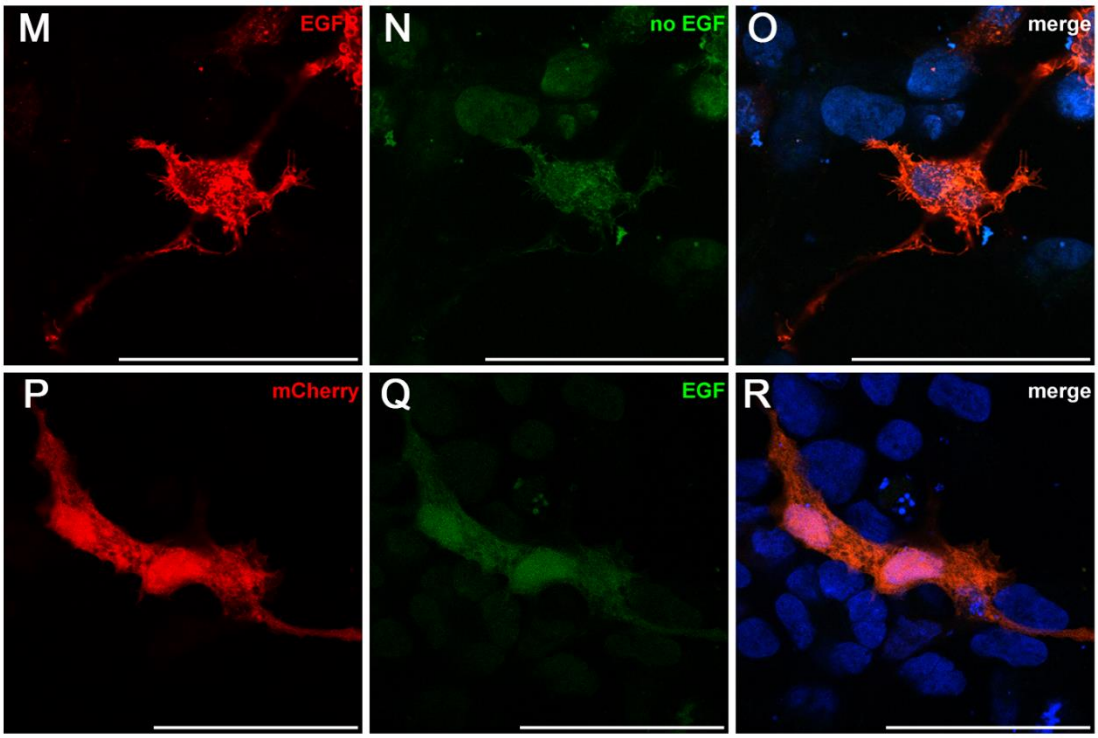

Figure 14. EGF binding to receptors. Fluorescent images of HEK293 cells transfected with ApoER2 (A-C), ApoER2Δ16 (D-F), VLDLR (G-I), EGFR (J-O) linked to a mCherry fluorophore and mCherry alone (P-R). Conditions (A-L, P-R) were treated for 1min with human EGF labelled with Dylight488(1 µg/µl,37°C), as control no EGF was added to EGFR expressing cells (M-O). After fixing and DAPI staining cells were mounted. Scale bar represents 50µm.

The expression of the receptors ApoER2_mcherry (Figure 14; A-C), ApoER2Δ16_mCherry (Figure 14; D-F), VLDLR_mCherry (Figure 13;G-I) and EGFR_mCherry (Figure 14; J-O) and mCherry (Figure 14; P-R) was induced and treatment with human EGF labelled with Dylight 488 (A-L,P-R) was carried out. Cells were fixed, DAPI stained and mounted on glass slides. Controls without EGF (Figure 14; M-O) and without receptor (Figure 14; P-R) were included. With fluorescence microscopy three different channels were used to detect the expressed receptors (mCherry, Figure 14; A, D, G, J,M,), the bound EGF (Dylight488, Figure 14; B, E, H, K, Q) and the nucleic acids (DAPI, Figure 14; C,F, I, L, O, R). It is clearly visible, that the receptors linked to mCherry, are not found in the nuclei of cells (Figure 14: A, D, G, J, M) whereas in the control condition, mCherry (Figure 13, P-R) alone is clearly present in the nuclei ([110],Figure 2C). High amounts of the ApoER2 variants, VLDLR and EGFR are found in the membrane as well as in the cytosol, whereas in the control condition with mCherry alone it seems that the fluorophore alone is not inserted in the membrane (Figure 14, P). It appears that, cells expressing EGFR form a lot of spikes, regardless of the presence of EGF (Figure 14; J, M). In the other conditions, some longer protrusions are formed but the overall cell shape looks much smoother when compared to EGFR expressing cells. As expected, no hitherto unknown binding was discovered. EGF only binds to EGFR which is nicely visible in Figure 14 J-M. Especially in the merge (Figure 14; L), the close proximity of receptor and ligand is visible, as the overlay of both channels the colours cannot be distinguished anymore and merge into a yellow structure.

To test whether Reelin is binding to EGFR, cells were again transfected as mentioned above and treated with Reelin which was stained with Dylight400. In Figure 15 HEK293 cells transfected with ApoER2_mCherry (A-C), ApoER2Δ16_mCherry (D-F), VLDLR_mCherry (G-I, M-O), EGFR_mCherry (J-L) and mCherry (P-R) are shown. Treatment with RCM was carried out for 3min at 37°C and cells were fixed, stained with Reelin primary AB G10 and as secondary AB Goat anti–Mouse IgG (H+L) Highly Cross-Adsorbed Secondary Antibody, Alexa Fluor 488 A-11001 822387 was used. Additionally, all experiments were repeated with another antibody conjugated to a Dylight 633 AB to exclude bleed through, which can happen when using filters

for fluorescence microscopy that detect light spectra which are to some point overlapping. (Additional data with Dylight 633 staining are included in Figure 25.) DAPI staining was carried out as above, cells were mounted on glass slides and imaged with LSM700. Upon Reelin treatment one can see that cells transfected with ApoER2 (Figure 15, A-C) develop many spikes and protrusions. Reelin signalling is crucial during brain development. It gets processed, diffuses and is bound by postmitotic neurons which at first express ApoER2. They are

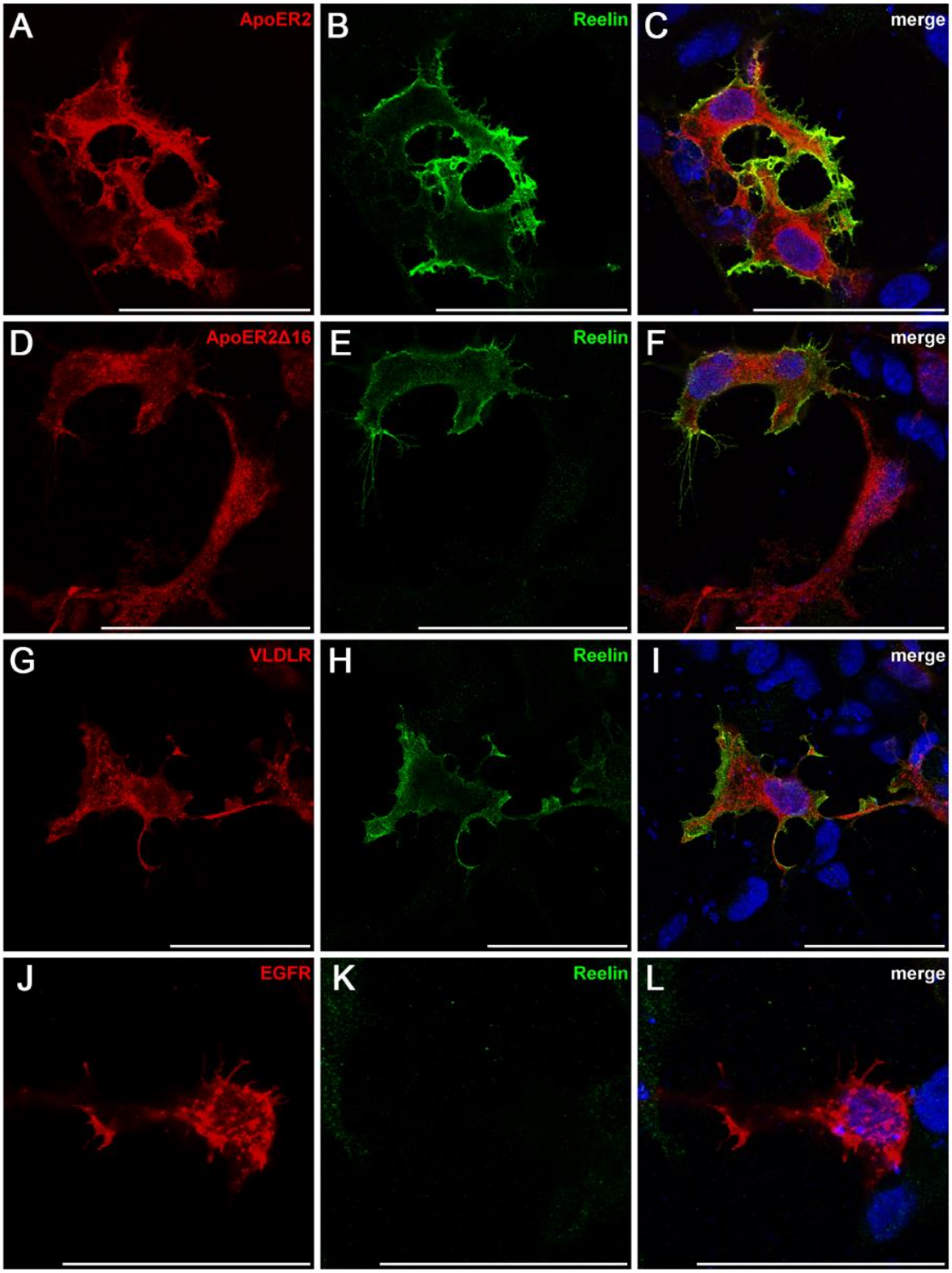

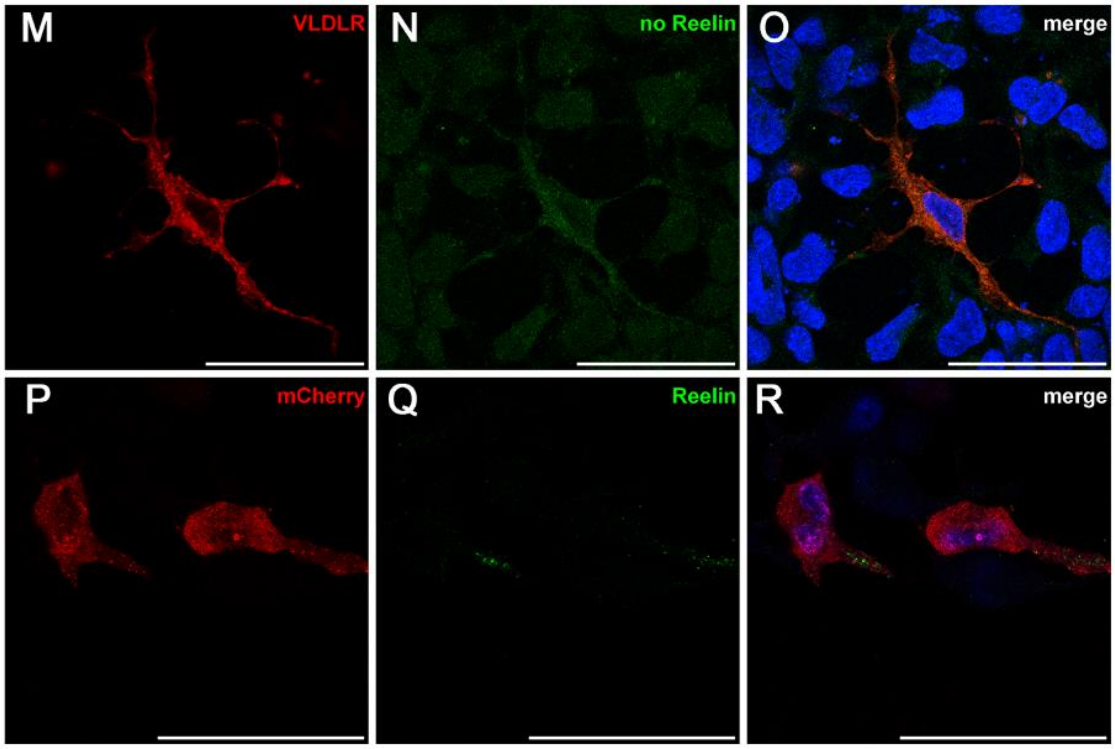

Figure 15 Reelin binding to receptors. Fluorescent images of HEK293 cells transfected with ApoER2 (A-C), ApoER2Δ16 (D-F), VLDLR (G-I, M-O), EGFR (J-L) linked to a mCherry fluorophore and mCherry alone (P-R). Conditions (A-L, P-R) were treated for 3min at

depolarized and multipolar migration of them is initiated, which leads to formation of protrusions in various directions. Neurons are re-polarized, and their movement is changes to locomotion and finally to terminal somal translocation. This process is orchestrated by full length reelin and an increasing expression of VLDLR [16,74].

This effect was not visible in cells treated with EGF (Figure 14,A-C). In Figure 15 D cells expressing ApoER2Δ16 are shown. Interestingly, only one of those two cells bind Reelin on the plasma membrane, although, no difference in levels of receptor expression and location can be detected. As the extracellular O-linked sugar domain is missing, there could be a structural difference that retains the variant in large numbers in the Golgi apparatus or the efficiency of membrane insertion is reduced. In Figure 15 G the distribution of VLDLR in the expressing cell is shown. When compared to cells expressing ApoER2 (Figure 15 A), less spikes are present but long protrusions are formed as well. In H (Figure 15) the bound Reelin is visible, and in the merge (Figure 15, I), the binding of it to the receptor is nicely demonstrated. The expression of EGFR (Figure 15, J) also looks good and no bound Reelin can be found in the green channel (Figure 15,K). The cells still formed a lot of spikes upon EGFR expression, which was already observed in the EGF binding experiment (Figure 14). In Figure 15, M-O the included control, were a cell expressing VLDLR, treated with MCM instead of RCM is shown. The cell structure with long protrusions is visible again, but the signal in the green channel is missing. The second included control, where mCherry alone was expressed is shown in Figure 15 P-R. MCherry (P) is distributed in the whole cell and Reelin is not present at the plasma membrane in this condition (Q). As expected, no binding that was not already described before could be detected and all interactions of the Reelin and the EGFR pathways, that were discovered before, could be reproduced. There is no overlap of both pathways at the receptor/ligand level.

In parallel an experiment was carried out by one of my colleagues to evaluate downstream events of the receptors. HEK293 cells expressing fluorescently tagged EGFR and Dab1 were fixed and analyzed via fluorescent microscopy. The results are shown in Figure 1D of Dlugosz et al,2021. [109].

A positive control with cells expressing ApoER2_mcherry in parallel with Dab1_mGFP and a negative control were fluorophores (mCherry, mGFP) only were expressed, was included. The colocalization can be detected through merging images derived from the green and red fluorescent channel. When proteins colocalize, the resulting image color is yellow. As this was the case, we could show that the EGFR receptor and the Dab1 protein colocalize when co-expressed in one cell. Additionally, we validated this on the protein level as well. For this, HEK293 cells were transfected with EGFR and Dab 1 and via co-immunoprecipitation with an EGFR-specific antibody Dab1 could be pulled down (Figure 1B,[109]). This was also possible with a Dab1 specific antibody. In this case EGFR could be pulled down (Figure 5,[109]). All previously mentioned components could also be found in mouse neurons, and we also were able to precipitate EGFR and small amounts of Dab1 could be detected (Figure 1C, [109]).

Colocalisation of Receptors

As it was already known that ApoER2 and VLDLR are capable of forming heterodimers and receptor clusters at the membrane, when co-expressed [16]. Another goal of my project was to find out if EGFR can also be included in such clusters when co-expressed with ApoER2 and/or VLDLR. For this ApoER2_mGFP, ApoER2Δ16_mGFP and VLDLR_mGFP together with EGFR_mCherry were expressed in HEK cells and visualized by fluorescence microscopy. As we already had the knowledge, that EGFR and Dab1 colocalize, we included this condition as a positive control as well as to further validate our results observed by other experiments. mGFP and mCherry transfected cells were used for negative controls [109].

In Figure 16,A expression of ApoER2 is shown. When compared to other experiments, that were carried out during my master project (Binding of EGF/Reelin to different receptors, morphological changes of cells transfected with different Receptors), it looks like there is a reduced amount of ApoER2_mGFP in the cell membrane under the conditions used in this experiment. Also, the amount of membrane spikes lined with ApoER2, which were observed in other experiments, are not seen here. In B expression of EGFRmCherry is shown. This receptor reaches the membrane and is also located in several protrusions formed by the cell. In the merge of both channels, it is visible, that only EGFR seems to reach the membrane, when both receptors are present in the cell. There is one strong yellow signal visible, which probably is the result of some aggregates of both proteins.

Although ApoER2 and EGFR seem to co-localize in some regions inside the cell, which could be organelles producing, altering, and transporting them, the protein that reaches the membrane is almost exclusively EGFR. In the case, where colocalization of ApoER2Δ16 and EGFR was assessed, the same results were obtained. ApoER2Δ16 is distributed throughout intracellular membranes but doesn't reach the spikey protrusions formed by the cells, where EGFR is found. In this case the localizations of both receptors seem to be even more exclusive (Figure 16; D-F). Co-expression of VLDLR and EGFR also results in different localization of both receptors. Again, EGFR is found majorly in the plasma membrane and its spiky protrusions, whereas VLDLR is located in organelles and vesicles within the cells (Figure 16; G-I).The first control that is shown in the figure is the one where the receptors of the Reelin Pathway were replaced by mGFP, which results in an even distribution of the green signal inside the cell in the nucleus. The spikes which are seen in cells expressing EGFR are still formed and visible because the receptor is inserted into the plasma membrane (Figure 16; J-L).

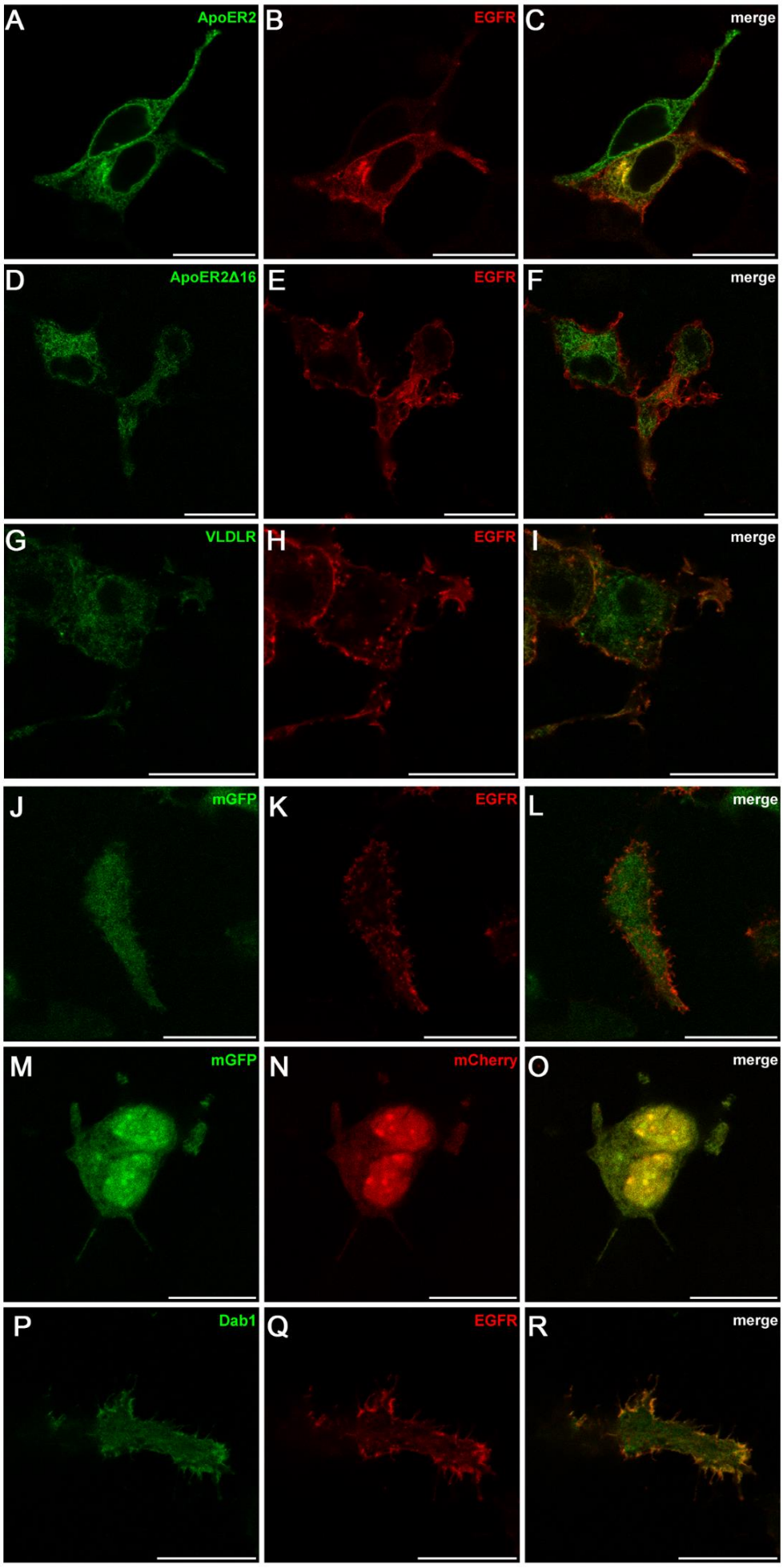
A
ApoER2
B
EGFR
C
merge
D
ApoER2Δ16
E
EGFR
F
merge
G
VLDLR
H
EGFR
I
merge
J
mGFP
K
EGFR
L
merge
M
mGFP
N
mCherry
O
merge
P
Dab1
Q
EGFR
R
merge

Figure 16 Colocalisation. HEK 293 cells cotransfected with plasmids carrying ApoER2_mGFP and EGFP_mCherry (A-C), ApoER2Δ16_mGFP and EGFR_mCherry (D-E), VLDLR_mGFP and EGFR_mCherry (G-I) are shown. As negative controls mGFP and EGFR_mCherry (J-K) and mGFP and mCherry (M-O) and as a positive control Dab1_mGFP and EGFR(P-R) are included. Cells were fixed, mounted and visualized with LSM700.

The second negative control was done by co-expression of both fluorophores that were used in the other conditions. As they are distributed in a similar way and not sorted to special compartments, the result of the channel merge is an even yellow signal (Figure 16; M-O).

The positive control was done with cells expressing Dab1 and EGFR and shows how colocalization of proteins with attached fluorophores looks like. Although Dab1 is an intracellular adaptor protein and found throughout the cytosol, the major amount is located very close to the membrane and therefore to the EGFR that is located there. Because of the closeness of both proteins, the signal in the merge again appears yellow. This was also shown in our paper and is mentioned above. With this very similar experiment we could show that EGFR and Dab1 that were co-expressed in HEK293 cells, are colocalizing ([109], Figure1D).

Morphological changes of cells transfected with different Receptors

As cells expressing the receptors seem to have differences in their shapes, we wanted to take a closer look at them to make sure, observations of morphological changes during our previous experiments with Reelin and EGF indeed are happening.

We saw formation of spikes in cells expressing ApoER2 which were treated with Reelin. Long protrusions were built by cells expressing VLDLR. When ApoER2Δ16 was present some protrusions were formed. In some cases of ApoER2Δ16 expression no spikes were visible at all. To validate this observation, we stained the cells for F-actin, which is part of the cellular cytoskeleton and therefore strongly associated with the cell membrane by Phalloidin staining for fluorescent microscopy [111].

By phalloidin staining, all cells, including the ones not expressing the receptors are stained. HEK293 cells were again transfected with plasmids carrying the genes of either ApoER2_mGFP, ApoER2Δ16_mGFP, Dab1_mGFP, VLDLR_mGFP or mGFP alone and after fixation they were stained with Phalloidin red. During PFA fixation of cells it is crucial to avoid using methanol[112] to prevent disruption of phalloidin. In Figure 17 A, a cell expressing ApoER2 is shown and in the spikes and some protrusions, which are formed, also contain the receptor.

Here (Figure 17 ,B) it is visible, that HEK293 cells, not expressing ApoER2 are also capable of forming protrusions without receptor expression. In the merge (Figure 17, C), where DAPI staining is included, one can see, that the receptor is located in close proximity to F-actin (white arrowhead). When (Figure 17, D), ApoER2Δ16 was expressed it seems, that the cell shape is completely different when compared to cells expressing ApoER2(A). The surface looks way smoother and overall, the cells look more elongated. With Phalloidin staining (E) it is visible, that those cells still have various small protrusions/filopodia, regardless of receptor expression. However, it looks like that there is a localization difference between ApoER2FL and ApoER2 Δ16. In the merge(F) it is clearly visible, that the ApoER2 Δ16 isoform doesn't sort to areas where small filopodial protrusions are formed (white arrowhead). In the next experiment, where the expression of the adaptor protein Dab1 was induced (G-I), one can see, that the intracellular protein is able to locate very close to the membrane, as it can be found in all spikes and protrusions the cell has formed. When compared to ApoER2, Dab1 seems to be equally distributed in the cytosol, as the green signal is more even, whereas the ApoER2 signal is present in varying concentrations, which makes sense because the receptor is known to cluster in the membrane and inside the cell it is either found in vesicles, the ER and the Golgi apparatus. In the experiment, where cells expressing VLDLR (J-L) the cells differ a bit in shape as they are more elongated when compared to cells expressing ApoER2. They seem to have more in common with the shape of cells expressing ApoER2Δ16. The receptor is found in the protrusions built by the cell (L, white arrowhead). In some cases, some aggregates have built, indicated by strong signals which can be seen in the upper cell that is depicted.

In the last row (Figure 17, M-O), the control cells expressing mGFP only are shown. The protein has no sorting signal attached and is evenly distributed in the cell and is not seen in the protrusions of the cell.

The shape differences of cells previously seen expressing different ApoER2 variants could not be verified, instead we could determine that the ApoER2Δ16 variant is not always inserted into the plasma membrane as the full-length isoform. To get to know the exact cause why this is the case one has to have a closer look at the exon 16 and the process of glycosylation in the ER. Dab1 and VLDLR are both colocalized with the actin network and found in extensions of cells.

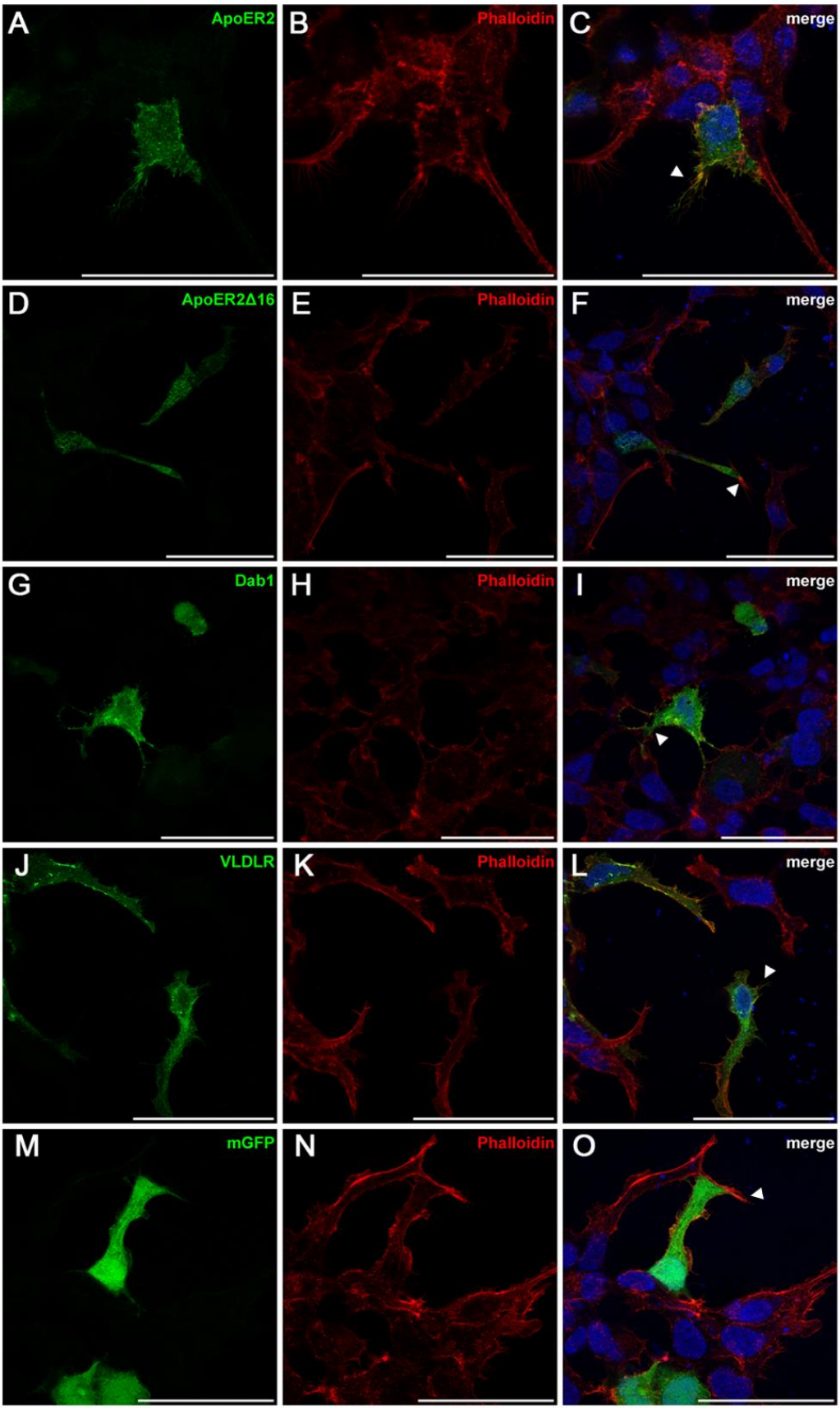

Figure 17 Cell shape changes. HEK293 cells expressing ApoER2_mGFP (A-C), ApoER2Δ16_mGFP (D-E), Dab1_mGFP (G-I), VLDLR_mGFP (J-K) and mGFP (M-O). Cells were fixed and stained with Phalloidin red (4,95µM) and DAPI. Afterwards they were mounted and visualized with LSM 700. Scale bars represent 50µm. White arrowheads indicate where protrusions formed by Actin structures are visible. In the conditions with cells expressing ApoER2Δ16_mGFP and mGFP the corresponding protein is not found in those areas whereas in other all other conditions a colour shift occurs due to overlapping actin and protein locations.

Dab1 and EGF/EGFR

Dab1 is an important adaptor protein in the Reelin pathway, which gets phosphorylated Src-family kinases when Reelin binds to ApoER2 or VLDLR. To discover hitherto unknown functions of Dab1 a corresponding knockout cell line was established in the lab.

Dab1 KO verification

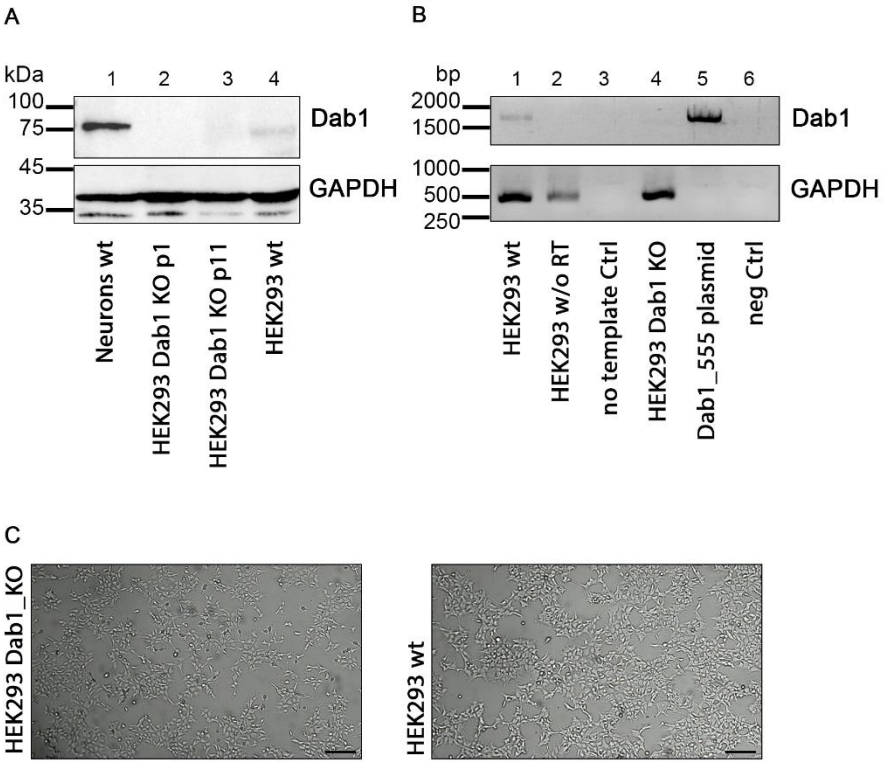

Figure 18 HEK293 Dab1 KO verification. **A**. Comparison of Protein expression of Dab1 through SDS-PAGE and Western blot in Neurons (DIV3, 1), HEK293 Dab1 KO after one (2) and 11 (3) passages and HEK293 wt(4). **B**. Control of Dab1 expression on mRNA level through RT-PCR. HEK293 wt (1) and HEK293 Dab1 KO cell lysates (4) were used and mRNA was extracted. Controls such as without Reverse Transcriptase Enzyme (2) and without template (3) were included. As a positive control Dab1_555 plasmid DNA was included in the subsequent PCR. The negative Control (6) without DNA was added for the PCR as well. GAPDH was included in both conditions (SDS-PAGE/Western blot and RT PCR) as loading control. **C**. HEK293 Dab1_KO and HEK293 wt cells were seeded with a density of $3x10^5$ cells/ml and pictures were taken after 24h.

The used cell line was HEK293 cells which is known to express low amounts of Dab1. The method used for the creation of the knockout line was CRISPR-Cas9 and it was done by a colleague before my project started. To make sure, that the establishment of the HEK293 Dab1 KO cell line worked, a verification on protein and further mRNA level was carried out.

First several clones were tested on protein levels via SDS-Page and Western blot. After some passages of the cells in culture dishes, we wanted to verify that they did not have regain their ability to express Dab1 after some time. Two lysates of HEK293 Dab1 KO cells, differing in their passage number (1 and 11) were compared (Figure 18A, lanes 2 and 3). As control Neurons which are known to express high numbers of Dab1 as well as HEK293 wt cells were included. Dab1 levels (panel 1) were detected with D4 antibody and GAPDH levels (panel 2) were included as loading control. As this was confirmed via SDS-Page followed by Western blotting, a RT-PCR was included to make sure, cells also lacked ability to build Dab1 on mRNA level and results are displayed in Figure 18B. Dab1 mRNA was found in HEK293 wt cells (panel 1, lane 1) and can be compared to the Dab1_555 positive control (panel 1, lane 5). In HEK293 Dab1 KO cells Dab1

mRNA was absent (panel 1, lane 4). Controls such as no RT (2), no template (3) and a negative control for the PCR (6) were included as well as a loading control with GAPDH (panel 2). Because of growth differences, that were observed during maintenance of the HEK293 wt and KO cell lines (Figure 18C), further experiments to characterize these differences were carried out. The methods chosen were the EdU- proliferation assay as well as the WST- metabolic activity/proliferation assay.

EdU- click it proliferation assay

To evaluate cell proliferation the EdU-click assay was used. 5-ethynyl-2'-deoxyuridinde (EdU) is an analogue of the thymidine nucleoside and is actively incorporated into newly synthesized DNA. Through a cycloaddition reaction a fluorescent azide is coupled to EdU and can be monitored with a fluorescent microscope [113].

The fluorescent dye being used was Alexa Fluor 488 and all cells where DNA replication took place were detected and counted and compared to the total amount of cells that were detected with DAPI staining. Exact protocol details can be found in the material and methods section above. The proliferation rate of HEK293 cells lacking Dab1 was compared to HEK293 wt. and an additional experiment where the k.o. phenotype was rescued via transfection with an expression plasmid for Dab1. The result of the experiment is presented in Figure 19. Already, when looking at the fluorescent microscopy images of the three conditions (Figure 19A), one could see, that there are less green colored nuclei in HEK293 Dab1 KO cells(A:D), when compared to the wt cells (A:A) and to the rescued (A:G) condition. For each condition ten technical replicates were created as different areas were observed and imaged. The DAPI stained nuclei are depicted in A:B, E, H and additionally a merge of both channels is included in A:C, F, I. The images of Figure 19A were further processed with ImageJ/Fiji, as shown in Figure 19B. First, the threshold of the images had to be adjusted to get areas with a size big enough for counting as well as to connect grainy colored areas for increased quality when counting. Next, images were processed to binary and watershed. The watershed option was used to separate nuclei that were positioned too close to each other. The processed images are shown in the upper column in Figure 19B (A-C for EdU, G-I for DAPI). Mostly, the processing worked nicely, but sometimes the separation did not work perfectly, and corrections were done by hand. As a next step, the areas bigger than 50µm2 were counted and exported into an excel sheet. The counts were put into relation to each other and visualized with GraphPad Prism which is shown in Figure 19C. The analysis via one-way ANOVA with multiple comparisons shows a significant growth difference (**p≤ 0.01) between cells expressing Dab1 (HEK293 wt, HEK293 Dab1 KO/Dab1_555) and the k.o. cells (HEK293 Dab1 KO). What can be observed as well, is that the phenotype established through Dab1 knockout, could be rescued via transfection of the cells with a plasmid carrying the DNA of the respective gene.

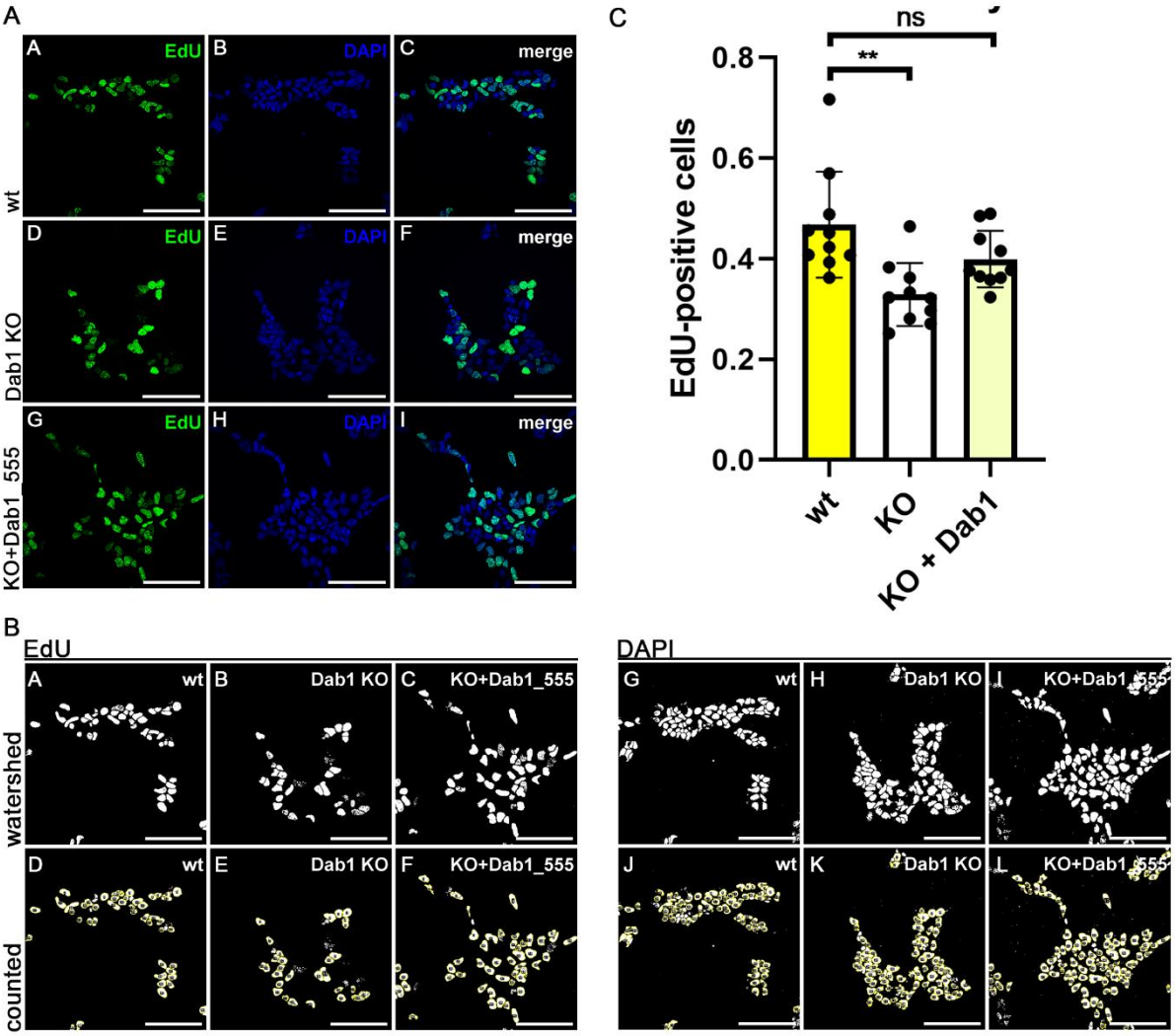

Figure 19 EdU proliferation assay. **A**. Fluorescent microscopy images of HEK293 wt, Dab1 KO and Dab1. KO expressing Dab1_555. They were treated with 10µM of EdU for 2h at 37°C and incorporated bases were made visible via Click-iT assay with AlexaFluor 488 (EdU, A, D, G). The total amount of DNA was stained with DAPI (B, E, H). The merged images of the depicted conditions are shown in C, F and I. **B**. For further analysis the images shown in A were threshold adjusted, processed to binary and watershed for EdU and DAPI channels separately (A-C, G-I). As a last step, particles bigger than 50µm2 were counted (D-F, J-K). **C**. Counted EdU and DAPI stained nuclei were set into relation and analysed via one-way ANOVA multiple comparisons test. Scale bars represent 100µm and for analysis ImageJ and GraphPad Prism were used and ten different fields of view were taken into account.

WST-1 proliferation/metabolic activity

To validate the DNA replication based proliferation assay a metabolic proliferation assay was performed. With the help of a tetrazolium salt (WST-1) the cell proliferation and metabolic activity can be measured. Formazan is formed by cleaving of WST-1 in metabolically active cells. NAD(P)H production during glycolysis is necessary for this reaction to happen. As glycolysis is a crucial process in viable cells, the amount of built formazan is correlating to the metabolic activity of cells. With colorimetric methods, formazan can be measured at λ 440-480 and differences in metabolic activity of cell lines can be compared. [114]

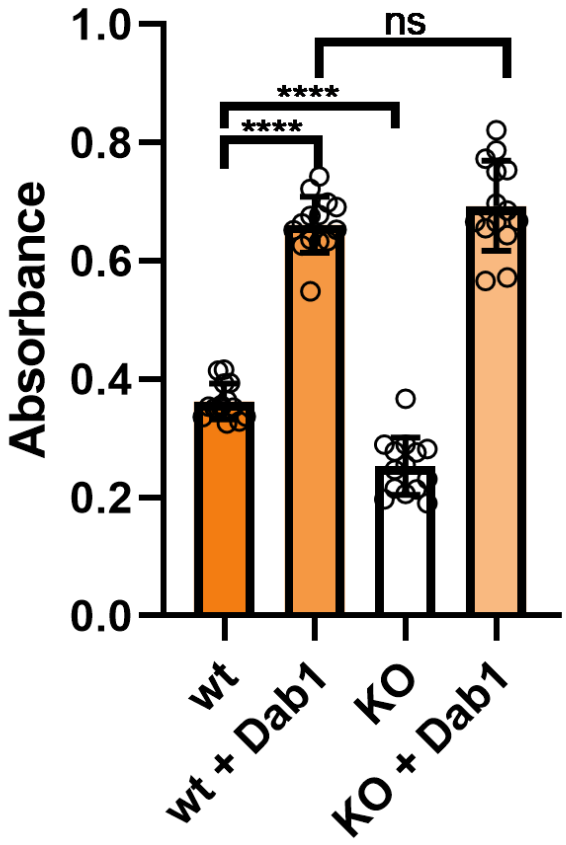

Figure 20 WST-1 assay analysis. HEK293 wt and HEK293 Dab1 KO cells transfected with pClneo(wt+KO conditions) or with Dab1_555. WST-1(10nM) was added to each well. Absorbance of 480/30nm was measured after 2h. Two independent experiments were carried out with 7 replicates of each condition. Analysis was done via excel and graph pad prism. One-way ANOVA with Tukey's multiple comparison test was carried out. ****p≤0.0001; ns not significant;circles, replicates.

Cells were seeded and prepared as mentioned in the material and methods section. Two independent experiments were carried out and for each condition seven replicates were done. The results of the analyzed assay are shown in Figure 20. To treat all cells in the same way, controls for each cell line were transfected with an empty plasmid (pCLneo, wt and KO). The metabolic activity and proliferation can be affected during the process of transfection. To check if, indeed, the reduced cell proliferation seen in cells lacking Dab1 again a rescue experiment was included (KO+Dab1). Furthermore, an over-expression experiment was also carried out to see if an increased amount of Dab1 in wt cells can changes metabolic activity of those cells. What could be seen, was, that the metabolic activity of Dab1KO cells is indeed reduced when compared to the wt cell line. This result goes along with the one we acquired with the EdU-assay. Additionally, we could see, that the metabolic activity increases after transfection with Dab1. Interestingly, the metabolic activity of cells transfected with Dab1 not only increases which corresponds to the results obtained with the proliferation assay, but it even exceeds activity seen in HEK293 wt cells by far. This effect could be observed after transfection of HEK293 Dab1 KO cells with the Dab1 plasmid (KO+ Dab1) as well as after transfection of the HEK293 wt cell line (wt+KO).

Dab1 Phosphorylation through EGFR/EGF

As shown in Binding of EGF/Reelin to different receptors we could exclude that a cross talk between the EGFR and Reelin pathway at receptor level exists. Interestingly, we could identify three NPXY motifs at the intracellular domain of EGFR Therefore we decided to check, if Dab1, which is known to interact with ApoER2 and VLDLR through the same motif, could possibly bind to EGFR. The three motifs that exist are highlighted in green in Figure 21 where the sequence acquired from NCBI is depicted. Additionally, the transmembrane region is highlighted in red. Sequence alignment of EGFR with ApoER2 and VLDLR was presented in Dlugosz et al, 2021 [109,115].

>NP_005219.2 epidermal growth factor receptor isoform a precursor [Homo sapiens]
MRPSGTAGAALLALLAALCPASRALEEKKVCQGTSNKLTQLGTFEDHFLSLQRMFNNCEVVLGNLEITYV
QRNYDLSFLKTIQEVAGYVLIALNTVERIPLENLQIIRGNMYYENSYALAVLSNYDANKTGLKELPMRNL
QEILHGAVRFSNNPALCNVESIQWRDIVSSDFLSNMSMDFQNHLGSCQKCDPSCPNGSCWGAGEENCQKL
TKIICAQQCSGRCRGKSPSDCCHNQCAAGCTGPRESDCLVCRKFRDEATCKDTCPPLMLYNPTTYQMDVN
PEGKYSFGATCVKKCPRNYVVTDHGSCVRACGADSYEMEEDGVRKCKKCEGPCRKVCNGIGIGEFKDSLS
INATNIKHFKNCTSISGDLHILPVAFRGDSFTHTPPLDPQELDILKTVKEITGFLLIQAWPENRTDLHAF
ENLEIIRGRTKQHGQFSLAVVSLNITSLGLRSLKEISDGDVIISGNKNLCYANTINWKKLFGTSGQKTKI
ISNRGENSCKATGQVCHALCSPEGCWGPEPRDCVSCRNVSRGRECVDKCNLLEGEPREFVENSECIQCHP
ECLPQAMNITCTGRGPDNCIQCAHYIDGPHCVKTCPAGVMGENNTLVWKYADAGHVCHLCHPNCTYGCTG
PGLEGCPTNGPKIPSIATGMVGALLLLLVVALGIGLFMRRRHIVRKRTLRRLLQERELVEPLTPSGEAPN
QALLRILKETEFKKIKVLGSGAFGTVYKGLWIPEGEKVKIPVAIKELREATSPKANKEILDEAYVMASVD
NPHVCRLLGICLTSTVQLITQLMPFGCLLDYVREHKDNIGSQYLLNWCVQIAKGMNYLEDRRLVHRDLAA
RNVLVKTPQHVKITDFGLAKLLGAEEKEYHAEGGKVPIKWMALESILHRIYTHQSDVWSYGVTVWELMTF
GSKPYDGIPASEISSILEKGERLPQPPICTIDVYMIMVKCWMIDADSRPKFRELIIEFSKMARDPQRYLV
IQGDERMHLPSPTDSNFYRALMDEEDMDDVVDADEYLIPQQGFFSSPSTSRTPLLSSLSATSNNSTVACI
DRNGLQSCPIKEDSFLQRYSSDPTGALTEDSIDDTFLPVPEYINQSVPKRPAGSVQNPVYHNQPLNPAPS
RDPHYQDPHSTAVGNPEYLNTVQPTCVNSTFDSPAHWAQKGSHQISLDNPDYQQDFFPKEAKPNGIFKGS
TAENAEYLRVAPQSSEFIGA

Figure 21. FASTA amino acid sequence result of EGFR precursor isoform. The transmembrane region is highlighted in red, NPXY motifs are highlighted in green.*(NCBI, 05/07/23)*

First, my colleague determined if EGFR could pull down Dab1 and compared the effect with ApoER2. Indeed, it was possible to pull down Dab1 in both conditions, while using HEK293 transfected cells as well as in mouse embryonic neurons (E13.5). Additionally, we wanted to check if both proteins are found in the same areas of cells. This was verified by expressing fluorescently tagged EGFR and Dab1 in HEK cells and imaging via confocal fluorescent microscopy. The results of both experiments can be found in Dlugosz et al 2021 in Figure 1[109]. As interaction and colocalization of both proteins could be detected, as a next step we wanted to know if it is possible to phosphorylate Dab1 in a HEK293 stable cell line via transfection of cells with EGFR and Dab1 and treatment with EGF. We could see that Dab1 phosphorylation upon EGF indeed was happening and we set up an experiment to follow the time course of levels of our proteins of interest. For the time course we treated the cells with 10ng/ml of hEGF. We also wanted to see if Dab1 phosphorylation depends on kinase activity of EGFR and its autophosphorylation. Thus, we decided to block this process with the help of known inhibitors. First the irreversibly binding tyrosine kinase inhibitor Neratinib was used. In Figure 22 four different blots of the time course experiment are shown.

For this specific experiment HEK293 cells were transfected with plasmids coding for EGFR and Dab1(A: lanes 1-6, B: lanes 8-13), VLDLR, EGFR and Dab 1 (A: lanes 7-12, B: 1-6), VLDLR and EGFR (A: 13, B: 7) and VLDLR and Dab1 (C, D). In Figure 22A (the original blot is shown in supplementary in Figure 24) total lysates were used for SDS-PAGE and Western blotting. Phosphorylated EGFR (panel 1, pEGFR) and Dab1 (panel 3, D4) were visualized with specific antibodies. To check if protein levels are comparable the housekeeping protein GAPDH was included. The blot was stripped and reblotted with an antibody against VLDLR to check the transfection efficiency. The goal of this experiment was to see if there is some Dab1 degradation happening, depending on the duration of treatment with EGF. As expected, upon EGF treatment, a robust phosphorylation of EGFR could be detected. Phosphorylation of the receptor was absent when EGF was omitted (IM:1,7) and when the cells were pretreated with the kinase inhibitor (Neratinib: 4,6,10,11). There were no differences of Dab1 levels observed in panel 3, which indicates that Dab1 does not get degraded after 20 min of EGF treatment.

In the second blot (Figure 22B) results from a Dab1 pull down with α54 antibody are shown. Phosphorylation of Dab1 (panel1) and EGFR (panel 3) were detected with PY99 and the blot was stripped and reblotted for Dab1 total levels (panel 2) with D4. Although Dab1 levels seem to differ (panel 2), most likely due to high levels of protein after the first staining of the blot. Through the high capability of HEK293 to express genes from transfected plasmids, detection of the corresponding proteins is easier. However, the disadvantage of this effect is that strong bands can be detected (B: 2,3,5,9,10,12), which may lead to a stripping and to a problem by re-probing the blots with a second antibody (B: panel 2). One can easily see, that especially, in lanes where

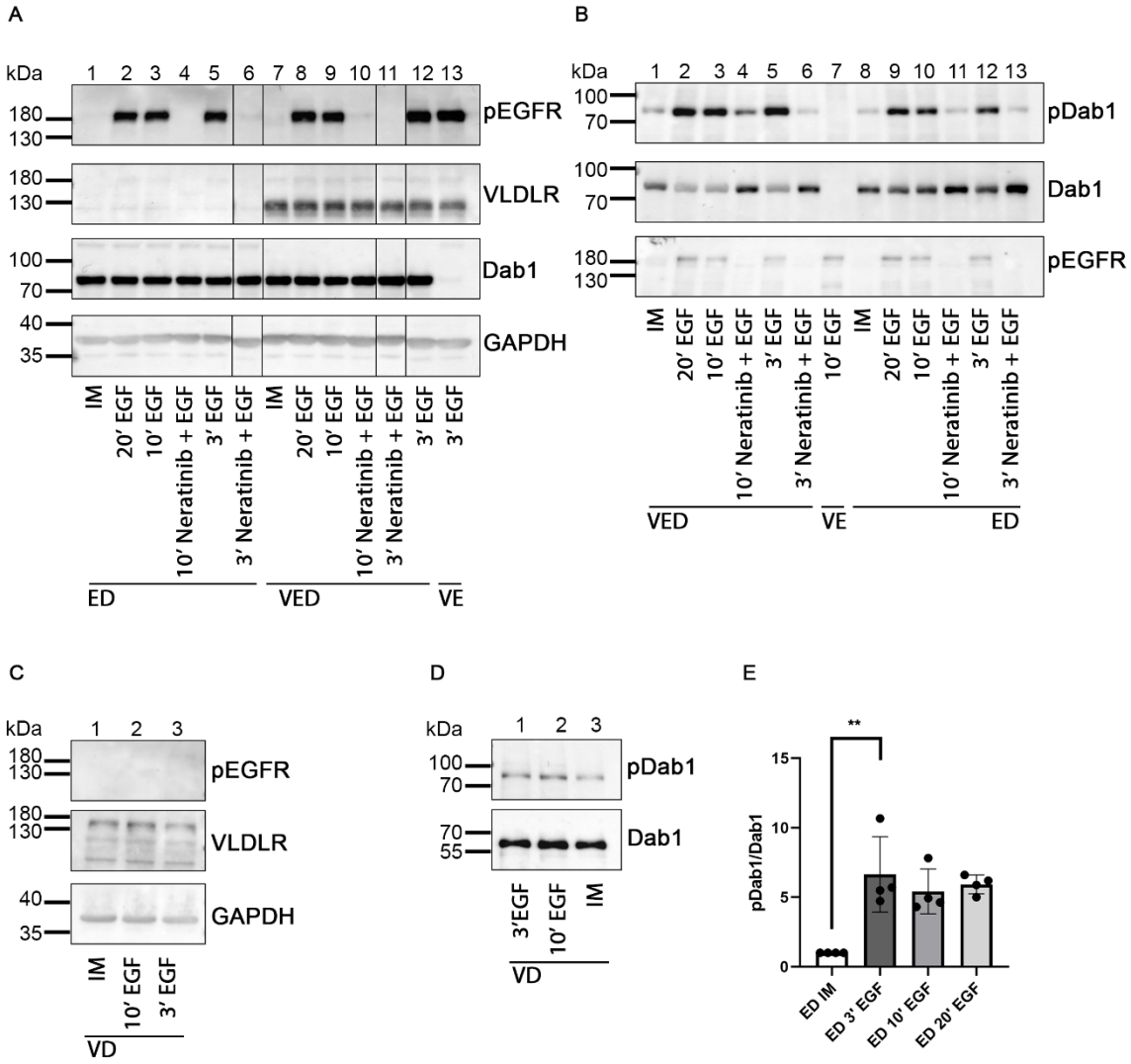

Figure 22 Dab1 Phosphorylation through EGF pathway with HEK293 cells. **A**. HEK29 cells transfected with EGFR and Dab1 (lanes 1-6), VLDLR, EGF and Dab1 (lanes 7-12) and VLDLR and EGFR (lane 13) were treated with IM (lanes 1,7) or with EGF for 3min (lanes 5,6,11-13), 10min (lanes 3,4,9,10) or 20min (lanes 2,8). Phosphorylated EGFR levels (panel 1), VLDLR (panel2) and Dab1(panel 3) levels were checked. Neratinib was included as Inhibitor for EGFR signalling (lanes 4,6,10,11) and total protein levels were compared through GAPDH controls (panel 4). Cells were lysed and analysed via SDS-PAGE and Western Blot. Lanes 6 and 11 were loaded incorrectly, the lanes were exchanged to simplify the figure. Original blots can be found in supplementary. **B**. Cell lysates were acquired in the same way as mentioned in A and used to run a Co-IP. Dab1 was pulled down via a54. pEGFR (panel 3) and pDab1(panel1) levels were checked with a phosphotyrosine specific AB (PY99). The Dab1 blot was stripped and reblotted with Dab1 AB for total AB levels. **C**. Control carried out in HEK293 cells with VLDLR and Dab1 transfection and EGF treatment for 3 and 10min. pEGFR (panel 1), VLDLR (panel 2) and GAPDH (panel 3) levels are shown and were acquired from total cell lysates. **D**. Dab1 phosphorylation control upon EGF treatment without EGFR. Dab1 phosphorylation via PY99 (panel1) and total Dab1 levels (panel 2) are shown after Immunoprecipitation with α54. **E**. Relative levels of phosphorylated Dab1 are presented. Western blots were scanned with ChemiDoc Touch Imaging System (BioRad), analysed via ImageLab (BioRad), set into relation in Excel and visualised with Graph Pad. Bands were normalised with Dab1 and mock controls were set to 1. Unpaired, two-tailed t-test was used for analysis. * $p \leq 0.05$, ** $p \leq 0.01$, ns, not significant; dots, number of independent experiments. Error bars represent standard deviation.

strong bands of pDab1 could be detected, the detection of Dab1 was decreased. Because of this, we decided to use less plasmid DNA for transfection of HEK293 in the following experiments and also decided to additionally include NIH3T3 cells, which tend to express less protein from transfected plasmids. EGFR phosphorylation and successive Dab1 phosphorylation by EGF treatment could be detected nicely through pull down, too. In my HEK293 overexpression system the phosphorylation levels of Dab1 and EGFR did not go down after 10 and 20min of treatment. My colleague redid this experiment, using less DNA for transfection, and could detect a reduction of phosphorylation (Figure 2A, [109]). We also included controls to make sure that the observed effect indeed depends on EGFR. Thus, we also included a condition where EGFR was missing. In Figure 22C the same as in A was done, with exclusion of EGFR. Of course, detection of phosphorylated EGFR (panel 1) was therefore not possible. VLDLR (panel 2) and GAPDH (panel 3) levels were evenly distributed in the different conditions. In Figure 22D, a pull down of Dab1 was carried out via α54 from cell lysates prepared in the same way as in C. The observed Dab1 phosphorylation levels were similar at a low level in all three conditions and after stripping the blot and reblotting it with D4, the levels of Dab1 were even as well. Blots from four different experiments were then analysed via Image Lab, a software provided by BioRad. With this application, the signals acquired via ChemiDoc can be set into relation, including total protein levels imaged via ponceau or GAPDH levels. Background signals can be subtracted, and the exact area of the detected bands can be defined. Adjusted Volumes (Intensity) were taken and copied to excel where pDab1 levels were set into relation with Dab1 total levels. The values obtained were transferred to Graph Pad and a two tailed t-test was performed. The results are shown in Figure 22E. A strong phosphorylation of Dab1 after 3 minutes of EGF treatment could be detected and with a p value under 0.01 the results were significant.

Last, I focused on our newly discovered crosstalk between EGFR and the Reelin pathway and designed an experiment to test the presence of this link in NIH3T3 cells. NIH3T3 cells were transfected via Ultracruz with plasmids coding for EGFR and Dab1 Figure 23A: lanes 1-4), ApoER2, EGFR and Dab1 (A: lanes 5-8) and VLDLR, EGFR and Dab1 (A: lanes 9-12). The proteins were detected as described above. In this case Dab1 phosphorylation was strongest after 3min of treatment with hEGF. After 10 and 20min a signal could still be detected but was already diminished greatly and almost as low as cells treated with IM only. EGFR phosphorylation, however, was stronger in cells transfected only with EGFR and Dab1 but not with ApoER2 and VLDLR. Additionally, the strongest phosphorylation signal of Dab1 is present in cells where only EGFR and Dab1 are present. This indicates, that ApoER2 and VLDLR might have a higher affinity towards Dab1 binding and compete with EGFR, if present. Again, inhibitors, blocking the kinase activity of EGFR were used to check the dependence of Dab1 phosphorylation on the active kinase domain of EGFR. This time Neratinib and, in addition, Gefitinib, an inhibitor, that reversibly binds EGFR, were used. The blot in Figure 23B shows that through blocking of EGFR autophosphorylation, Dab1 phosphorylation also could be prevented, suggesting a direct interaction of them with each other. In Figure 23E analysed data acquired from A and another experiment were visualized. The analysis was done in the same way as described above for HEK293 cells. This time data from only two independent experiments are shown. Although no significant difference could be detected in this specific experiment, a trend which shows increased phosphorylation of Dab1 upon EGF treatment can be seen. For our publication, results from four different experiments were taken for analysis and shows a robust phosphorylation of Dab1 after EGF treatment in NIH3T3 (Figure 2D,[109]) as tested by the two tailed t-test.

However, how exactly Dab1 gets phosphorylated still needs to be elucidated. It could be a direct interaction and activated EGFR itself phosphorylates Dab1 or some other kinase could be involved downstream of EGFR.

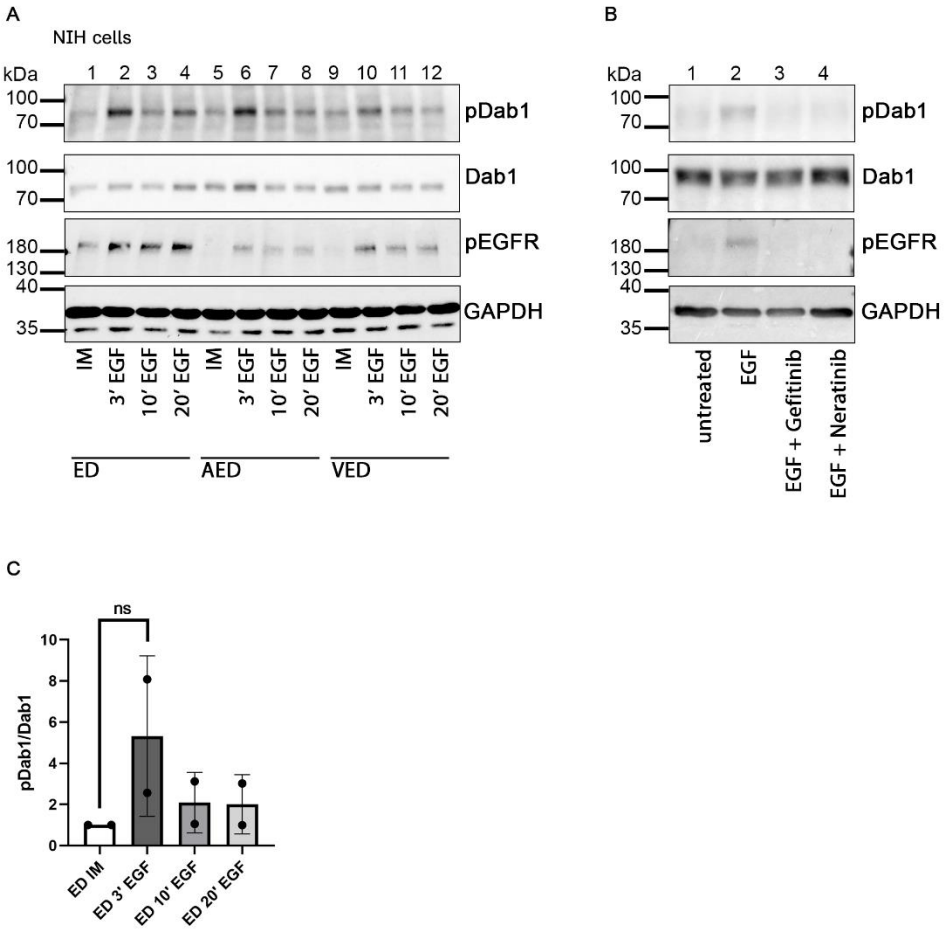

Figure 23 Dab1 Phosphorylation through EGF pathway with NIH3T3 cells **A**. NIH3T3 cells were transfected with EGFR and Dab1 (lanes 1-4), ApoER2, EGFR and Dab1 (lanes 5-8) and with VLDLR, EGFR and Dab1 (lanes 9-12). Cells were treated with IM (lanes 1,5,9,) or EGF for 3min (2,6,10), 10min (3,7,11) and 20min (4,8,12). Cells were lysed and analysed via SDS-PAGE and Western Blot. Phosphorylated EGFR (panel 3) and phosphorylated Dab1(panel1) levels were checked with a phosphotyrosine specific AB (PY99). The Dab1 blot was stripped and reblotted with Dab1 AB for total AB levels. GAPDH control was included for comparison of total protein levels. **B**. NIH3T3 cells were treated with EGF for 3 min (lane 2) and conditions including Gefitinib (lane 3) and Neratinib (lane 4) inhibitors were included. Phosphorylated EGFR (panel 3) and Dab1 (panel 1) levels were checked with PY99. GAPDH loading control (panel 4) was included and the Dab1 blot was stripped and reblotted to check total Dab1 levels (panel2). In each figure all panels correspond to the same blot. **C**. Relative levels of phosphorylated Dab1 are presented. Western blots were scanned with ChemiDoc Touch Imaging System (BioRad), analysed via ImageLab (BioRad), set into relation in Excel and visualised with Graph Pad. Bands were normalised with Dab1 and mock controls were set to 1. Unpaired, two-tailed t-test was used for analysis. * $p \leq 0.05$, ** $p \leq 0.01$, ns, not significant; dots, number of independent experiments. Error bars represent standard deviation.

Discussion

As presented in the results section my thesis is a compilation of results derived from different projects running in the lab during my work. Mainly my work consisted of experiments focusing on the EGFR and Reelin pathway to take us one step closer to understanding certain functions of these broad signalling cascade pathways.

One part of this work was focused on optimizing protocols for experiments which did not produce conclusive results at this time. I succeeded to optimize pull down experiments which according to my results heavily depend on the use of very fresh reagents.

Another interesting finding was that ApoER2Δ16, which lacks the o-linked sugar domain is not always properly sorted to the cell membrane und thus, not available for Reelin binding. Revealing

the cause for this effect would be very interesting. It could be, that large amounts of the protein are retained in the ER or Golgi, as some mechanism detects them as not properly folded. Furthermore, it could also be retained in endosomes. To resolving this problem, it would be first necessary to define the exact localization of the receptor inside the cell. Organelle sorting by ultracentrifugation could be one option to tackle this problem. Another possibility to check the exact localization of the mis-sorted receptor would be by confocal microscopy using markers for the different membrane compartments of the cell.

One interesting result of my work was the drastic decrease of bound N-Wasp to Dab1 in presence of Reelin. N-Wasp is an activator of the Arp2/3 complex and is involved in actin cytoskeleton remodelling. It is known to play an essential role in dendritic maturation and oligodendrocyte myelination[116,117]. It could be that without Reelin treatment cells are somehow in a resting state and N-Wasp is tethered to Dab1 while it is not needed and released and activated upon Reelin treatment. Of course, N-Wasp could also be involved in other pathways Dab1 plays a role in, for example the VEGFR pathway or the EGFR pathway. As the interaction of Dab1 and N-Wasp was also detected in primary cells this observation is most likely not an artifact produced by overexpressing cell lines. Maybe through studies with Isoforms or mutated Dab1, the mechanism of the interaction its function can be uncovered. It could be, that a phosphorylation or conformational change of Dab1 upon Reelin treatment decreases the affinity of it to N-Wasp.

Another thing, where many improvements await to be done is the setup of the wound healing assay. To sum it up, for further optimization of this experiment a way to acquire data in a more consistent way, to find significant differences, would be important. Thus, a method to dramatically increase transfection efficiency is needed. The use of stable cell lines expressing the gene of interest could be a big improvement. Unfortunately, the existing cell lines were contaminated with mycoplasma or had problems with protein expression. Additionally, it would be important to further optimize the protocol with NIH3T3 cells as they are a rather suitable model system for neurons under certain conditions [118] . Another potential step would be to check the 200µl tips prior to their use to determine that all of them look the same or maybe use the same tip for all conditions and wash it in between. As already mentioned, an increase of serum could improve the health of cells, too. A stronger reaction to ligands/reagents could possibly be the result, as cells are in a better shape. Because of these difficulties that still have to be solved and a lack of time, the treatment of the cells with full length Reelin was not included in the final experiment. Yet another option would be to use a completely different experimental set up such as a transwell or gradient assay [119].

In our paper[109], we could show, that Dab not only plays an important role in the Reelin pathway but is also bound by EGFR. This binding is mediated by the NPxY motif located on the intracellular domain of the receptor. Through EGF treatment, it was possible to phosphorylate Dab1, which is dependent on the kinase activity of the receptor. This could be validated by us via blocking it with inhibitors. My work in this paper mainly consists of showing that this system works in NIH3T3 cells, whereas my colleagues focused more on HEK293 cells and primary mouse neurons. Additionally, Dab1 plays an important role during proliferation and metabolic activity. This we could show via generating a Dab1 k.o. cell line based on HEK293 cells. In the publication, my part was to prove, that cells lacking Dab1 show reduced metabolic activity and proliferation. With EdU and WST assay it was shown that this was indeed the case.

As we could identify a hitherto unknown link of the EGFR and the Reelin pathway due to interaction of EGFR to Dab1, during our research some important next steps came to our mind[109]. To check where exactly Dab1 is bound to EGFR, mutations of its NPXY motives could be introduced and protein proximity assessed via Flim FRET[16] could be performed. Additionally, it would be interesting, which of the five phosphorylation sites of Dab1 are phosphorylated in the brain upon EGFR signalling. We could detect that Dab1 phosphorylation of tyrosine 232 is happening upon EGF but not upon Reelin treatment. It would be interesting as well, to see if different EGFR ligands change the Dab1 phosphorylation pattern. So far, we have just tested

EGF. Further we could detect a diminished signal of Dab1 P when ApoER2 and VLDLR were present in our experimental setup which indicates that Dab1 has a higher affinity to the Reelin receptors. Overall, the newly discovered link between the EGF and Reelin pathway in the intestines is very exciting and could possibly give rise to a new therapeutic target for the treatment of colorectal cancer [109,120,121].

Sources

1. Santana, J. & Marzolo, M. P. The functions of Reelin in membrane trafficking and cytoskeletal dynamics: implications for neuronal migration, polarization and differentiation. *Biochemical Journal* **474**, 3137–3165 (2017).

2. Jossin, Y. Reelin functions, mechanisms of action and signaling pathways during brain development and maturation. *Biomolecules* **10**, 1–31 (2020).

3. Bock, H. H. & May, P. Canonical and non-canonical reelin signaling. *Front Cell Neurosci* **10**, 195731 (2016).

4. D'Arcangelo, G. *et al.* A protein related to extracellular matrix proteins deleted in the mouse mutant reeler. *Nature 1995 374:6524* **374**, 719–723 (1995).

5. Falconer, D. S. Two new mutants, 'trembler' and 'reeler', with neurological actions in the house mouse (Mus musculus L.). *J Genet* **50**, 192–205 (1951).

6. Dulabon, L. *et al.* Reelin binds alpha3beta1 integrin and inhibits neuronal migration. *Neuron* **27**, 33–44 (2000).

7. Pinto-Lord, M. C., Evrard, P. & Caviness, V. S. Obstructed neuronal migration along radial glial fibers in the neocortex of the reeler mouse: a Golgi-EM analysis. *Brain Res* **256**, 379–393 (1982).

8. Jossin, Y. *et al.* The central fragment of Reelin, generated by proteolytic processing in vivo, is critical to its function during cortical plate development. *J Neurosci* **24**, 514–521 (2004).

9. D'Arcangelo, G. *et al.* Reelin Is a Ligand for Lipoprotein Receptors. *Neuron* **24**, 471–479 (1999).

10. Weeber, E. J. *et al.* Reelin and ApoE Receptors Cooperate to Enhance Hippocampal Synaptic Plasticity and Learning. *Journal of Biological Chemistry* **277**, 39944–39952 (2002).

11. Lee, G. H. & D'Arcangelo, G. New Insights into Reelin-Mediated Signaling Pathways. *Front Cell Neurosci* **10**, 1–8 (2016).

12. Yasui, N., Nogi, T. & Takagi, J. Structural basis for specific recognition of reelin by its receptors. *Structure* **18**, 320–331 (2010).

13. Manoharan, M., Muhammad, S. A. & Sowdhamini, R. Sequence Analysis and Evolutionary Studies of Reelin Proteins. *Bioinform Biol Insights* **9**, 187 (2015).

14. Engeroff, K., Warm, D., Bittner, S. & Blanquie, O. Different activity patterns control various stages of Reelin synthesis in the developing neocortex. *Cerebral Cortex* (2023) doi:10.1093/CERCOR/BHAD210.

15. Jossin, Y., Gui, L. & Goffinet, A. M. Processing of Reelin by Embryonic Neurons Is Important for Function in Tissue But Not in Dissociated Cultured Neurons. *The Journal of Neuroscience* **27**, 4243 (2007).

16. Dlugosz, P., Tresky, R. & Nimpf, J. Differential Action of Reelin on Oligomerization of ApoER2 and VLDL Receptor in HEK293 Cells Assessed by Time-Resolved Anisotropy and Fluorescence Lifetime Imaging Microscopy. *Front Mol Neurosci* **12**, 1–23 (2019).

17. Yasui, N. *et al.* Functional Importance of Covalent Homodimer of Reelin Protein Linked via Its Central Region. *J Biol Chem* **286**, 35247 (2011).

18. Okugawa, E. *et al.* Physiological significance of proteolytic processing of Reelin revealed by cleavage-resistant Reelin knock-in mice. *Sci Rep* **10**, 1–13 (2020).

19. Hashimoto-Torii, K. *et al.* Interaction between Reelin and Notch signaling regulates neuronal migration in the cerebral cortex. *Neuron* **60**, 273 (2008).

20. Ampuero, E., Jury, N., Härtel, S., Marzolo, M. P. & van Zundert, B. Interfering of the Reelin/ApoER2/PSD95 Signaling Axis Reactivates Dendritogenesis of Mature Hippocampal Neurons. *J Cell Physiol* **232**, 1187–1199 (2017).

21. Kushima, I. *et al.* High-resolution copy number variation analysis of schizophrenia in Japan. *Molecular Psychiatry 2016 22:3* **22**, 430–440 (2016).

22. Eastwood, S. L. & Harrison, P. J. Cellular basis of reduced cortical reelin expression in schizophrenia. *American Journal of Psychiatry* **163**, 540–542 (2006).

23. Riva, M. *et al.* Aberrant survival of hippocampal Cajal-Retzius cells leads to memory deficits, gamma rhythmopathies and susceptibility to seizures in adult mice. *Nat Commun* **14**, 1531 (2023).

24. Ludington-Hoe, S. M. *et al.* Neurophysiologic Assessment of Neonatal Sleep Organization: Preliminary Results of a Randomized, Controlled Trial of Skin Contact With Preterm Infants. *Pediatrics* **117**, e909–e923 (2006).

25. Nalivaeva, N. N. *et al.* The amyloid precursor protein: A biochemical enigma in brain development, function and disease. *FEBS Lett* **587**, 2046–2054 (2013).

26. Hoe, H. S. & Rebeck, G. W. Regulated Proteolysis of APP and ApoE Receptors. *Molecular Neurobiology 2008 37:1* **37**, 64–72 (2008).

27. Knuesel, I. Reelin-mediated signaling in neuropsychiatric and neurodegenerative diseases. *Prog Neurobiol* **91**, 257–274 (2010).

28. Tsuneura, Y., Nakai, T., Mizoguchi, H. & Yamada, K. New Strategies for the Treatment of Neuropsychiatric Disorders Based on Reelin Dysfunction. *International Journal of Molecular Sciences 2022, Vol. 23, Page 1829* **23**, 1829 (2022).

29. Botella-López, A. *et al.* β-amyloid controls altered Reelin expression and processing in Alzheimer's disease. *Neurobiol Dis* **37**, 682–691 (2010).

30. Herz, J. & Strickland, D. K. LRP: a multifunctional scavenger and signaling receptor. *Journal of Clinical Investigation* **108**, 779 (2001).

31. Gallo, C. M., Ho, A. & Beffert, U. ApoER2: Functional Tuning Through Splicing. *Front Mol Neurosci* **13**, 563831 (2020).

32. Dlugosz, P. & Nimpf, J. The Reelin Receptors Apolipoprotein E receptor 2 (ApoER2) and VLDL Receptor. *Int J Mol Sci* **19**, 3090 (2018).

33. Trommsdorff, M. *et al.* Reeler/disabled-like disruption of neuronal migration in knockout mice lacking the VLDL receptor and ApoE receptor 2. *Cell* **97**, 689–701 (1999).

34. Hack, I. *et al.* Divergent roles of ApoER2 and Vldlr in the migration of cortical neurons. *Development* **134**, 3883–3891 (2007).

35. Andrade, N. *et al.* ApoER2/VLDL receptor and Dab1 in the rostral migratory stream function in postnatal neuronal migration independently of Reelin. *Proc Natl Acad Sci U S A* **104**, 8508 (2007).

36. Beffert, U. *et al.* Modulation of Synaptic Plasticity and Memory by Reelin Involves Differential Splicing of the Lipoprotein Receptor Apoer2. *Neuron* **47**, 567–579 (2005).

37. Wasser, C. R. *et al.* Differential splicing and glycosylation of Apoer2 alters synaptic plasticity and fear learning. *Sci Signal* **7**, ra113 (2014).

38. Petit-Turcotte, C. *et al.* The apoE receptor apoER2 is involved in the maintenance of efficient synaptic plasticity. *Neurobiol Aging* **26**, 195–206 (2005).

39. Ohkubo, N. *et al.* Apolipoprotein E and Reelin ligands modulate tau phosphorylation through an Apolipoprotein E receptor/disabled-1/glycogen synthase kinase-3β cascade. *The FASEB Journal* **17**, 295–297 (2003).

40. Rossi, D. *et al.* Reelin reverts biochemical, physiological and cognitive alterations in mouse models of Tauopathy. *Prog Neurobiol* **186**, (2020).

41. Khialeeva, E. & Carpenter, E. M. Nonneuronal roles for the reelin signaling pathway. *Developmental Dynamics* **246**, 217–226 (2017).

42. Beffert, U. *et al.* ApoE Receptor 2 Controls Neuronal Survival in the Adult Brain. *Current Biology* **16**, 2446–2452 (2006).

43. Brandes, C. *et al.* Alternative Splicing in the Ligand Binding Domain of Mouse ApoE Receptor-2 Produces Receptor Variants Binding Reelin but Not α2-Macroglobulin. *Journal of Biological Chemistry* **276**, 22160–22169 (2001).

44. Dlugosz, P. & Nimpf, J. The Reelin Receptors Apolipoprotein E receptor 2 (ApoER2) and VLDL Receptor. *Int J Mol Sci* **19**, 3090 (2018).

45. May, P., Bock, H. H., Nimpf, J. & Herz, J. Differential Glycosylation Regulates Processing of Lipoprotein Receptors by γ-Secretase. *Journal of Biological Chemistry* **278**, 37386–37392 (2003).

46. Balmaceda, V. *et al.* ApoER2 processing by presenilin-1 modulates reelin expression. *The FASEB Journal* **28**, 1543–1554 (2014).

47. Telese, F. *et al.* LRP8-Reelin-regulated Neuronal (LRN) Enhancer Signature Underlying Learning and Memory Formation. *Neuron* **86**, 696 (2015).

48. Gao, J. *et al.* The E3 ubiquitin ligase IDOL regulates synaptic ApoER2 levels and is important for plasticity and learning. *Elife* **6**, e29178–e29178 (2017).

49. Sotelo, P., Farfán, P., Benitez, M. L., Bu, G. & Marzolo, M. P. Sorting nexin 17 regulates ApoER2 recycling and reelin signaling. *PLoS One* **9**, (2014).

50. Poirier, S. *et al.* The proprotein convertase PCSK9 induces the degradation of low density lipoprotein receptor (LDLR) and its closest family members VLDLR and ApoER2. *J Biol Chem* **283**, 2363–2372 (2008).

51. Hinrich, A. J. *et al.* Therapeutic correction of ApoER2 splicing in Alzheimer's disease mice using antisense oligonucleotides. *EMBO Mol Med* **8**, 328–345 (2016).

52. Andersen, O. M. *et al.* Essential role of the apolipoprotein E receptor-2 in sperm development. *J Biol Chem* **278**, 23989–23995 (2003).

53. Naji, D. H. *et al.* Significant genetic association of a functional TFPI variant with circulating fibrinogen levels and coronary artery disease. *Mol Genet Genomics* **293**, 119 (2018).

54. Komaravolu, R. K., Waltmann, M. D., Konaniah, E., Jaeschke, A. & Hui, D. Y. ApoER2 (Apolipoprotein E Receptor-2) Deficiency Accelerates Smooth Muscle Cell Senescence via Cytokinesis Impairment and Promotes Fibrotic Neointima After Vascular Injury. *Arterioscler Thromb Vasc Biol* **39**, 2132–2144 (2019).

55. Ulrich, V. *et al.* Genetic variants of ApoE and ApoER2 differentially modulate endothelial function. *Proc Natl Acad Sci U S A* **111**, 13493–13498 (2014).

56. Baitsch, D. *et al.* Apolipoprotein E induces antiinflammatory phenotype in macrophages. *Arterioscler Thromb Vasc Biol* **31**, 1160–1168 (2011).

57. Sakai, K. *et al.* A neuronal VLDLR variant lacking the third complement-type repeat exhibits high capacity binding of ApoE containing lipoproteins. *Brain Res* **1276**, 11 (2009).

58. Howell, B. W., Hawkes, R., Soriano, P. & Cooper, J. A. Neuronal position in the developing brain is regulated by mouse disabled-1. *Nature 1997 389:6652* **389**, 733–737 (1997).

59. Sheldon, M. *et al.* Scrambler and yotari disrupt the disabled gene and produce a reeler - like phenotype in mice. *Nature 1997 389:6652* **389**, 730–733 (1997).

60. Howell, B. W., Herrick, T. M. & Cooper, J. A. Reelin-induced tryosine phosphorylation of Disabled 1 during neuronal positioning. *Genes Dev* **13**, 643 (1999).

61. Howell, B. W., Herrick, T. M., Hildebrand, J. D., Zhang, Y. & Cooper, J. A. Dab1 tyrosine phosphorylation sites relay positional signals during mouse brain development. *Curr Biol* **10**, 877–885 (2000).

62. Strasser, V. *et al.* Receptor Clustering Is Involved in Reelin Signaling. *Mol Cell Biol* **24**, 1378 (2004).

63. Assadi, A. H. *et al.* Interaction of reelin signaling and Lis1 in brain development. *Nat Genet* **35**, 270–276 (2003).

64. Pramatarova, A. *et al.* Nck beta interacts with tyrosine-phosphorylated disabled 1 and redistributes in Reelin-stimulated neurons. *Mol Cell Biol* **23**, 7210–7221 (2003).

65. Huang, Y. *et al.* Tyrosine phosphorylated Disabled 1 recruits Crk family adapter proteins. *Biochem Biophys Res Commun* **318**, 204–212 (2004).

66. Feng, L., Allen, N. S., Simo, S. & Cooper, J. A. Cullin 5 regulates Dab1 protein levels and neuron positioning during cortical development. *Genes Dev* **21**, 2717–2730 (2007).

67. Franco, S. J., Martinez-Garay, I., Gil-Sanz, C., Harkins-Perry, S. R. & Müller, U. Reelin regulates cadherin function via Dab1/Rap1 to control neuronal migration and lamination in the neocortex. *Neuron* **69**, 482–497 (2011).

68. Jossin, Y. & Cooper, J. A. Reelin, Rap1 and N-cadherin orient the migration of multipolar neurons in the developing neocortex. *Nat Neurosci* **14**, 697–703 (2011).

69. Sekine, K. *et al.* Reelin controls neuronal positioning by promoting cell-matrix adhesion via inside-out activation of integrin α5β1. *Neuron* **76**, 353–369 (2012).

70. Matsunaga, Y. *et al.* Reelin transiently promotes N-cadherin-dependent neuronal adhesion during mouse cortical development. *Proc Natl Acad Sci U S A* **114**, 2048–2053 (2017).

71. Park, T. J. & Curran, T. Crk and Crk-Like Play Essential Overlapping Roles Downstream of Disabled-1 in the Reelin Pathway. *The Journal of Neuroscience* **28**, 13551 (2008).

72. Leemhuis, J. & Bock, H. H. Reelin modulates cytoskeletal organization by regulating Rho GTPases. *Commun Integr Biol* **4**, 254 (2011).

73. Zhang, B. *et al.* Alternative splicing of disabled-1 controls multipolar-to-bipolar transition of migrating neurons in the neocortex. *Cerebral Cortex* **28**, 3457–3467 (2018).

74. Honda, T., Hirota, Y. & Nakajima, K. Heterozygous Dab1 Null Mutation Disrupts Neocortical and Hippocampal Development. *eNeuro* **10**, (2023).

75. Howell, K. R., Hoda, M. N. & Pillai, A. VEGF activates NR2B phosphorylation through Dab1 pathway. *Neurosci Lett* **552**, 30–34 (2013).

76. Duit, S., Mayer, H., Blake, S. M., Schneider, W. J. & Nimpf, J. Differential functions of ApoER2 and very low density lipoprotein receptor in Reelin signaling depend on differential sorting of the receptors. *Journal of Biological Chemistry* **285**, 4896–4908 (2010).

77. Levental, I., Levental, K. R. & Heberle, F. A. Lipid rafts: controversies resolved, mysteries remain. *Trends Cell Biol* **30**, 341 (2020).

78. Pike, L. J. Rafts defined: a report on the Keystone Symposium on Lipid Rafts and Cell Function. *J Lipid Res* **47**, 1597–1598 (2006).

79. Allen, J. A., Halverson-Tamboli, R. A. & Rasenick, M. M. Lipid raft microdomains and neurotransmitter signalling. *Nat Rev Neurosci* **8**, 128–140 (2007).

80. Head, B. P., Patel, H. H. & Insel, P. A. Interaction of membrane/lipid rafts with the cytoskeleton: Impact on signaling and function. *Biochimica et Biophysica Acta (BBA) - Biomembranes* **1838**, 532–545 (2013).

81. Babonis, L. S. & Martindale, M. Q. Phylogenetic evidence for the modular evolution of metazoan signalling pathways. *Philosophical Transactions of the Royal Society B: Biological Sciences* **372**, (2017).

82. Barberán, S., Martín-Durán, J. M. & Cebrià, F. Evolution of the EGFR pathway in Metazoa and its diversification in the planarian Schmidtea mediterranea. *Sci Rep* **6**, (2016).

83. Yamada, M., Ikeuchi, T. & Hatanaka, H. The neurotrophic action and signalling of epidermal growth factor. *Prog Neurobiol* **51**, 19–37 (1997).

84. Tissue expression of EGFR - Summary - The Human Protein Atlas. https://www.proteinatlas.org/ENSG00000146648-EGFR/tissue.

85. Gallo, V. & Deneen, B. Glial Development: The Crossroads of Regeneration and Repair in the CNS. *Neuron* **83**, 283 (2014).

86. Yang, Y. P. *et al.* A Chimeric Egfr Protein Reporter Mouse Reveals Egfr Localization and Trafficking In Vivo. *Cell Rep* **19**, 1257–1267 (2017).

87. Singh, B. & Coffey, R. J. Trafficking of Epidermal Growth Factor Receptor Ligands in Polarized Epithelial Cells. *Annu Rev Physiol* **76**, 275 (2014).

88. Harris, R. C., Chung, E. & Coffey, R. J. EGF receptor ligands. *Exp Cell Res* **284**, 2–13 (2003).

89. Abou-Fayçal, C., Hatat, A. S., Gazzeri, S. & Eymin, B. Splice Variants of the RTK Family: Their Role in Tumour Progression and Response to Targeted Therapy. *Int J Mol Sci* **18**, (2017).

90. Barbieri, E., Di Fiore, P. P. & Sigismund, S. Endocytic control of signaling at the plasma membrane. *Curr Opin Cell Biol* **39**, 21–27 (2016).

91. Sakthianandeswaren, A. *et al.* Predictive Biomarkers for Monoclonal Antibody Therapies Targeting EGFR (Cetuximab, Panitumumab) in the Treatment of Metastatic Colorectal Cancer. *Advances in the Molecular Understanding of Colorectal Cancer* (2018) doi:10.5772/INTECHOPEN.80690.

92. Roskoski, R. The ErbB/HER family of protein-tyrosine kinases and cancer. *Pharmacol Res* **79**, 34–74 (2014).

93. Schneider, M. R. & Yarden, Y. The EGFR-HER2 module: a stem cell approach to understanding a prime target and driver of solid tumors. *Oncogene 2016 35:23* **35**, 2949–2960 (2015).

94. Levantini, E., Maroni, G., Del Re, M. & Tenen, D. G. EGFR signaling pathway as therapeutic target in human cancers. *Semin Cancer Biol* **85**, 253–275 (2022).

95. Li, Y. *et al.* Toward the next generation EGFR inhibitors: an overview of osimertinib resistance mediated by EGFR mutations in non-small cell lung cancer. *Cell Commun Signal* **21**, 71 (2023).

96. SuperScript™ IV VILO™ Master Mix with ezDNase™ Enzyme Manual. https://www.thermofisher.com/document-connect/document-connect.html?url=https://assets.thermofisher.com/TFS-Assets%2FLSG%2Fmanuals%2FsuperscriptIV_VILO_master_mix_UG.pdf.

97. Platinum™ SuperFi II DNA Polymerase Manual. https://www.thermofisher.com/document-connect/document-connect.html?url=https://assets.thermofisher.com/TFS-Assets%2FLSG%2Fmanuals%2FMAN0018859_Platinum_SuperFi_II_DNA_Pol_UG.pdf.

98. Mayer, H., Duit, S., Hauser, C., Schneider, W. J. & Nimpf, J. Reconstitution of the Reelin Signaling Pathway in Fibroblasts Demonstrates that Dab1 Phosphorylation Is Independent of Receptor Localization in Lipid Rafts. *Mol Cell Biol* **26**, 19–27 (2006).

99. Ma, L. *et al.* Ligand-dependent recruitment of the ErbB4 signaling complex into neuronal lipid rafts. *Journal of Neuroscience* **23**, 3164–3175 (2003).

100. Stockinger, W. *et al.* The Low Density Lipoprotein Receptor Gene Family DIFFERENTIAL EXPRESSION OF TWO 2-MACROGLOBULIN RECEPTORS IN THE BRAIN*. *Journal of Biological Chemistry* **273**, 32213–32221 (1998).

101. Burrell, T. C., Divekar, S. D., Weeber, E. J. & Rebeck, G. W. Fyn tyrosine kinase increases Apolipoprotein E Receptor 2 levels and phosphorylation. *PLoS One* **9**, (2014).

102. Gene Set - HEK293. https://maayanlab.cloud/Harmonizome/gene_set/HEK293/BioGPS+Cell+Line+Gene+Expression+Profiles.

103. Zagranichnaya, T. K., Wu, X., Danos, A. M. & Villereal, M. L. Gene expression profiles in HEK-293 cells with low or high store-operated calcium entry: can regulatory as well as regulated genes be identified? *Physiol Genomics* **21**, 14–33 (2005).

104. Li, M., Husic, N., Lin, Y. & Snider, B. J. Production of Lentiviral Vectors for Transducing Cells from the Central Nervous System. *J Vis Exp* 4031 (2012) doi:10.3791/4031.

105. Yue, P. Y. K., Leung, E. P. Y., Mak, N. K. & Wong, R. N. S. A simplified method for quantifying cell migration/wound healing in 96-well plates. *J Biomol Screen* **15**, 427–433 (2010).

106. Mackay, C. R. Moving targets: cell migration inhibitors as new anti-inflammatory therapies. *Nat Immunol* **9**, 988–998 (2008).

107. Liang, C. C., Park, A. Y. & Guan, J. L. In vitro scratch assay: a convenient and inexpensive method for analysis of cell migration in vitro. *Nat Protoc* **2**, 329–333 (2007).

108. Dong Cho Han, Rodriguez, L. G. & Guan, J. L. Identification of a novel interaction between integrin beta1 and 14-3-3beta. *Oncogene* **20**, 346–357 (2001).

109. Dlugosz, P., Teufl, M., Schwab, M., Kohl, K. E. & Nimpf, J. Disabled 1 Is Part of a Signaling Pathway Activated by Epidermal Growth Factor Receptor. *International Journal of Molecular Sciences 2021, Vol. 22, Page 1745* **22**, 1745 (2021).

110. Chen, Y., Long, H., Wu, Z., Jiang, X. & Lan, M. EGF Transregulates Opioid Receptors through EGFR-mediated GRK2 Phosphorylation and Activation. *Mol Biol Cell* **19**, 2973 (2008).

111. Wulf, E., Deboben, A., Bautz, F. A., Faulstich, H. & Wieland, T. Fluorescent phallotoxin, a tool for the visualization of cellular actin. *Proc Natl Acad Sci U S A* **76**, 4498 (1979).

112. Hua, K. & Ferland, R. J. Fixation methods can differentially affect ciliary protein immunolabeling. *Cilia* **6**, (2017).

113. Salic, A. & Mitchison, T. J. A chemical method for fast and sensitive detection of DNA synthesis in vivo. *Proc Natl Acad Sci U S A* **105**, 2415–2420 (2008).

114. Ishiyama, M. *et al.* A combined assay of cell viability and in vitro cytotoxicity with a highly water-soluble tetrazolium salt, neutral red and crystal violet. *Biol Pharm Bull* **19**, 1518–1520 (1996).

115. epidermal growth factor receptor isoform a precursor [Homo sapiens] - Protein - NCBI. https://www.ncbi.nlm.nih.gov/protein/NP_005219.2?report=fasta.

116. Hasegawa, K., Matsui, T. K., Kondo, J. & Kuwako, K. I. N-WASP-Arp2/3 signaling controls multiple steps of dendrite maturation in Purkinje cells in vivo. *Development* **149**, (2022).

117. Katanov, C. *et al.* N-Wasp Regulates Oligodendrocyte Myelination. *J Neurosci* **40**, 6103–6111 (2020).

118. Wang, Z. *et al.* Differentiation of neuronal cells from NIH/3T3 fibroblasts under defined conditions. *Dev Growth Differ* **53**, 357–365 (2011).

119. Zhao, W., Zhao, H., Li, M. & Huang, C. Microfluidic devices for neutrophil chemotaxis studies. *J Transl Med* **18**, (2020).

120. Garcia-Miranda, P., Peral, M. J. & Ilundain, A. A. Rat small intestine expresses the reelin-Disabled-1 signalling pathway. *Exp Physiol* **95**, 498–507 (2010).

121. Vázquez-Carretero, M. D. *et al.* Small and large intestine express a truncated Dab1 isoform that assembles in cell-cell junctions and co-localizes with proteins involved in endocytosis. *Biochimica et Biophysica Acta (BBA) - Biomembranes* **1860**, 1231–1241 (2018).

122. Tissir, F. & Goffinet, A. M. Reelin and brain development. *Nature Reviews Neuroscience 2003 4:6* **4**, 496–505 (2003).

List of figures

List of tables

Supplementary Figures

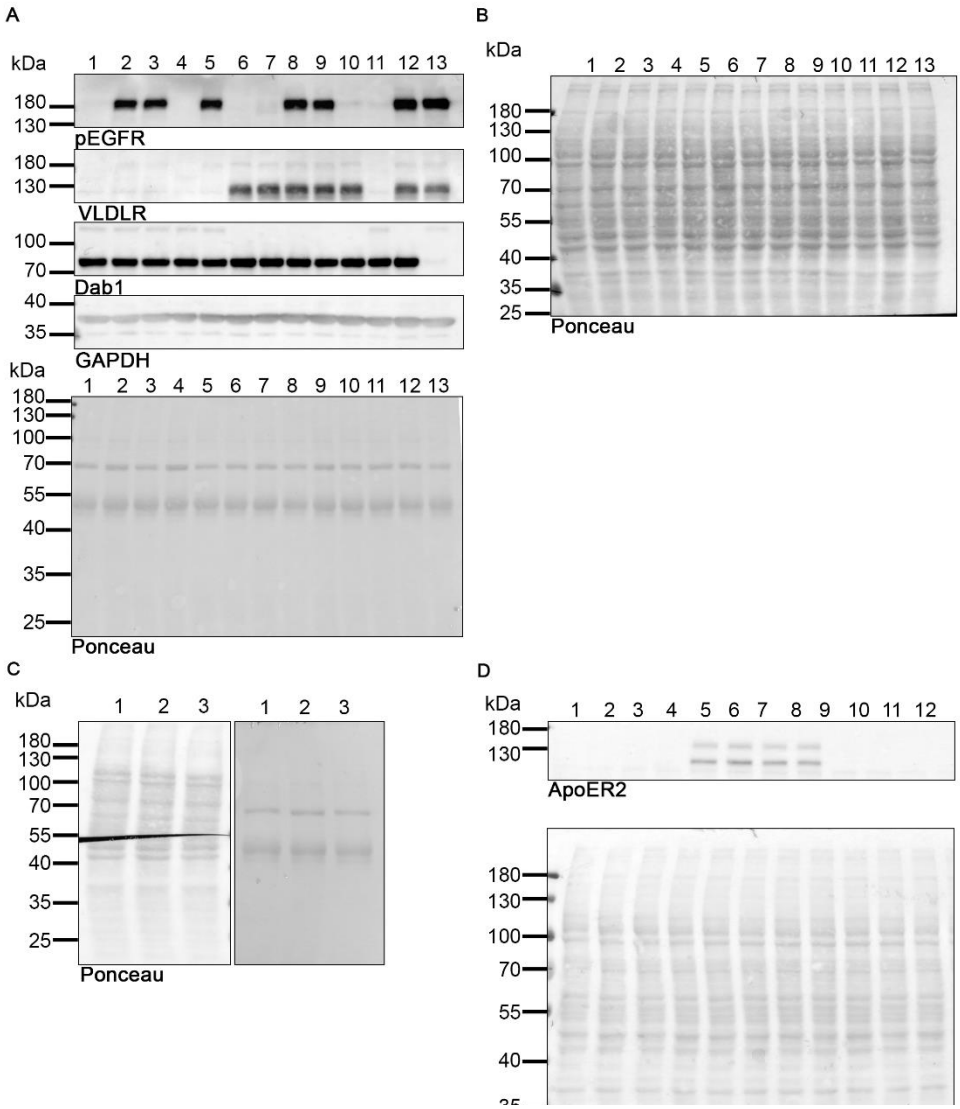

Figure 24 **A**. Original blot of Figure 22A. where lanes 6 and 11 are loaded incorrectly and Ponceau staining **B**. Ponceau staining of blot depicted in Figure 22B. **C**. Ponceau staining of Figure 22.C and D. **D**. ApoER2 level blotted after stripping of the pEGFR panel and Ponceau staining of the blot shown in Figure 23. and. Ponceau staining was included to assess the quality of the run blot.

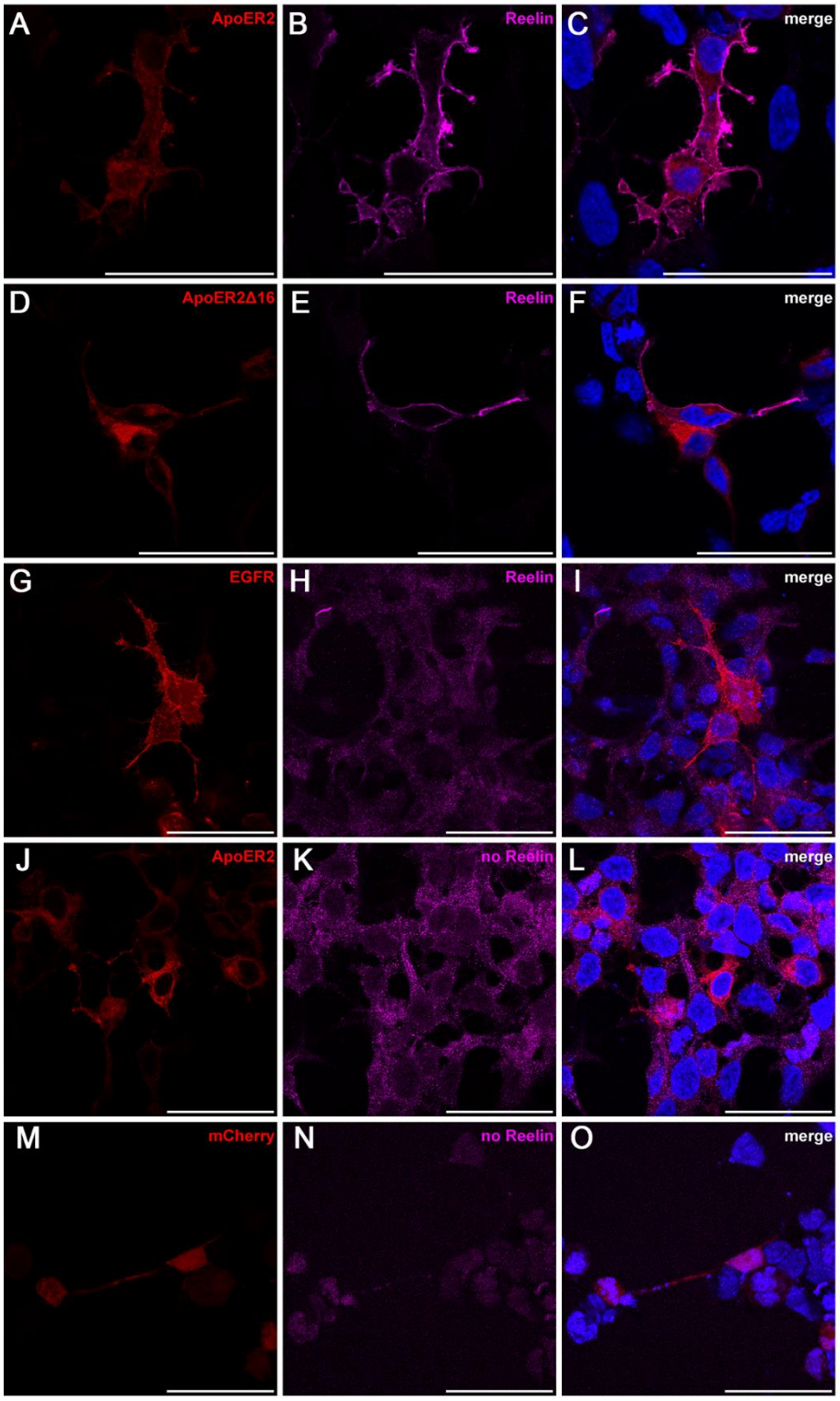

Figure 25 Reelin binding to receptors. Fluorescent images of HEK293 cells transfected with ApoER2 (A-C, J-L), ApoER2Δ16 (D-F), EGFR (G-I), linked to a mCherry fluorophore and mCherry alone (M-O). Conditions (A-I, M-O) were treated for 3min at 37°C with RCM, as control MCM was added to ApoER2 expressing cells (J-L). After fixing and DAPI staining cells were mounted. Scale bar represents 50µm.